UNICA

UNIVERSITÀ
DEGLI STUDI
DI CAGLIARI

Ph.D. DEGREE IN

Physics

Cycle XXXVIII

TITLE OF THE Ph.D. THESIS

TMD Approach in High Energy Physics: Theory and Applications

Scientific Disciplinary Sector(s)

02/PHYS-02

Ph.D. Student:	Simone Anedda
Supervisor:	Prof.Francesco Murgia
Co-Supervisor:	Prof. Giuseppe Bozzi, Prof. Cristian Pisano

Final exam. Academic Year 2024/2025

Thesis defence session: February 2026

Contents

Introduction

Hadrons, such as protons and neutrons, are the building blocks of visible matter in the universe. Unlike elementary particles (like leptons), they are made up of quarks and gluons, collectively known as partons, bound by strong interaction. The underlying theory, Quantum Chromodynamics (QCD), is a non-Abelian gauge theory developed in the early 1970s with colour as its charge and gluons as self-interacting gauge bosons.

A distinctive feature of QCD is the way the strong interaction manifests itself at different energy scales: at short distances, quarks and gluons interact weakly, allowing for the application of perturbative methods (asymptotic freedom); at large distances, colour confinement prevents coloured particles from being observed in isolated states, making the study of hadron structure particularly fascinating and challenging. This dichotomy implies that the quark-gluon dynamics we seek to uncover must be inferred from colour-neutral hadronic final states measured by detectors, and the use of a theoretical approach that allows us to distinguish between short-distance physics and long-distance structure embodied by universal functions.

The modern picture of hadron structure emerged from a sequence of decisive experiments and parallel theoretical advances. Deep inelastic electron-nucleon scattering (DIS) at the Stanford Linear Accelerator Center (SLAC) in 1967-69 revealed scaling behaviour in the inclusive cross section, showing how the nucleon is composed of point-like constituents. Breidenbach et al. [1] observed that the structure functions exhibit only a weak dependence on the photon virtuality, an empirical regularity later termed Bjorken scaling. Theoretically, Bjorken related the scaling limit to current-algebra arguments [2], and Callan and Gross derived the relation $F_2(x) \simeq 2xF_1(x)$ for scattering off spin-1/2 constituents [3], thereby providing a crucial consistency check for point-like quarks. This interpretation was formalised by Feynman's parton model, which offers a simple yet powerful description of hadron structure, in which DIS is explained as incoherent scattering off quasi-free constituents at high momentum transfer, described in terms of distribution functions [4].

Soon after, precise measurements revealed small, but systematic deviations from exact scaling ("scaling violation"). The theoretical breakthrough came in 1973, when Gross, Wilczek [5] and Politzer [6] demonstrated that non-Abelian gauge theories are asymptotically free. This led to QCD as the theory of strong interactions and explained why partons behave as nearly free particles at high Q^2, while remaining confined at low energy.

Though exact scaling is expected in the parton model, QCD predicts a logarithmic Q^2 dependence of the structure functions; indeed, gluon radiation and parton splitting lead to small, logarithmic deviations from exact scaling. This insight gave rise to the QCD evolution equations, derived independently by Dokshitzer [7], Gribov and Lipatov [8], and Altarelli and Parisi [9] in the 1970s, now universally referred to as the DGLAP equations. These equations describe how parton distributions evolve with the energy scale, and their predictions were later confirmed experimentally by muon–nucleon scattering experiments such as those conducted by the European Muon Collaboration (EMC) [10], the BCDMS collaboration [11] at CERN and later at HERA [12].

A complementary theoretical development was Wilson's operator product expansion (OPE), which provided a systematic method to separate short-distance (perturbative) contributions from long-distance (non-perturbative) effects. Based on the ideas of OPE and the renormalisation group, factorisation theorems were established for certain classes of high-energy reactions (such as inclusive DIS, Drell-Yan, and hadron production in e^+e^- annihilation) [13]: cross sections can be written as convolutions of universal parton distribution functions (PDFs) or fragmentation functions (FFs), non-perturbative but measurable quantities, with hard-scattering coefficients calculable in perturbation theory.

In collinear factorisation, partons (hadrons) are characterised by their longitudinal momentum fraction x (z) with respect to the parent hadrons (partons). Universal PDFs and FFs, combined with perturbatively resummed hard parts (e.g., CSS resummation for low transverse momentum), describe a wide range of processes from inclusive DIS and Drell-Yan to pp collisions at the LHC, and remain the standard language for precision phenomenology.

Despite its successes, the collinear approach has intrinsic limitations that have led to the need for a more general formalism. In fact, it neglects the intrinsic momentum k_T of partons and is insensitive to spin-momentum correlations in the transverse plane; as a result, it cannot fully account for observables that depend on the azimuthal structure or on the spectrum at low transverse momentum. The Transverse-Momentum-Dependent (TMD) framework addresses these issues by introducing TMD PDFs and FFs that explicitly depend on both x (or z) and k_T, and by incorporating appropriate soft factors and evolution equations (like e.g., in the Collins-Soper-Sterman approach or in soft collinear effective theories (SCET)). Thus, TMDs account for a much richer structure involving correlations (e.g., the Sivers and Boer-Mulders functions) among the spin, or polarisation state, and the intrinsic motion of partons and hadrons. These correlations manifest themselves in observable spin and azimuthal asymmetries in inclusive and semi-inclusive hadronic processes.

Rigorous TMD factorisation has been proven for three fundamental processes characterised by two distinct energy scales: a perturbative one, related to a large momentum transfer in the process, Q, and a much smaller second scale, q_T, comparable to the QCD scale and such that $Q \gg q_T \sim \Lambda_{QCD}$, which is related to the intrinsic parton motion

inside hadrons [14–17]. These processes are: (1) Semi-inclusive deep inelastic scattering (SIDIS), $\ell\, p(N) \to \ell'\, h + X$; (2) The Drell-Yan (DY) process for inclusive dilepton production in hadronic collisions, $AB \to \gamma^*,\, Z \to \ell^+\ell^- + X$; (3) Two almost back-to-back hadron production in lepton-antilepton annihilations, $\ell^+\ell^- \to \gamma^*,\, Z \to h_1\, h_2 + X$, also known as semi-inclusive $\ell^+\ell^-$ annihilation (SIA).

Indeed, most of the available experimental information on quark TMDs comes from these three processes. Concerning phenomenology, the full (leading and, in some cases, next-to-leading twist) structure of azimuthal dependences for particle production in (un)polarised processes has been derived in the TMD approach for SIDIS [18–20] and DY [21] processes, as well as for hadron-pair SIA production [22, 23]. In particular, Refs. [20, 23] present, respectively for the SIDIS and SIA cases, an independent derivation within the TMD approach and the helicity formalism that will be adopted also in the next sections. Other processes, like Higgs [24, 25], photon pair [26], J/ψ pair [27], J/ψ+photon [28] and C-even quarkonium production [29, 30] in hadronic collisions, where the dominance of the colour-singlet quarkonium formation mechanism is assumed, represent another source of valuable information on TMDs, in particular the almost unknown gluon ones. For these reactions, TMD factorisation is not fully proven yet and there are some indications for possible factorisation-breaking effects for processes involving four hadrons, see e.g. Ref. [31].

A central goal of modern hadronic physics is to obtain a three-dimensional picture of the nucleon (and, more generally, of quark–gluon dynamics) by extracting TMDs from experimental data. To this end, we have to solve an inverse problem: measured two-scale observables (with $q_T \ll Q$) are deconvolved into universal TMD PDFs/FFs and perturbative hard parts. Ref. [32] lays out a practical workflow: (i) identify "good" two-scale observables (cross sections or asymmetries) that admit TMD factorisation; (ii) select complementary data sets that jointly constrain a closed set of TMDs; (iii) compute/validate the short-distance hard parts; (iv) implement the scale evolution of TMDs so measurements at different Q can be compared; (v) perform global fits minimizing the difference between data and theoretical calculations based on the factorization formalisms to extract the set of universal TMDs that can best describe the data within the experimental uncertainties.

Within the workflow outlined above, we will follow two directions. First, we suggest considering photon-photon scattering as a clean, factorisable channel to access TMD fragmentation through azimuthal modulations in inclusive almost back-to-back hadron pair production. TMD factorization is expected to hold, given the clarity of the initial electromagnetic state and the presence of final-state interactions only. This makes $\gamma\gamma \to h_1 h_2 + X$ a "good" two-scale observable, complementing semi-inclusive deep inelastic scattering and e^+e^- annihilation processes, which provide most of the present phenomenological information on TMDs.

Second, we study Higgs production through gluon fusion in the low-q_T regime, which

provides a probe for gluon TMDs. For colour-singlet final state and $q_T \ll m_H$, the cross section factorises into a hard function and gluon TMDs that evolve with the Collins-Soper kernel; the spectrum is directly sensitive to the unpolarised $f_1^g(x, k_\perp)$ and, in refined analyses, to the linearly polarised $h_1^{\perp g}(x, k_\perp)$. Empirically, gluon TMDs remain poorly constrained compared to their quark counterparts; for this reason we want to exploit the LHC measurements of H transverse momentum in the TMD region, in order to fit the measured low-q_T Higgs spectrum, and more precisely, obtain the non-perturbative contribution with the relative uncertainties. A first consistent extraction of the non-perturbative contribution from Higgs q_T data would put gluon TMDs on a similar path to that already followed by quark TMDs, which are now comparatively well constrained. The resulting information on the gluon sector can then be applied to other gluon-initiated processes (e.g., low-q_T vector-boson plus jet or heavy-quarkonium channels), providing stronger global constraints and cross-checks of TMD universality and evolution. Furthermore, such a fit would advance our understanding of the three-dimensional, momentum-space composition of the nucleon's gluons, significantly improving our knowledge of hadronic structure. This thesis is structured as follows:

Chapter 1 is a review of the theoretical framework that underpins the TMD approach. It starts with a review of the operator definitions of quark and gluon TMDs, the factorization of two-scale observables, and the roles of the renormalization and rapidity scales. It then discusses perturbative evolution and matching, clarifying how logarithms of the hard scale are resummed and where genuinely non-perturbative information is required.

Chapter 2 turns to photon–photon collisions across different processes, showing how they can provide a clean environment to access TMD fragmentation physics. It introduces the relevant kinematics and helicity formalism, derives the structure of azimuthal modulations, and illustrates how selected asymmetries isolate specific TMD fragmentation functions; a concise phenomenological study shows the sensitivity of projected measurements.

Chapter 3 addresses gluon TMDs using the low-q_T Higgs transverse-momentum spectrum in gluon fusion. It formulates the $gg \to H$ cross section in TMD factorization, details the experimental inputs and fiducial selections (notably the $H \to \gamma\gamma$ and $H \to 4\ell$ channels), and presents first results together with a discussion of theoretical and experimental systematics. Technical material, including hard and matching coefficients, numerical strategies, and phase-space factors, is collected in dedicated appendices where appropriate.

Chapter 1

Theoretical framework

Quantum Chromodynamics is the accepted theory of the strong interaction that describes the structure and dynamics of hadrons. Its Lagrangian density reads

$$\mathcal{L} \;=\; \sum_q \bar{\psi}_q (i \not{D} \;-\; m_q)\psi_q - \frac{1}{4} F^a_{\mu\nu} F^{a\,\mu\nu} \,, \tag{1.1}$$

where ψ_q denote the quark fields of flavour q with mass m_q, and the sum runs over the N_f active flavours, $q \in \{u, d, s, c, b, t\}$. The covariant derivative is $D_\mu = \partial_\mu - ig\, A^a_\mu T^a$ and the field–strength tensor is

$$F^a_{\mu\nu} = \partial_\mu A^a_\nu \;-\; \partial_\nu A^a_\mu \;+\; g\, f^{abc} A^b_\mu A^c_\nu \,, \tag{1.2}$$

where A^a_μ are the gauge (gluon) fields, T^a are the generators in the fundamental representation of the group $SU(N_c)$ (with $a \in \{1, ..., N_c^2 - 1\}$), f^{abc} are the structure constants, and $N_c = 3$ is the number of colours. Non–Abelian gauge theories such as QCD are renormalizable; see, e.g., [33]. Consequently, the coupling constant acquires a scale dependence through the renormalization scale μ. Assuming that the strong coupling $\alpha_S(\mu_0) = g^2(\mu_0)/(4\pi)$ is small at some reference scale μ_0, its running for $\mu > \mu_0$ can be determined perturbatively. At leading order one finds

$$\alpha_S(\mu) = \frac{\alpha_S(\mu_0)}{1 + \frac{\beta_0}{4\pi}\alpha_S(\mu_0) \ln \frac{\mu^2}{\mu_0^2}} \,, \tag{1.3}$$

with $\beta_0 = \frac{11}{3} N_c - \frac{2}{3} N_f$. Increasing μ at fixed μ_0 thus decreases $\alpha_S(\mu)$; for example, one finds $\alpha_S(91\text{ GeV}) \sim 0.12$ at the Z–boson mass scale. In the limit $\mu \to \infty$, $\alpha_S(\mu) \to 0$, thus exhibiting asymptotic freedom [34]. Conversely, if we want to evolve towards $\mu < \mu_0$, we must account for the increase in $\alpha_S(\mu)$. Indeed, when μ approaches hadronic scales $\mu \sim M_{had} \sim 1$ GeV, α_S is close to unity, leading to a breakdown of the perturbative expansion. Consequently, the interaction is too strong, and non-perturbative techniques are required to tackle QCD; in this sense, PDFs and their generalizations are non-perturbative objects and cannot be derived within perturbative QCD. Two other features of QCD are:

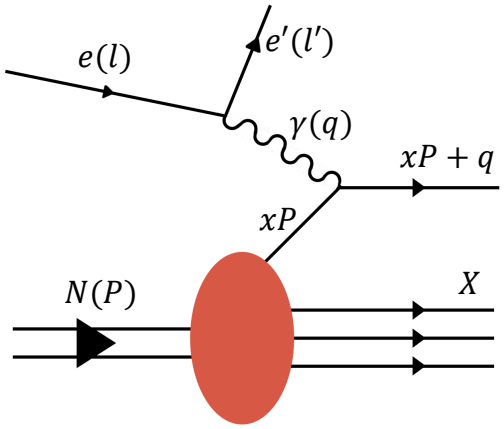

Figure 1.1: The amplitude of deep-inelastic scattering in the Bjorken-limit, where the electron scatters elastically off a charged parton carrying the momentum fraction $x \simeq x_{_B}$ of the nucleon's momentum P.

colour confinement, describing the empirical fact that free colour charges have never been observed in nature; and the spontaneous breaking of chiral symmetry, which is approximately present in the Lagrangian (due to $m_q \ll M_{had}$ for light flavours $q = u, d, s$), but is not manifest in the hadron spectrum. Modern knowledge of the partonic structure of hadrons comes from collinear QCD. In this framework, as discussed above, the cross section factorizes into short-distance, perturbatively calculable hard parts, and universal, process-independent non-perturbative functions, known as the collinear parton distribution functions (PDFs) and fragmentation functions (FFs). A canonical example is inclusive DIS, whose kinematics can be described by the following variables:

$$s = (P + l)^2\,, \quad Q^2 = -q^2\,, \quad x_{_B} = \frac{Q^2}{2\,P \cdot q}\,, \quad y = \frac{P \cdot q}{P \cdot l}\,, \tag{1.4}$$

where s is the square of the centre-of-mass energy, $x_{_B}$ is the Bjorken scaling variable, y denotes the energy loss of the electron in the target rest frame, and the momentum transfer Q defines the hard scale of the process. The QCD factorization formula for the unpolarised cross section [1] can be written as:

$$\mathrm{d}\sigma_{\mathrm{DIS}}^{(\mathrm{unp})} = \sum_a \int_{x_B}^1 \frac{\mathrm{d}x}{x}\, f_1^a(x, \mu_F)\, \mathrm{d}\hat{\sigma}^a\left(\frac{x_B}{x}, \frac{Q}{\mu_R}, \alpha_S(\mu_R)\right) + \mathcal{O}\left(\frac{\Lambda_{\mathrm{QCD}}}{Q}\right). \tag{1.5}$$

where f_1^a is the unpolarised (spin–averaged) PDF with $a = u, \bar{u}, d, \bar{d}, ..., g$. The partonic cross section $d\hat{\sigma}^a$ can be computed order–by–order in perturbation theory. While the tree–level term coincides with the parton model result, radiative QCD corrections appear at next–to–leading order (NLO), such as virtual one–loop corrections to the process $\gamma^* q \to q$

[1] In the TMD formalism, one often writes f_1^a for unpolarized PDFs instead of f^a, or q and g, which are also widely used.

as well as real radiative corrections $\gamma^* q \to g q$ and the photon–gluon fusion process $\gamma^* g \to q\bar{q}$.

Both the partonic cross section and the PDFs depend on unphysical scales: the renormalization scale μ_R, which enters the running coupling $\alpha_S(\mu_R)$ and the hard parts, and the factorization scale μ_F, at which collinear singularities are absorbed into the PDFs. At $\mathcal{O}(\alpha_S)$, ultraviolet divergences from loop integrals are removed by renormalization (introducing μ_R), whereas collinear singularities associated with nearly collinear radiation are factorized into the PDFs (introducing μ_F). In dimensional regularization, μ_R appears when loop integrals are evaluated in $4 - 2\epsilon$ dimensions; μ_F arises from the subtraction of collinear poles and the definition of the PDF scheme (typically $\overline{\text{MS}}$). It is common practice to choose $\mu_R \simeq \mu_F \simeq Q$ to avoid large logarithms $\ln(Q/\mu)$, although the two scales are conceptually distinct.

In this way, PDFs and partonic cross sections are both scale and scheme dependent; however, these dependences must drop out for the full cross section, which is a physical observable. As in the case of $\alpha_S(\mu)$, perturbative QCD predicts the scale dependence of the PDFs through the DGLAP evolution equation,

$$\frac{d\, f_1^a(x,\mu)}{d \ln \mu^2} \;=\; \sum_b \int_x^1 \frac{dx'}{x'}\; P_{ab}\Big(\frac{x}{x'}, \alpha_s(\mu)\Big)\; f_1^b(x',\mu)\,, \tag{1.6}$$

where the splitting functions

$$P_{ab}(x,\alpha_s) \;=\; \frac{\alpha_S}{2\pi}\; P_{ab}^{(1)}(x) \;+\; \left(\frac{\alpha_S}{2\pi}\right)^2 P_{ab}^{(2)}(x) \;+\; ... \tag{1.7}$$

can be computed order–by–order. Because of the quark–gluon coupling and the gluon self–coupling, a parton can split into other partons, thus P_{ab} measure the probability of finding a parton a inside a parton b. Although μ is formally arbitrary, in practice, the perturbative calculations require choosing the scale to be close to the hard scale Q of the process to avoid divergences. Otherwise, large logarithms $\alpha_S^n(\mu) \ln^n(Q/\mu)$ (due to n–loop contributions) spoil the convergence of the perturbative series. Consequently, μ is usually set equal to the hard scale of the process.

Let us consider now the distributions of spin–$\frac{1}{2}$ quark carrying a longitudinal momentum fraction x of its parent hadron. For a spin–$\frac{1}{2}$ nucleon target one can define: (i) the unpolarised quark density $f_1^q(x)$ in an unpolarised nucleon; (ii) the helicity distribution $g_1^q(x)$ in a longitudinally polarised nucleon; and (iii) the transversity distribution $h_1^q(x)$ in a transversely polarised nucleon, where the quark's transverse polarisation is aligned with that of the nucleon. Analogous distributions exist for antiquarks as well. In order to provide a definition of the quark distributions in terms of QCD operators, we introduce the following correlator:

$$\Phi^q(x,S) \;=\; \int \frac{d(\lambda\cdot P)}{4\pi} e^{i\lambda\cdot p}\, \langle P,S|\, \bar{\psi}_q(0)\, \mathcal{W}[0,\lambda]\, \psi_q(\lambda)\, |P,S\rangle\, |_{\lambda^+=|\boldsymbol{\lambda}_\perp|=0}\,, \tag{1.8}$$

where P^μ and S^μ are the hadron momentum and polarisation four-vectors. Gauge invariance of the QCD operator $\bar{\psi}_q(0)\mathcal{W}[0,\lambda]\psi_q(\lambda)$ is ensured by the Wilson line $\mathcal{W}[0,\lambda]$, a path–ordered exponential of the gluon field

$$\mathcal{W}[\gamma] \;=\; P\,\exp\left[-ig\int_\gamma dx^\mu A^c_\mu(x)T^c\right], \tag{1.9}$$

which connects the quark fields along a path γ appropriate to the process and factorisation scheme. Quark distribution functions are essentially traces of the correlator in Eq. (1.8),

$$\Phi^{q\,[\Gamma]}(x) \;\equiv \frac{1}{2}\,\mathrm{Tr}[\Phi^q\,\Gamma]\,, \tag{1.10}$$

where Γ is a specific Dirac structure. At leading twist, only three Dirac structures contribute,

$$\Gamma \in \left\{\gamma^+,\,\gamma^+\gamma_5,\,i\sigma^{\alpha+}\gamma_5\right\}, \tag{1.11}$$

with

$$\gamma^+ \equiv \frac{\gamma^0+\gamma^3}{\sqrt{2}}\,, \qquad \sigma^{\alpha\beta} = \frac{i}{2}[\gamma^\alpha,\gamma^\beta]\,, \tag{1.12}$$

yielding, respectively, to the unpolarised (used in Eq. (1.5)), helicity and transversity quark PDFs:

$$\Phi^{q[\gamma^+]}(x) \;=\; f_1^q(x)\,, \qquad \Phi^{q[\gamma^+\gamma_5]}(x) \;=\; S_L\,g_1^q(x)\,, \qquad \Phi^{q[i\sigma^{j+}]}(x) \;=\; S_\perp^j\,h_1^q(x)\,, \tag{1.13}$$

where the transverse index is $j = 1,2$, the nucleon polarisation is described by $S^\mu = (0,\boldsymbol{S}_\perp,S_L)$ in the nucleon rest frame. As a result of charge conjugation symmetry, the corresponding antiquark distributions are given by

$$f_1^{\bar{q}}(x) = -f_1^q(-x), \quad g_1^{\bar{q}}(x) = g_1^q(-x), \quad h_1^{\bar{q}}(x) = -h_1^q(-x)\,. \tag{1.14}$$

The chiral properties follow from the decomposition $\psi_{R,L} = \frac{1}{2}(1\pm\gamma_5)\psi$:

$$\begin{gathered}\bar{\psi}\gamma^+\psi \;=\; \bar{\psi}_R\gamma^+\psi_R \,+\, \bar{\psi}_L\gamma^+\psi_L, \quad \bar{\psi}\gamma^+\gamma_5\psi \;=\; \bar{\psi}_R\gamma^+\gamma_5\psi_R \,-\, \bar{\psi}_L\gamma^+\gamma_5\psi_L, \\ \bar{\psi}i\sigma^{j+}\gamma_5\psi \;=\bar{\psi}_L i\sigma^{j+}\gamma_5\psi_R \,-\, \bar{\psi}_R i\sigma^{j+}\gamma_5\psi_L\,,\end{gathered} \tag{1.15}$$

so f_1 and g_1 are chiral–even, whereas h_1 is chiral–odd. In inclusive DIS chiral–odd contributions are suppressed by m_q/Q, but they can be accessed in other processes such as semi–inclusive DIS (SIDIS) and Drell–Yan.

For gluons in a spin–$\frac{1}{2}$ hadron, only two twist–2 collinear distributions exist: the unpolarised density $f_1^g(x)$ and the helicity distribution $g_{1L}^g(x)$. A collinear gluon transversity distribution for the nucleon is forbidden at twist–2 by angular–momentum conservation: a spin–1/2 nucleon cannot provide the required two–unit spin flip.

An analogous classification applies to collinear fragmentation functions. For spinless hadrons in the final state (e.g., pions) only the unpolarised FF $D_1^{h/q}(z)$ appears at leading

twist, whereas for polarised hadrons (e.g., Λ hyperons) one has the helicity $G_1^{h/q}(z)$ and the transversity $H_1^{h/q}(z)$, describing longitudinal and transverse spin transfer, respectively. Here z (also denoted as z_h) is the light-cone momentum fraction carried by the observed hadron relative to the fragmenting parton.

We can obtain an operator definition of the collinear gluon PDFs and fragmentation functions as in Eq. (1.8), suitably modifying the QCD operators. These collinear PDFs and FFs, evolved with DGLAP equations, underpin the successful description of a wide class of observables.

Now we must ask when collinear QCD is sufficient to describe physical processes, and when it is not. When the measured observable is inclusive over transverse momentum (e.g. DIS structure functions) or probes kinematics with $q_T \sim Q$ (hard recoil generated by perturbative radiation), fixed-order collinear factorization provides an accurate description. In such cases, the intrinsic transverse motion of partons can be integrated out without compromising predictability.

There exists, however, a broad and phenomenologically crucial class of observables for which the above conditions are not met. Whenever we measure a transverse-momentum spectrum much smaller than the hard scale, $q_T \ll Q$, fixed-order predictions develop large logarithms $\ln(Q/q_T)$ and even unphysical $1/q_T^2$ singular behaviour order by order. This signals the need for an all-orders resummation of $\ln(Q/q_T)$. In this two-scale regime, the appropriate framework is *TMD factorization*, in which the cross section factorizes into (i) a hard, perturbatively calculable coefficient, (ii) universal TMD PDFs/FFs that depend on $(x, k_\perp)$—up to a process-dependent gauge-link structure—and (iii) a soft factor (which in modern definitions is absorbed into the TMDs). The associated evolution involves both renormalization-scale and rapidity (Collins–Soper) evolution, enabling controlled predictions from $q_T \to 0$ with matching to fixed order at larger q_T.

Concrete phenomenological triggers for TMDs. Typical situations where collinear factorization alone becomes insufficient include:

- *Small-q_T spectra for colourless final states* (DY,W/Z,Higgs): when $q_T \ll Q$, large $\ln(Q/q_T)$ towers require all-orders resummation and $q_T \to 0$ region is described by TMD factorization.

- *Azimuthal and spin asymmetries* in SIDIS and DY (e.g. Sivers/Collins effects): these observables are intrinsically sensitive to spin-$k_\perp$ correlations and cannot be captured by collinear PDFs/FFs alone.

- *Back–to–back hadron pairs* in e^+e^-: the small transverse-momentum imbalance directly probes TMD FFs.

1.1 Quark and Gluon TMDs

The theoretical framework of TMD factorization is inherently more involved than its collinear counterpart. In collinear calculation, crucial cancellations arise after integrating over the partonic transverse momentum. In the TMD context, those integrals are not performed: the dependence on $k_\perp$ is retained explicitly, so contributions that would cancel upon integration must be consistently accounted for. The Collins, Soper and Sterman (CSS) formalism provides a systematic framework to handle these complications of transverse-momentum dependence. Classic applications include the Drell–Yan (DY) process, semi-inclusive deep-inelastic scattering (SIDIS), and back-to-back hadron production in electron–positron annihilation at small transverse momentum, where CSS TMD factorization applies and constrains the functional form of TMDs. For comprehensive treatments of TMD definitions and TMD factorization, see, e.g., Ref. [32].

Transverse tensor conventions

We work with the Minkowski metric $g^{\mu\nu} = \mathrm{diag}(1,-1,-1,-1)$ and the antisymmetric tensor $\epsilon^{\mu\nu\rho\sigma}$, with $\epsilon^{0123} = +1$. We introduce two light-like reference vectors n^μ and $\bar{n}^\mu$, which can be aligned, for instance, with the $\pm z$ directions,

$$n^\mu = \frac{1}{\sqrt{2}}(1,0,0,1), \qquad \bar{n}^\mu = \frac{1}{\sqrt{2}}(1,0,0,-1), \tag{1.16}$$

so that $n^2 = \bar{n}^2 = 0$ and $n\cdot\bar{n} = 1$. The transverse projector and antisymmetric tensor are

$$g_\perp^{\mu\nu} = g^{\mu\nu} - \left(n^\mu\bar{n}^\nu + n^\nu\bar{n}^\mu\right), \qquad \epsilon_\perp^{\mu\nu} = \epsilon^{\mu\nu\rho\sigma}n_\rho\bar{n}_\sigma, \tag{1.17}$$

which satisfy $g_\perp^{\mu\nu}n_\nu = g_\perp^{\mu\nu}\bar{n}_\nu = \epsilon_\perp^{\mu\nu}n_\nu = \epsilon_\perp^{\mu\nu}\bar{n}_\nu = 0$. With the above choice of n and $\bar{n}$, the transverse plane coincides with the xy–plane, and the components of $g_\perp^{\mu\nu}$ and $\epsilon_\perp^{\mu\nu}$ are

$$g_\perp^{11} = g_\perp^{22} = -1, \quad g_\perp^{ij} = 0 \text{ otherwise (for } i,j = 1,2), \quad \text{and} \quad \epsilon_\perp^{12} = +1,\ \epsilon_\perp^{21} = -1, \tag{1.18}$$

all other components being zero. It is then convenient to identify $\delta_\perp^{ij} \equiv -\,g_\perp^{ij} = \mathrm{diag}(1,1)$.

Leading Quark TMD PDFs

For a spin-$\frac{1}{2}$ hadron with momentum P and covariant spin vector S, the unsubtracted quark TMD distributions can be obtained by taking the trace over the Dirac indices of the product of the correlator Φ^q, multiplied by the Dirac structures Γ. Namely,

$$\Phi^{q\,[\Gamma]}(x,\boldsymbol{k}_\perp) = \int \frac{d(\lambda\cdot P)\,d^2\lambda_\perp}{(2\pi)^3} e^{i\,k\cdot\lambda}\,\langle P,S|\,\bar{\psi}_i(0)\,\mathcal{W}[0,\lambda]\,\frac{\Gamma}{2}\,\psi_j(\lambda)\,|P,S\rangle\,|_{\mathrm{LF}}\,, \tag{1.19}$$

where the nonlocality is restricted to the light-front LF ($\lambda\cdot\overline{n} \equiv \lambda^+ = 0$). The path-ordered gauge link $\mathcal{W}[0,\lambda]$ is the staple-like Wilson line; its direction (future- or past-pointing) encodes the colour flow of the process and is the origin of the process dependence of T-odd TMDs, Ref. [32]. As in the PDF case, the Γ matrices of (1.11) are associated with unpolarised, longitudinally and transversely polarised quarks and antiquarks, respectively. However, due to the presence of $\boldsymbol{k}_\perp$, eight leading power TMDs exist, compared to the three leading twist collinear PDFs. The projections of the correlator onto the Dirac structures are explicitly given by

$$\begin{aligned}
\Phi_U^{q[\gamma^+]}(x,\boldsymbol{k}_\perp,\mu,\zeta) &= f_1(x,k_\perp) - \frac{\epsilon_\perp^{\rho\sigma}\, k_{\perp\rho}\, S_{\perp\sigma}}{M}\, f_{1T}^\perp(x,k_\perp),\\
\Phi_L^{q[\gamma^+\gamma^5]}(x,\boldsymbol{k}_\perp,\mu,\zeta) &= S_L\, g_1(x,k_\perp) + \frac{\boldsymbol{k}_\perp\cdot\boldsymbol{S}_\perp}{M}\, g_{1T}^\perp(x,k_\perp),\\
\Phi_T^{q[i\sigma^{\alpha+}\gamma^5]}(x,\boldsymbol{k}_\perp,\mu,\zeta) &= S_\perp^\alpha\, h_1(x,k_\perp) + \frac{S_L\, k_\perp^\alpha}{M}\, h_{1L}^\perp(x,k_\perp)\\
&\quad + \frac{\left(k_\perp^\alpha k_\perp^\rho - \frac{1}{2}\delta_\perp^{\alpha\rho} k_\perp^2\right) S_{\perp\rho}}{M^2}\, h_{1T}^\perp(x,k_\perp) - \frac{\epsilon_\perp^{\alpha\rho}\, k_{\perp\rho}}{M}\, h_1^\perp(x,k_\perp)\,.
\end{aligned} \tag{1.20}$$

The expressions Eq. (1.20) define TMDs of antiquarks according to

$$\mathrm{TMD}^{\bar{q}}(x,k_\perp) = \pm\mathrm{TMD}^{q}(-x,k_\perp) \quad \text{with} \quad \begin{cases} + & \text{for } g_1,\ f_{1T}^\perp,\ h_{1L}^\perp,\ h_1^\perp,\\ - & \text{for } f_1,\ h_1,\ g_{1T}^\perp,\ h_{1T}^\perp. \end{cases} \tag{1.21}$$

The partonic interpretation of the leading quark TMDs is as follows; three of them have collinear counterparts:

- $f_1(x,k_\perp)$ describes the distribution of unpolarised quarks inside an unpolarised hadron, similar to the unpolarised collinear distribution $f_1(x)$.
- $g_1(x,k_\perp)$ is the helicity distribution, that is the distribution of longitudinally polarised quarks inside a longitudinally polarised hadron, similar to the collinear helicity distribution $g_1(x)$.
- $h_1(x,k_\perp)$ is the transversity distribution, that is the distribution of transversely polarised quarks inside a transversely polarised hadron, similar to the collinear transversity distribution $h_1(x)$.

The remaining distributions arise only when measuring transverse momenta and have no collinear counterparts:

- $f_{1T}^\perp(x,k_\perp)$ is the Sivers function [35], which describes the distribution of unpolarised quarks inside a transversely polarised hadron. Since it is T-odd, it was originally believed to vanish due to symmetry arguments [36]. It was later clarified that it is non-vanishing when the Wilson lines are properly accounted for in the definitions of the unsubtracted TMD PDF and the soft function [37–39].

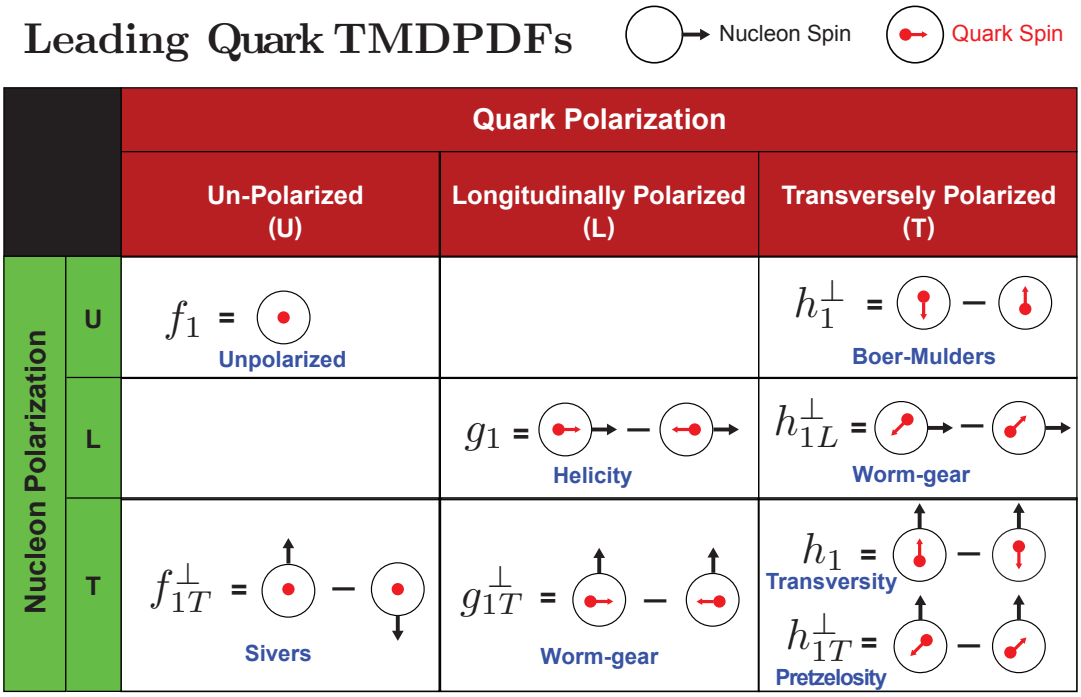

Figure 1.2: Leading power quark TMD parton distribution function for a spin-$\frac{1}{2}$ (or for an unpolarised or spin 0) hadron.

- $g_{1T}^\perp(x, k_\perp)$ is the distribution of longitudinally polarised quarks in a transversely polarised hadron, and vice versa, $h_{1L}^\perp(x, k_\perp)$ describes transversely polarised quarks in a longitudinally polarised hadron [40]. They are referred to in the literature as "worm-gear" T and L functions, or Kotzinian–Mulders functions [41, 42].

- $h_1^\perp(x, k_\perp)$ is the Boer–Mulders function [43], which describes a transversely polarised quark in an unpolarised hadron. Like the Sivers function $f_{1T}^\perp(x, k_\perp)$, it is time-reversal odd.

- $h_{1T}^\perp(x, k_\perp)$ is the pretzelosity function, which contributes to the distribution of a transversely polarised quark in a transversely polarised hadron [44], in addition to the transversity $h_1(x, k_\perp)$. This is due to the monopole structure (proportional to $\delta_\perp$ and associated with h_1) and the quadrupole one (proportional to $\left(k_\perp^\alpha k_\perp^\rho - \frac{1}{2}\delta_\perp^{\alpha\rho} k_\perp^2\right)$ and associated with $h_{1T}^\perp$) in the transverse plane.

Because of parity conservation in QCD, the empty fields in Fig. 1.2 would correspond to distributions of unpolarised (longitudinally polarised) quarks inside a longitudinally polarised (unpolarised) hadron that are forbidden.

Leading Gluon TMD PDF

In the same way, it is possible to define a total of eight leading power gluon TMDs. The gluon correlator is defined as

$$\Phi^{\alpha\beta}(x, \boldsymbol{k}_\perp) = \int \frac{d(\lambda\cdot P)\, d^2\lambda_\perp}{(2\pi)^3} e^{i\,k\cdot\lambda} \langle P,S|\, F^{n\alpha}(0)\, \mathscr{W}[0,\lambda]\; F^{n\beta}(\lambda)\, |P,S\rangle\, |_{\rm LF}\,, \tag{1.22}$$

where, compared to the quark correlator in Eq. (1.8), the quark fields have been replaced by the field strength tensor $F_{\mu\nu}(\lambda) \equiv F^a_{\mu\nu}(\lambda)T^a$, related to the potential by $F_{\mu\nu} = \partial_\mu A_\nu - \partial_\nu A_\mu - ig[A_\mu, A_\nu]$; the gauge link $\mathscr{W}$ is the staple-like Wilson line in the adjoint representation. Due to the tensor structure of the gluon field strength tensor, the gluon TMD correlator carries a tensor structure as well. In addition, α and β have to be transverse indices, which is kept implicit in Eq. (1.22).

At leading power the spin-decomposition of the correlator for a spin-$\frac{1}{2}$ hadron is

$$\begin{aligned} x\Phi^{\alpha\beta}(x, \boldsymbol{k}_\perp, \mu, \zeta) = \frac{1}{2}\Bigg[&- g_\perp^{\alpha\beta}\, f_1^g(x,k_\perp) + \frac{k_\perp^2}{M^2}\left(\frac{g_\perp^{\alpha\beta}}{2} + \frac{k_\perp^\alpha k_\perp^\beta}{k_\perp^2}\right) h_1^{\perp g}(x,k_\perp)\Bigg] \\ &+ \frac{S_L}{2}\Bigg[- i\,\epsilon_\perp^{\alpha\beta}\, g_{1L}^g(x,k_\perp) - \frac{k_\rho\, \epsilon_\perp^{\rho\{\alpha} k_\perp^{\beta\}}}{2M^2}\, h_{1L}^{\perp g}(x,k_\perp)\Bigg] \\ &+ \frac{1}{2}\Bigg\{ g_\perp^{\alpha\beta}\, \frac{k_{\perp\rho} S_{\perp\sigma}\, \epsilon_\perp^{\rho\sigma}}{M}\, f_{1T}^{\perp g}(x,k_\perp) - i\,\epsilon_\perp^{\alpha\beta}\, \frac{\boldsymbol{k}_\perp\cdot\boldsymbol{S}_\perp}{M}\, g_{1T}^g(x,k_\perp) \\ &\quad + \frac{k_{\perp\rho}\, \epsilon_\perp^{\rho\{\alpha} k_\perp^{\beta\}}}{2M^2}\, \frac{\boldsymbol{k}_\perp\cdot\boldsymbol{S}_\perp}{M}\, h_{1T}^{\perp g}(x,k_\perp) - \frac{k_{\perp\rho}\, \epsilon_\perp^{\rho\{\alpha} S_\perp^{\beta\}}}{4M}\, h_{1T}^g(x,k_\perp)\Bigg\}\,, \end{aligned} \tag{1.23}$$

where $a^{\{\alpha} b^{\beta\}} = a^\alpha b^\beta + a^\beta b^\alpha$. Because the gluon is spin 1, the allowed tensor structure differs from the quark case and includes linear-polarization terms (helicity-2 structures), e.g. $h_1^{\perp g}$, in addition to helicity-0 and helicity-1 structures. A compact classification is given in Fig. 1.3. A useful helicity interpretation follows from the ±1 gluon helicity basis $\uparrow = (\hat{e}_1 + i\hat{e}_2)/\sqrt{2}$ and $\downarrow = (\hat{e}_1 - i\hat{e}_2)/\sqrt{2}$.

- The symmetric helicity 0 combination $\uparrow\downarrow + \downarrow\uparrow$ gives the unpolarised configurations that appear for the unpolarised and transversely polarised hadrons, with distribution f_1^g and f_{1T}^g.

- The antisymmetric helicity 0 combination $\uparrow\downarrow - \downarrow\uparrow$ yields the helicity distributions g_{1L}^g and g_{1T}^g for the longitudinally and transversely polarised hadrons, respectively.

- The helicity 2 combinations $\uparrow\uparrow + \downarrow\downarrow$ and $\uparrow\uparrow - \downarrow\downarrow$ are given in Eq. (1.23) by the $h_1^{\perp g}$, $h_{1L}^{\perp g}$, h_{1T}^g and $h_{1T}^{\perp g}$ terms for all the possible spin-$\frac{1}{2}$ hadron polarization.

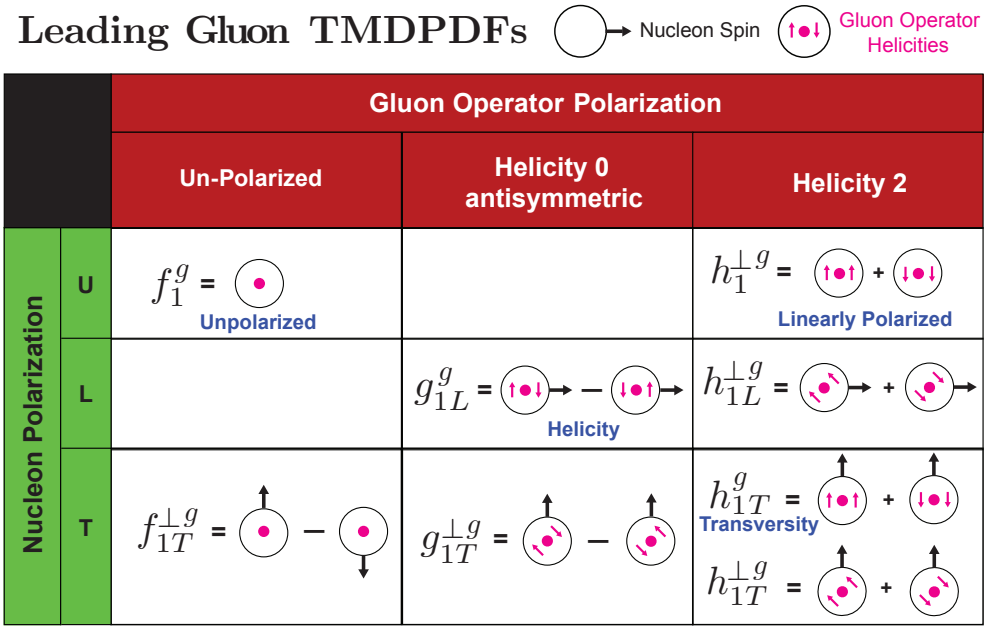

Figure 1.3: Leading power gluon TMD parton distribution functions for a spin-$\frac{1}{2}$ (or for an unpolarised or spin 0) hadron.

Leading Quark TMD FFs

The projections of the quark TMD fragmentation correlator onto specific Dirac structures Γ, for a quark fragmenting into a detected hadron (with mass M_h and spin vector S), can be expressed as

$$\begin{aligned}\Delta^{[\Gamma]}(z,\boldsymbol{p}_\perp) =& \frac{1}{2z}\,\mathrm{Tr}\sum_X \int \frac{d(\lambda\cdot P_h)d^2\lambda_\perp}{(2\pi)^3}\, e^{i\lambda\cdot k}\,\Gamma \\ &\times\Big\langle 0\Big|(\mathcal{W}\,\psi_i)(\lambda)\Big|h,X\Big\rangle\Big\langle h,X\Big|(\bar\psi_j\,\mathcal{W})(0)\Big|0\Big\rangle\,,\end{aligned} \tag{1.24}$$

where z is the hadron's light-cone momentum fraction, $p_\perp$ is the hadron transverse momentum with respect to the fragmenting quark direction, and $\mathcal{W}$ denotes the appropriate Wilson lines. The projections onto the leading Dirac structures (as in the PDF case) yield the eight leading power quark TMD FFs:

$$\begin{aligned}\Delta_U^{[\gamma^+]}(z,p_\perp;\mu,\zeta) &= D_1(z,p_\perp) + \frac{1}{z}\,\frac{\epsilon_\perp^{\rho\sigma}\,p_{\perp\rho}S_{\perp\sigma}}{M_h}\,D_{1T}^\perp(z,p_\perp)\,,\\
\Delta_L^{[\gamma^+\gamma^5]}(z,p_\perp;\mu,\zeta) &= S_L\,G_1(z,p_\perp) + \frac{1}{z}\,\frac{p_\perp\cdot S_\perp}{M_h}\,G_{1T}^\perp(z,p_\perp)\,,\\
\Delta_T^{[i\sigma^{\alpha+}\gamma^5]}(z,p_\perp;\mu,\zeta) &= S_\perp^\alpha\,H_1(z,p_\perp) - \frac{1}{z}\,\frac{S_L\,p_\perp^\alpha}{M_h}\,H_{1L}^\perp(z,p_\perp)\\
&\quad - \frac{1}{z^2}\,\frac{\left(p_\perp^\alpha p_\perp^\rho - \frac{1}{2}\delta_\perp^{\alpha\rho}p_\perp^2\right)S_{\perp\rho}}{M_n^2}\,H_{1T}^\perp(z,p_\perp) + \frac{1}{z}\,\frac{\epsilon_\perp^{\alpha\rho}p_{T\rho}}{M_h}\,H_1^\perp(z,p_\perp)\,.\end{aligned} \tag{1.25}$$

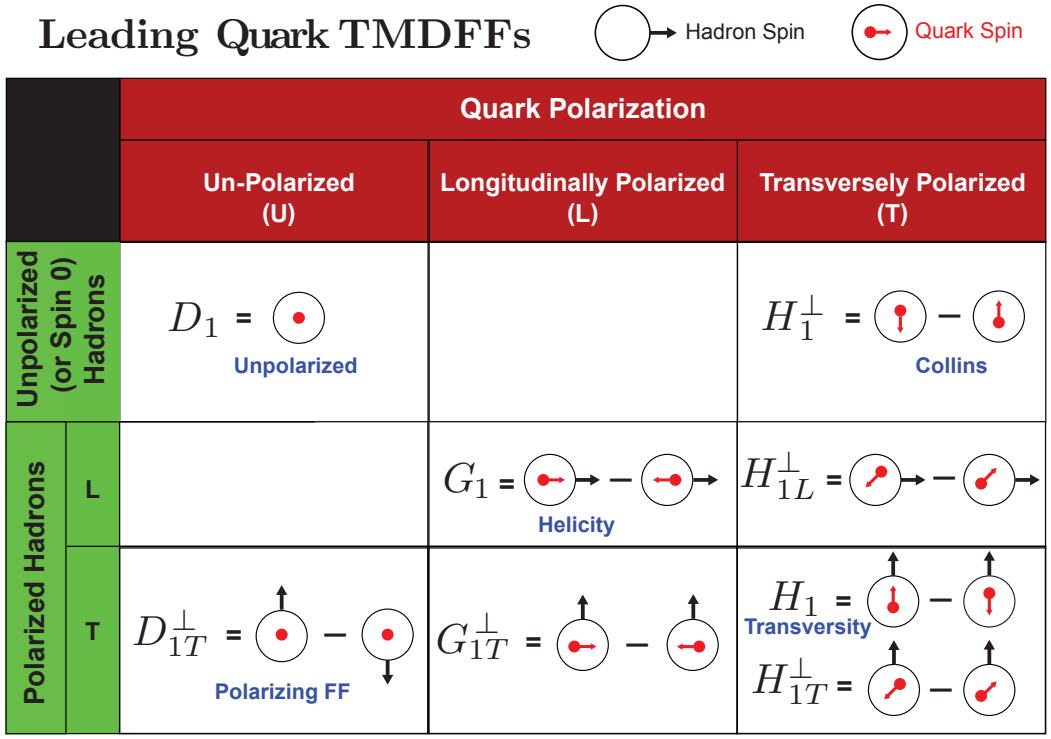

Figure 1.4: Leading power quark TMD fragmentation functions for a spin-$\frac{1}{2}$ (or for an unpolarised or spin 0) hadron.

This decomposition is analogous to the PDF case in Eq. (1.20) and has a similar interpretation in terms of quark and hadron polarizations, as summarized in Fig. 1.4. Here we again encounter two T-odd functions, namely the polarizing FF $D_{1T}^\perp$ and the Collins function $H_1^\perp$.

Helicity formalism. It is often convenient to describe parton PDFs and FFs in the helicity basis, which makes the role of the parton and hadron polarizations explicit.
As an example, in the fragmentation sector, following the approach adopted in Ref. [23, 45], we can define

$$\widehat{D}_{\lambda_c,\lambda_c'}^{\lambda_h,\lambda_h'}(z,\boldsymbol{p}_\perp) = \sum_{X,\lambda_X} \widehat{\mathcal{D}}_{\lambda_h,\lambda_X;\lambda_c}(z,\boldsymbol{p}_\perp)\,\widehat{\mathcal{D}}^*_{\lambda_h',\lambda_X;\lambda_c'}(z,\boldsymbol{p}_\perp)\,. \tag{1.26}$$

where $\widehat{\mathcal{D}}_{\lambda_c,\lambda_c'}^{\lambda_h,\lambda_h'}$ is the fragmentation amplitude describing the process $c \to h + X$ in which the parton c from the elementary scattering $ab \to cd$ generates the detected final hadron h.
If we define ϕ_h as the azimuthal angle of the hadron h in the helicity reference frame of parton c, we can rewrite the fragmentation function as

$$\widehat{\mathcal{D}}_{\lambda_h,\lambda_X\,;\lambda_c}(z,\boldsymbol{p}_\perp) = \mathcal{D}_{\lambda_h,\lambda_X\,;\lambda_c}(z,p_\perp)\;\mathrm{e}^{\,i\,\lambda_c\,\phi_h}\,, \tag{1.27}$$

where $p_\perp = |\boldsymbol{p}_\perp|$, so that

$$\widehat{D}^{\lambda_h,\lambda'_h}_{\lambda_c,\lambda'_c}(z,p_\perp) = D^{\lambda_h,\lambda'_h}_{\lambda_c,\lambda'_c}(z,p_\perp)\,\exp\Big[i(\lambda_c-\lambda'_c)\,\phi_h\Big]\,, \tag{1.28}$$

where $D^{\lambda_h,\lambda'_h}_{\lambda_c,\lambda'_c}(z,p_\perp)$ is the azimuthal-independent modulus of $\widehat{D}^{\lambda_h,\lambda'_h}_{\lambda_c,\lambda'_c}(z,p_\perp)$, which can be obtained by replacing $\widehat{\mathcal{D}} \to \mathcal{D}$ in Eq. (1.26).
From Eq.(1.26) we can get the following relation, valid for both quarks and gluons,

$$\Big(\widehat{D}^{\lambda'_h,\lambda_h}_{\lambda'_c,\lambda_c}\Big)^* = \widehat{D}^{\lambda_h,\lambda'_h}_{\lambda_c,\lambda'_c}\,. \tag{1.29}$$

which, in particular, gives

$$\begin{aligned}
\Big(\widehat{D}^{+-}_{+-}\Big)^* &= \widehat{D}^{-+}_{-+}, \qquad & \Big(\widehat{D}^{+-}_{-+}\Big)^* &= \widehat{D}^{-+}_{+-},\\
\Big(D^{++}_{+-}\Big)^* &= D^{++}_{-+}, \qquad & \Big(D^{+-}_{++}\Big)^* &= D^{+-}_{++}.
\end{aligned} \tag{1.30}$$

Concerning the parity properties of the $\mathcal{D}$ helicity amplitudes, they satisfy the standard parity relation,

$$\mathcal{D}_{-\lambda_h,\,-\lambda_X\,;\,-\lambda_c} = \eta\,\mathrm{e}^{\,i\pi\,(s_c-S_h-S_X)}\,\mathrm{e}^{\,i\pi\,(\lambda_c-\lambda_h+\lambda_X)}\,\mathcal{D}_{\lambda_h,\,\lambda_X\,;\,\lambda_c}\,, \tag{1.31}$$

where η is the intrinsic parity factor such that $\eta^2 = 1$. Consequently,

$$D^{-\lambda_h,\,-\lambda'_h}_{-\lambda_c,\,-\lambda'_c}(z,p_\perp) = \exp\Big[i\pi\Big((\lambda_c-\lambda'_c)-(\lambda_h-\lambda'_h)\Big)\Big]\,D^{\lambda_h,\,\lambda'_h}_{\lambda_c,\,\lambda'_c}(z,p_\perp)\,. \tag{1.32}$$

Notice that the additional phase factor leads in some cases to different behaviours between the quark ($\lambda_c = \pm 1/2$) and gluon ($\lambda_c = \pm 1$) cases. Exploiting the parity relation, the corresponding quark (upper signs) and gluon (lower signs) fragmentation functions obey the relations

$$\begin{aligned}
D^{++}_{++} &= D^{--}_{--}, \qquad & D^{++}_{--} &= D^{--}_{++},\\
D^{++}_{+-} &= \mp\, D^{--}_{-+}, \qquad & D^{++}_{-+} &= \mp\, D^{--}_{+-},\\
D^{+-}_{++} &= -\,D^{-+}_{--}, \qquad & D^{-+}_{++} &= -\,D^{+-}_{--},\\
D^{+-}_{+-} &= \pm\, D^{-+}_{-+}, \qquad & D^{-+}_{-+} &= \pm\, D^{+-}_{+-}.
\end{aligned} \tag{1.33}$$

These constraints leave us with only six independent amplitudes,

$$D^{++}_{++},\; D^{++}_{--},\; D^{++}_{+-},\; D^{+-}_{++},\; D^{+-}_{+-},\; D^{+-}_{-+}. \tag{1.34}$$

Finally, suitable linear combinations of these (in principle) complex quantities yield eight independent real functions; in fact, contracting them with the helicity density matrices of the quark and the hadron provides the complete set of leading quark TMD fragmentation

functions. The final expressions are reported below; for further details, see Ref. [23].

$$
\begin{aligned}
\widehat{D}_{h/q}(z,\boldsymbol{p}_\perp) &= D_{h/q} \;=\; (D^{++}_{++} + D^{++}_{--}) \\
\Delta\widehat{D}_{h/q,s_T}(z,\boldsymbol{p}_\perp) &= \Delta^N D_{h/q^\uparrow}\,\sin(\phi_{s_q}-\phi_h) \;=\; 4\,\mathrm{Im}\,D^{++}_{+-}\,\sin(\phi_{s_q}-\phi_h) \\
\Delta\widehat{D}^{h/q}_{S_Z/s_L}(z,\boldsymbol{p}_\perp) &= \Delta D^{h/q}_{S_Z/s_L} \;=\; (D^{++}_{++} - D^{++}_{--}) \\
\Delta\widehat{D}^{h/q}_{S_Z/s_T}(z,\boldsymbol{p}_\perp) &= \Delta D^{h/q}_{S_Z/s_T}\,\cos(\phi_{s_q}-\phi_h) \;=\; 2\,\mathrm{Re}\,D^{++}_{+-}\,\cos(\phi_{s_q}-\phi_h) \\
\Delta\widehat{D}^{h/q}_{S_X/s_L}(z,\boldsymbol{p}_\perp) &= \Delta D^{h/q}_{S_X/s_L} \;=\; 2\,\mathrm{Re}D^{+-}_{++} \\
\Delta\widehat{D}^{h/q}_{S_X/s_T}(z,\boldsymbol{p}_\perp) &= \Delta D^{h/q}_{S_X/s_T}\,\cos(\phi_{s_q}-\phi_h) \;=\; (D^{+-}_{+-} + D^{+-}_{-+})\,\cos(\phi_{s_q}-\phi_h) \\
\Delta\widehat{D}^{h}_{S_Y/q}(z,\boldsymbol{p}_\perp) &= \Delta D^{h}_{S_Y/q} \;=\; \Delta^N D_{h^\uparrow/q} \;=\; -\,2\,\mathrm{Im}\,D^{++}_{+-} \\
\Delta^-\widehat{D}^{h/q}_{S_Y/s_T}(z,\boldsymbol{p}_\perp) &= -\,\Delta D^{h/q}_{S_Y/s_T}\,\sin(\phi_{s_q}-\phi_h) \;=\; (D^{+-}_{+-} - D^{+-}_{-+})\,\sin(\phi_{s_q}-\phi_h)
\end{aligned}
\tag{1.35}
$$

where S_J $(J = X, Y, Z)$ denotes the components of the hadron spin along the axes of its helicity frame, and s_T (s_L) denotes the transverse (longitudinal) component of the quark spin in its own helicity frame.
To conclude, we present the correspondence with the Amsterdam notation adopted in the previous subsection (see Eq. 1.25 and Fig. 1.4):

$$
\begin{aligned}
D_{h/q} = D^{++}_{++} + D^{++}_{--} &= D_1(z,p_\perp) \\
\Delta D^{h}_{S_Y/q} = \Delta^N D_{h^\uparrow/q} = -2\;\mathrm{Im}\,D^{+-}_{++} &= \frac{p_\perp}{zM_h}\,D^\perp_{1T}(z,p_\perp) \\
\Delta D^{h/q}_{S_Z/s_L} = D^{++}_{++} - D^{++}_{--} &= G_{1L}(z,p_\perp) \\
\Delta D^{h/q}_{S_X/s_L} = 2\;\mathrm{Re}\,D^{++}_{+-} &= -\,\frac{p_\perp}{zM_h}\,G_{1T}(z,p_\perp) \\
\Delta D^{h/q}_{S_Z/s_T} = 2\;\mathrm{Re}\,D^{+-}_{++} &= -\,\frac{p_\perp}{zM_h}\,H^\perp_{1L}(z,p_\perp) \\
\Delta^N D_{h/q^\uparrow} = 4\;\mathrm{Im}\,D^{++}_{+-} &= \frac{2p_\perp}{zM_h}\,H^\perp_1(z,p_\perp) \\
\frac{1}{2}\Big[\Delta D_{S_X/s_T} + \Delta^- D_{S_Y/s_T}\Big] = D^{+-}_{+-} &= H_1(z,p_\perp) \\
\frac{1}{2}\Big[\Delta D_{S_X/s_T} - \Delta^- D_{S_Y/s_T}\Big] = D^{+-}_{-+} &= \frac{p_\perp^2}{2z^2M_h^2}\,H^\perp_{1T}(z,p_\perp)
\end{aligned}
\tag{1.36}
$$

1.2 TMD factorization in Drell-Yan processes

To introduce TMDs and the basic ideas behind TMD factorization, we consider the factorization theorem for the unpolarised Drell-Yan process, $pp \to \gamma^*/Z \to \ell^+\ell^-$.

Kinematics.

In an inclusive Drell-Yan process,

$$
h_1(P_1) \,+\, h_2(P_2) \to \gamma^*/Z(q) \,+\, X \to \ell^+(l) \,+\, \ell^-(l') \,+\, X\,, \tag{1.37}
$$

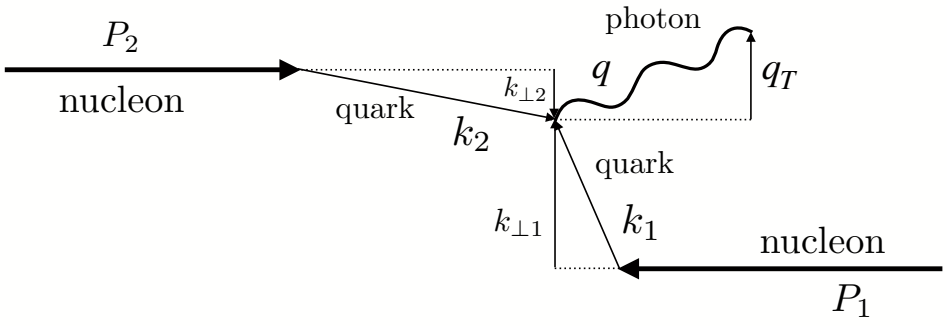

Figure 1.5: Kinematics relevant to the Drell–Yan process. In the hadronic center-of-mass frame the two incoming nucleons travel along the (z) direction with four-momenta P_1^μ and P_2^μ. A quark with four-momentum k_1^μ and transverse momentum $\boldsymbol{k}_{\perp 1}$ annihilates with a (anti)quark of four-momentum k_2^μ and transverse momentum $\boldsymbol{k}_{\perp 2}$. The hard scattering produces a time-like gauge boson, a virtual photon or Z, with four-momentum q^μ, and transverse-momentum conservation implies $\boldsymbol{q}_T = \boldsymbol{k}_{\perp 1} + \boldsymbol{k}_{\perp 2}$ (up to power-suppressed recoil).

two hadrons with momenta P_1 and P_2 collide at a centre-of-mass energy squared $s = (P_1 + P_2)^2$ producing a neutral vector boson with momentum q and invariant mass $Q = \sqrt{q^2} = \sqrt{s}$. The boson subsequently decays into a lepton anti-lepton pair. In the hadronic centre-of-mass frame, we define the magnitude of the lepton-pair transverse momentum and its rapidity as

$$q_T = \sqrt{q_x^2 + q_y^2}, \quad y = \frac{1}{2}\ln\left(\frac{q_0 + q_z}{q_0 - q_z}\right) \tag{1.38}$$

with the z-axis aligned with the beam direction.

In the small-q_T regime ($q_T \ll Q$), the Drell-Yan cross section admits a TMD-factorized form [14]. In particular, the differential cross section can be written in terms of the unpolarised TMDs of the two hadrons as

$$\begin{aligned}\frac{\mathrm{d}\sigma}{\mathrm{d}Q\,\mathrm{d}y\,\mathrm{d}q_T} &= \frac{16\pi^2\alpha^2 q_T}{9Q^3} H(Q,\mu)\sum_q c_q(Q) \\ &\times \int \mathrm{d}^2\boldsymbol{k}_{\perp 1}\mathrm{d}^2\boldsymbol{k}_{\perp 2}\, x_1 f_1^q(x_1,\boldsymbol{k}_{\perp 1};\mu,\zeta_1)\, x_2 f_1^{\bar{q}}(x_2,\boldsymbol{k}_{\perp 2};\mu,\zeta_2)\delta^{(2)}(\boldsymbol{k}_{\perp 1} + \boldsymbol{k}_{\perp 2} - \boldsymbol{q}_T)\,,\end{aligned} \tag{1.39}$$

where α is the electromagnetic coupling and $H(Q,\mu)$ is the hard factor encoding the perturbative short-distance dynamics, depending on the hard scale Q and on the renormalization scale μ. The sum runs over the active quarks and anti-quarks, and c_q are the respective electroweak charges. In the second line of Eq. (1.39) the TMDs f_1^q and $f_1^{\bar{q}}$ appear in a convolution over the intrinsic transverse momenta of the annihilating partons from hadrons h_1 and h_2. The partonic light-cone momentum fractions are (neglecting

subleading corrections in $k_\perp/Q$)

$$x_{1,2} = \frac{Q}{\sqrt{s}} e^{\pm y} \tag{1.40}$$

and the delta function $\delta^{(2)}(\boldsymbol{k}_{\perp 1} + \boldsymbol{k}_{\perp 2} - \boldsymbol{q}_T)$ enforces transverse momentum conservation at parton level.

Since TMD distributions arise from a two-scale theoretical framework [17], they depend on two factorization scales. One is the usual renormalization scale μ associated with UV divergences; the other is the rapidity scale (also called Collins-Soper scale) ζ_i, which regulates the rapidity divergences. Both scales are essential and should be treated independently. A more detailed discussion of the renormalization of the TMDs, from their bare to the renormalised definition, is provided in [32]. As customary, μ may be chosen arbitrarily, while the rapidity scales for the two TMDs must satisfy the kinematic constraint $\zeta_1\zeta_2 = Q^4$, leading to hard factors that do not depend explicitly on these scales [16]. Our choice for these scales is discussed in Sec.1.3. It is convenient to rewrite Eq.(1.39) in b_T-space (the conjugate space to the transverse momenta $k_\perp$), in this way the convolution in transverse momenta simplifies into a product of functions. Thus, we introduce the Fourier transform of each TMD[2]:

$$\tilde{f}_1^q(x, b_T; \mu, \zeta) = \int d^2\boldsymbol{k}_\perp e^{i\boldsymbol{k}_\perp \cdot \boldsymbol{b}_T} f_1^q(x, \boldsymbol{k}_\perp; \mu, \zeta) \tag{1.41}$$

Using Eq. (1.41), the convolution in Eq. (1.39) becomes

$$\begin{aligned}
&\int d^2\boldsymbol{k}_{\perp 1} d^2\boldsymbol{k}_{\perp 2}\, x_1 f_1^q(x_1, \boldsymbol{k}_{\perp 1}; \mu, \zeta_1)\, x_2 f_1^{\bar{q}}(x_2, \boldsymbol{k}_{\perp 2}; \mu, \zeta_2)\, \delta^{(2)}(\boldsymbol{k}_{\perp 1} + \boldsymbol{k}_{\perp 2} - \boldsymbol{q}_T) \\
&= \int \frac{d^2\boldsymbol{b_T}}{(2\pi)^2} e^{i\boldsymbol{q}_T \cdot \boldsymbol{b}_T}\, x_1 \tilde{f}_1^q(x_1, b_T; \mu, \zeta_1)\, x_2 \tilde{f}_1^{\bar{q}}(x_2, b_T; \mu, \zeta_2) \\
&= \frac{1}{2\pi} \int_0^\infty db_T\, b_T\, J_0(q_T b_T)\, x_1 \tilde{f}_1^q(x_1, b_T; \mu, \zeta_1)\, x_2 \tilde{f}_1^{\bar{q}}(x_2, b_T; \mu, \zeta_2)
\end{aligned} \tag{1.42}$$

where J_0 is the Bessel function of the first kind of order zero, with integral representation[3]

$$J_0(x) = \frac{1}{2\pi} \int_0^{2\pi} d\theta e^{ix\cos\theta}\,. \tag{1.43}$$

Inserting Eq. (1.42) into the differential cross section, Eq. (1.39), yields

$$\begin{aligned}
\frac{d\sigma}{dQdyd\boldsymbol{q}_T} &= \frac{8\pi\alpha^2 q_T}{9Q^3} H(Q, \mu) \\
&\times \sum_q c_q(Q) \int_0^\infty db_T\, b_T\, J_0(q_T b_T)\, x_1 \tilde{f}_1^q(x_1, b_T; \mu, \zeta_1)\, x_2 \tilde{f}_1^{\bar{q}}(x_2, b_T; \mu, \zeta_2)\,.
\end{aligned} \tag{1.44}$$

[2]Henceforth, we refer to the b_T-dependent function $\tilde{f}_1$ as to "TMD", even though it is the Fourier transform of the momentum-space distribution f_1.

[3]The form with J_0 assumes azimuthal symmetry, i.e., $\tilde{f}_1$ depends only on $b_T = |b_T|$. When an explicit azimuthal dependence is present(e.g., in polarised observables), the angular integral instead projects onto higher-order Bessel functions J_n with $n > 0$.

1.3 Evolution and matching

In this section we summarize the main steps needed to solve, for TMDs, both the renormalisation-group equation (RGE) and the rapidity-evolution equation (also referred to as the Collins-Soper equation). Since the evolution structure is the same for TMD PDFs and FFs, and the solution of the equations only depends on whether we are evolving a quark or a gluon function, we continue to consider the DY example to show how the evolution and matching enter into the characterisation of TMDs in practice.

As already mentioned above in Eq. (1.39), the (μ, ζ) dependence of the TMDs $f_1^{q(\bar{q})}$ arises from removing ultraviolet and rapidity divergences in their operator definition[4]. The solution of the evolution equations allows us to express the distribution $\tilde{f}_1^{q(\bar{q})}$ at some final scales (μ, ζ) in terms of the same distribution at the initial scales (μ_0, ζ_0). This is achieved by computing the evolution kernel, $R[(\mu, \zeta) \leftarrow (\mu_0, \zeta_0)]$, also known as the Sudakov form factor. To evaluate the Sudakov form factor R, we start from the RGE and the CS equation:

$$\frac{\partial \ln \tilde{f}_1}{\partial \ln \mu} = \gamma(\mu, \zeta), \qquad \frac{\partial \ln \tilde{f}_1}{\partial \ln \sqrt{\zeta}} = K(\mu), \tag{1.45}$$

where γ is the anomalous dimension governing RG evolution in μ, and K is the anomalous dimension of the Collins-Soper evolution in $\sqrt{\zeta}$ [46]. In addition to the evolution equation in Eq. (1.45), the rapidity anomalous dimension K needs to be renormalised and thus it obeys its own RGE:

$$\frac{\partial K}{\partial \ln \mu} = -\gamma_K(\alpha_s(\mu))\,, \tag{1.46}$$

with γ_K known as the cusp anomalous dimension. Since the crossed double derivatives of $\tilde{f}_1$ must be equal, using Eqs. (1.45) and (1.46) we obtain

$$\frac{\partial \gamma}{\partial \ln \sqrt{\zeta}} = -\gamma_K(\alpha_s(\mu))\,. \tag{1.47}$$

Using the point $\zeta = \mu^2$ as a boundary condition, this integrates to

$$\gamma(\mu, \zeta) = \gamma_F(\alpha_s(\mu)) - \gamma_K(\alpha_s(\mu))\, \ln \frac{\sqrt{\zeta}}{\mu}\,, \tag{1.48}$$

where $\gamma_F(\alpha_S(\mu)) \equiv \gamma(\mu, \mu^2)$. If the TMD $\tilde{f}_1$ is known at the scale (μ_0, ζ_0), the solution to the evolution equation given in Eq. (1.45) reads

$$\tilde{f}_1(\mu, \zeta) = R[(\mu, \zeta) \leftarrow (\mu_0, \zeta_0)]\, \tilde{f}_1(\mu_0, \zeta_0), \tag{1.49}$$

with R, accounting for the perturbative evolution of $\tilde{f}_1$, defined as

$$R[(\mu, \zeta) \leftarrow (\mu_0, \zeta_0)] = \exp\left\{ K(\mu_0)\, \ln \frac{\sqrt{\zeta}}{\sqrt{\zeta_0}} + \int_{\mu_0}^{\mu} \frac{d\mu'}{\mu'} \left[\gamma_F\Big(\alpha_s(\mu')\Big) - \gamma_K\Big(\alpha_s(\mu')\Big)\, \ln \frac{\sqrt{\zeta}}{\mu'} \right] \right\}. \tag{1.50}$$

[4] In what follows we focus on the μ and ζ dependences; other arguments that are not essential for the discussion are temporarily suppressed to lighten the notation.

There are several equivalent implementations of Eq. (1.50). Here we follow the standard treatment of Ref. [16]. As the next step, we rewrite the exponent in terms of the perturbatively calculable ingredients.

At a non-perturbative transverse scale $q_T \sim b_T^{-1} \sim \Lambda_{QCD}$, TMDs are genuinely non-perturbative objects. However, phenomenology is also sensitive to the region $q_T \sim b_T^{-1} \gg \Lambda_{QCD}$. In this regime, more precisely at small b_T, $\tilde{f}_1$ can be matched onto the collinear PDF through an operator expansion; we can write the initial scale TMD PDFs at small values of b_T as [16]:

$$\tilde{f}_1^i(x, b_T; \mu_0, \zeta_0) = \sum_{j=g,q(\bar{q})} \int_x^1 \frac{dy}{y} C_{ij}(y; \mu_0, \zeta_0)\, f_j\left(\frac{x}{y}, \mu_0\right) \equiv [\, C \otimes f_1 \,](x, b_T; \mu_0, \zeta_0)\,, \quad (1.51)$$

where the sum runs over all the parton flavours and C_{ij} are perturbative matching kernels, also called matching coefficients. Thus, the only non-perturbative input in Eq. (1.51) is the collinear PDF f_j[5]. With this notation, the evolved TMD reads

$$\tilde{f}_1(x, b_T; \mu, \zeta) = R\left[b_T;\, (\mu, \zeta) \leftarrow (\mu_0, \zeta_0)\right] [\, C \otimes f_1 \,](x, b_T; \mu_0, \zeta_0). \quad (1.52)$$

Matching and evolution are affected by non-perturbative effects that become relevant at large b_T, which are handled phenomenologically. In the CSS approach, this is implemented by a multiplicative non-perturbative function f_{NP} (diagonal in flavour space) together with a prescription that smoothly damps the perturbative content at large b_T (b_* prescription), discussed below.

1.3.1 Perturbative part

For phenomenological applications, we must choose the values of both the initial and final scales (μ_0, ζ_0) and (μ, ζ). It turns out that in the $\overline{\text{MS}}$ renormalization scheme there exists a particular scale,

$$\mu_b(b_T) = \frac{2e^{-\gamma_E}}{b_T}, \quad (1.53)$$

with γ_E the Euler constant, that avoids large logarithms in the perturbative expansion of both the Collins-Soper kernel K and the matching coefficients C when they are evaluated at $\mu_0 = \sqrt{\zeta_0} = \mu_b$.

Once more, in order to avoid divergences, we choose the same final renormalization scale μ as the one used in the hard factor H in Eq. (1.44); indeed, μ has to be of order Q to avoid large logarithms in H, therefore we set $\mu = Q$. Variations around this choice can be propagated by solving RGE for the strong coupling constant α_S. As explained above, the rapidity scales $\zeta_{1,2}$ obey the constraint $\zeta_1\zeta_2 = Q^4$, therefore, a common and convenient choice is $\zeta_1 = \zeta_2 = Q^2$. However, we stress that any alternative choice satisfying that

[5]The symbol $\otimes$ denotes the Mellin convolution, the sum over the flavours is implied and the matching function C has to be regarded as a matrix in flavour space multiplying a column vector of collinear PDFs

constraint is equivalent at the level of the cross section; in fact, from Eq. (1.50) it can be seen that the evolution factors R entering in the two TMDs in Eq. (1.44) combine such that the results depend on the product $\zeta_1\zeta_2$.

With these scales fixed, we briefly recall now the required perturbative ingredients. The hard function has the expansion

$$H(Q,Q) \;=\; 1 \,+\, \sum_{n}^{\infty} \left(\frac{\alpha_S(Q)}{4\pi}\right)^n H^{(n)}\,, \tag{1.54}$$

where $H^{(n)}$ for the DY case can be read off from, e.g., Ref. [47] up to the two-loop accuracy. Beyond $\mathcal{O}(\alpha_s^2)$ the hard factor can acquire a non-trivial flavour structure (see, e.g., Ref. [48]); in such cases H should be moved inside the flavour sum in Eq. (1.44).

Next, we consider the matching function C introduced in Eq. (1.51) to express the TMD distribution in the small b_T region. The perturbative expansion at the initial scale is

$$C_{ij}(x,b_T;\mu_b,\mu_b^2) \;=\; \delta_{ij}\delta(1-x) \,+\, \sum_{n=1}^{\infty} \left(\frac{\alpha_S(\mu_b)}{4\pi}\right)^n C_{ij}^{(n)}(x)\,, \tag{1.55}$$

where the $C_{ij}^{(n)}$, known up to $n=2$, have been computed in Refs. [49, 50], and $\mathcal{O}(\alpha_S^3)$ results for quark channels are presented in Ref. [48]. Finally, the anomalous dimensions entering the Sudakov form factor in Eq. (1.50) can be expanded as

$$\begin{aligned} K(\mu_b) &= \sum_{n=0}^{\infty} \left(\frac{\alpha_S(\mu_b)}{4\pi}\right)^{n+1} K^{(n)}, \\ \gamma_F(\alpha_S(\mu)) &= \sum_{n=0}^{\infty} \left(\frac{\alpha_S(\mu)}{4\pi}\right)^{n+1} \gamma_F^{(n)}, \\ \gamma_K(\alpha_S(\mu)) &= \sum_{n=0}^{\infty} \left(\frac{\alpha_S(\mu)}{4\pi}\right)^{n+1} \gamma_K^{(n)}. \end{aligned} \tag{1.56}$$

For reference, the coefficients $K^{(n)}$ can be found up to $n=3$ in Ref. [50] and up to $n=2$ in Ref. [48]. $\gamma_F^{(n)}$ and $\gamma_K^{(n)}$ are given in Refs. [48, 50] up to $n=2$. Notice that different conventions exist in the literature for these coefficients, reflecting alternative definitions of the CS kernel.

Logarithmic accuracy.

In this section, we discuss how to combine Eqs.(1.54)-(1.56) consistently to compute the cross section in Eq. (1.44). In particular, we adopt the convention used in Ref. [51] for the definition of the logarithmic ordering.

TMD factorization resums large logarithms of Q/q_T or, equivalently, of Q/μ_b. The resummation is encoded in the Sudakov form factor R defined in Eq. (1.50), whose schematic expansion is

$$R = 1 + \sum_{n=1}^{\infty} \left(\frac{\alpha_S(Q)}{4\pi}\right)^n \sum_{k=1}^{2n} L^k\, R^{(n,k)}\,, \tag{1.57}$$

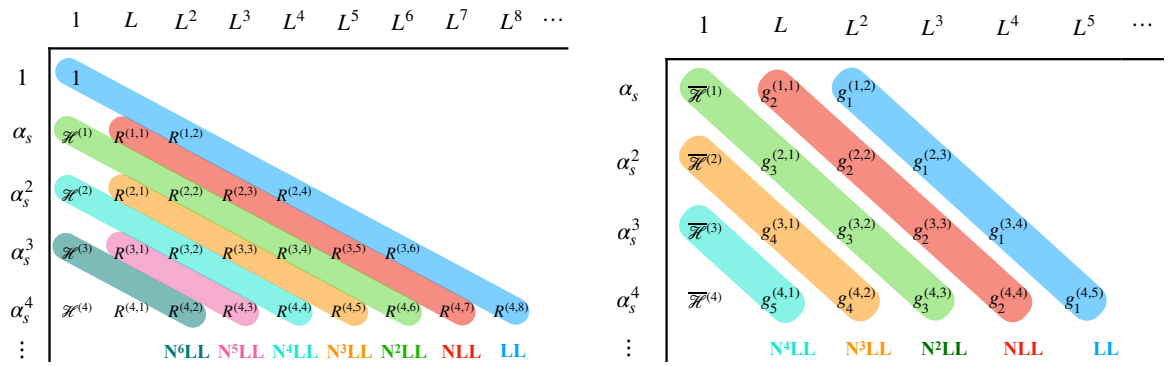

Figure 1.6: Graphical representation of logarithmic countings: in the left panel the counting is done at the level of the cross section, in the right panel at the level of the logarithm of the cross section.

with

$$L = \ln\left(\frac{Q^2}{\mu_b^2}\right). \tag{1.58}$$

The inner sum up to $2n$ displays the double logarithmic character of the resummation. This structure traces back to the evolution equations in Eq. (1.45), which resum two distinct categories of logarithms. With our scale choice $\mu_0 = \sqrt{\zeta_0} = \mu_b$ and $\mu = \sqrt{\zeta} = Q$, the μ- and ζ-evolution logarithms coincide, generating up to two powers of L per power of α_S. Consequently, Eq. (1.57) must include all powers of α_S whenever $\alpha_S L^2 \gtrsim 1$. It is convenient to reorganise the series by logarithmic accuracy,

$$R = 1 + \sum_{k=0}^{\infty} R_{\mathrm{N}^k\mathrm{LL}}\,, \tag{1.59}$$

with

$$R_{\mathrm{N}^k\mathrm{LL}} = \sum_{n=1+\lfloor k/2\rfloor}^{\infty} \left(\frac{\alpha_S(Q)}{4\pi}\right)^n L^{\,2n-k}\, R^{(n,\,2n-k)}, \tag{1.60}$$

where $\lfloor k/2\rfloor$ is the integer part of $k/2$. According to this definition, the leading logarithmic (LL) approximation corresponds to $k = 0$ in Eq. (1.59), the next-to-leading logarithmic (NLL) to $k = 1$, and so forth.

If we multiply the expression of $R_{\mathrm{N}^k\mathrm{LL}}$ by an additional explicit factor α_S^p, the tower is effectively shifted by two orders

$$\left(\frac{\alpha_S(Q)}{4\pi}\right)^p R_{\mathrm{N}^k\mathrm{LL}} = \sum_{m=1+\lfloor (k+2p)/2\rfloor}^{\infty} \left(\frac{\alpha_S(Q)}{4\pi}\right)^m L^{\,2m-(k+2p)}\, R^{(m-p,\,2m-(k+2p))} \;\sim\; R_{\mathrm{N}^{\,k+2p}\mathrm{LL}}\,, \tag{1.61}$$

where $\sim$ indicates identical logarithmic accuracy on both sides.

This is a crucial point in the discussion: in the cross section the Sudakov form factor is multiplied by powers of α_S arising from the hard factor H and/or the matching kernel C. Thus, Eq. (1.61) implies that (at cross section level) including one additional power of α_S in the perturbative expansion of H and/or C raises the overall logarithmic accuracy by two orders relative to the leading contribution. For instance, at LL and NLL accuracy, the function H and C may be taken at $\mathcal{O}(1)$; at NNLL and N^{3}LL, $\mathcal{O}(\alpha_S)$ corrections in H and C are required; and so on. This counting is illustrated in the left panel of Fig.1.6, where diagonal bands represent the terms included in $R_{\mathrm{N}^k\mathrm{LL}}$, and $\mathcal{H}^{(N)}$ denotes the perturbative coefficients of either H, C, or combinations thereof.

In general, the above counting applies to any process whose amplitude factorizes in the appropriate limit, as in TMD factorization. In the particular case of DY, the phase space for the emission of n real particles factorizes in b_T-space (see, e.g., Ref. [52]). These two aspects allow one to exponentiate soft-collinear emission, and consequently write the Sudakov form factor in the following general form[6]:

$$R = \exp\Big[\tfrac{1}{2} L\, g^{(1)}(\alpha_S L) + \tfrac{1}{2} g^{(2)}(\alpha_S L) + \tfrac{1}{2}\alpha_S\, g^{(3)}(\alpha_S L) + \cdots\Big]\,. \tag{1.62}$$

where the functions $g^{(i)}$ are defined with the boundary condition $g^{(i)}(0) = 0$. Compared to the general organization in Eq. (1.57), this exponentiation relates all terms of the form $\alpha_S^n L^m$ with $n+1 < m \leq 2n$ to lower-order contributions. In Eq. (1.62), the logarithmic counting is performed at the level of the exponent: $Lg^{(1)}$ resums the LL series $\alpha_S^n L^{n+1}$; $g^{(2)}$ resums the NLL series $\alpha_S^n L^{n-1}$; $\alpha_S g^{(3)}$ resums the NNLL series $\alpha_S^n L^{n-1}$; and so on. This counting is driven by the condition $\alpha_S L^2 \gtrsim 1$, which extends the validity of the resummed result (truncated at a given level: NLL, NNLL, etc.) to larger values of the divergent L (for smaller values of q_T).

The logarithmic counting applied to the arguments of the exponential is equivalent to considering the logarithm of the cross section [47]. In fact, neglecting for simplicity the matching functions, we schematically have

$$\ln\left(\frac{d\sigma}{dQ\,dy\,dq_T}\right) \propto \ln H + L\, g^{(1)} + g^{(2)} + \alpha_S\, g^{(3)} + \cdots\,. \tag{1.63}$$

Expanding $\ln H$ gives

$$\ln\Big(1 + \alpha_S H^{(1)} + \alpha_S^2 H^{(2)}\Big) = \alpha_S H^{(1)} + \alpha_S^2\left(H^{(2)} - \frac{H^{(1)2}}{2}\right) + \mathcal{O}(\alpha_S^3)\,. \tag{1.64}$$

Here the $\alpha_S H^{(1)}$ term contributes to the $\alpha_S^n L^{n-1}$ (NLL) tower, while $\alpha_S^2\Big(H^{(2)} - \frac{H^{(1)2}}{2}\Big)$ contributes to the $\alpha_S^n L^{n-2}$ (N^{3}LL). The same counting applies to the matching functions C. Hence, including $\mathcal{O}(\alpha_S)$ terms in H and C introduces NNLL corrections; including $\mathcal{O}(\alpha_S^2)$ terms upgrades the accuracy to N^{3}LL; and so forth. A schematic visualization

[6]The factors 1/2 in the argument of the exponential are justified by the fact that each of the two TMDs involved in the cross section contains an evolution factor R

Accuracy	$\boldsymbol{H}$, $\boldsymbol{C}$	$\boldsymbol{K}$, $\boldsymbol{\gamma_F}$	$\boldsymbol{\gamma_K}$	**PDF & α_S evol.**
LL	0	—	1	—
NLL	0	1	2	LO
NLL′	1	1	2	NLO
NNLL	1	2	3	NLO
NNLL′	2	2	3	NNLO
N^{3}LL	2	3	4	NNLO

Table 1.1: Truncation order in the expansions of Eqs. (1.54)–(1.56) for the two logarithmic countings considered in this work. The last column reports the order used for the evolution of the collinear PDFs and α_S.

of this logic is shown in the right panel of Fig. 1.6, where bands indicate logarithmic tower and $\overline{\mathcal{H}}$ represents the relevant coefficients in $\ln H$, $\ln C$, or their combinations. This logarithmic counting has been employed in several works (see, e.g., Refs. [47, 53–55]). In what follows we adopt this "standard counting" and denote accuracies as NLL, NNLL, etc.

A slightly different convention, widely used in literature, is the "primed" counting (see, e.g., Ref. [56, 57]). Expanding the Sudakov factor in Eq. (1.62) and multiplying by the hard function of Eq. (1.54), the cross section has the schematic form

$$\frac{d\sigma}{dQ\,dy\,dq_T} \propto 1 + L\,g^{(1)} + g^{(2)} + H^{(1)}\,\alpha_S\,L\,g^{(1)} + \cdots\,, \tag{1.65}$$

where the last term arises from the product of the $\mathcal{O}(\alpha_S)$ term of H and $Lg^{(1)}$. Since this contribution scales as $\alpha_S^n L^n$, like $g^{(2)}$, one may argue that achieving NLL accuracy requires including not only $g^{(2)}$ but also $H^{(1)}$ [56]. The same reasoning holds at higher orders: at a given logarithmic accuracy, one includes one extra order in H (and/or C) relative to the standard scheme. We refer to this as "primed counting", denoted NLL',NNLL', etc. The apparent contradiction with the standard definition is resolved by noting that the first term in the expansion of $\alpha_S L g^{(1)}$ is proportional to $\alpha_S^2 L^2$, i.e. it belongs to the NNLL tower $\alpha_S^n L^{2n-2}$ and is formally sub-leading with respect to the NLL accuracy governed by $g^{(2)}$ in the exponent.

Table 1.1 summarises the perturbative ingredients required for a consistent computation of Eq. (1.44) under both the standard and primed countings. The table entries indicate the higher power of α_S to which each quantity should be computed, and the last column specifies the corresponding accuracy in computing the evolution of the collinear PDFs and of the coupling α_S.

Finally, we note that some works employ a different notation for perturbative accuracies and/or different evolution frameworks. For example, Refs. [58–60] do not use the

definitions summarised in Tab. 1.1 because the double-scale evolution of TMDs is carried out within the "ζ-prescription", which differs from the standard CSS formalism.

1.3.2 Non perturbative part

As explained above, within the $\overline{\text{MS}}$ scheme it is possible to avoid large logarithms by choosing μ_b as the initial scale (μ_0, ζ_0). Accordingly, in the perturbative expansions of K, Eq. (1.56), and C, Eq. (1.55), the strong coupling α_S is evaluated at μ_b. As b_T grows, $\alpha_S(\mu_b)$ increases and eventually diverges when μ_b approaches the Landau pole at Λ_{QCD}. Since the computation of q_T dependent observables requires a Fourier transform of the TMDs, one must also handle the large b_T region where the perturbative treatment in the previous section breaks down. To overcome this limitation, it is customary to adopt a prescription that avoids integrating over the Landau pole. In this work, we follow the prescription of Ref. [61]. We therefore introduce an auxiliary scale b_{max}, denoting the largest b_T value for which perturbation theory is trusted, chosen such that

$$\alpha_S\left(\frac{2e^{-\gamma_E}}{b_{max}}\right) \ll 1. \tag{1.66}$$

In addition, we wish to prevent μ_b from becoming much larger than the hard scale Q ($\mu_b \gg Q$). While not strictly necessary, this feature facilitates the expansion of the cross section integrated in q_T, whose leading term reproduces the leading order collinear result [62]. To this end, we define

$$b_{min} = \frac{2e^{-\gamma_E}}{Q}, \tag{1.67}$$

and

$$b_{max} = 2e^{-\gamma_E}\,\text{GeV}^{-1} \approx 1.123\,\text{GeV}^{-1}. \tag{1.68}$$

With these choices, the scale μ_b is constrained between 1 GeV and Q, and consequently the collinear PDFs are never computed below 1 GeV and the lower limit in the μ'-integral appearing in the perturbative Sudakov factor (Eq. (1.50)) never exceeds the upper limit.

Then, we introduce a smooth monotonic map $b_*(b_T)$ with the limiting behaviours

$$\begin{aligned} b_*(b_T) &\to b_{\text{min}} \quad \text{for } b_T \to 0, \\ b_*(b_T) &\to b_{\text{max}} \quad \text{for } b_T \to \infty. \end{aligned} \tag{1.69}$$

In particular, we adopt the functional form of Ref. [63], which ensures a rapid and smooth approach to the asymptotic limits,

$$b_*(b_T) = b_{\text{max}}\left(\frac{1-\exp\left(-\dfrac{b_T^4}{b_{\text{max}}^4}\right)}{1-\exp\left(-\dfrac{b_T^4}{b_{\text{min}}^4}\right)}\right)^{1/4}. \tag{1.70}$$

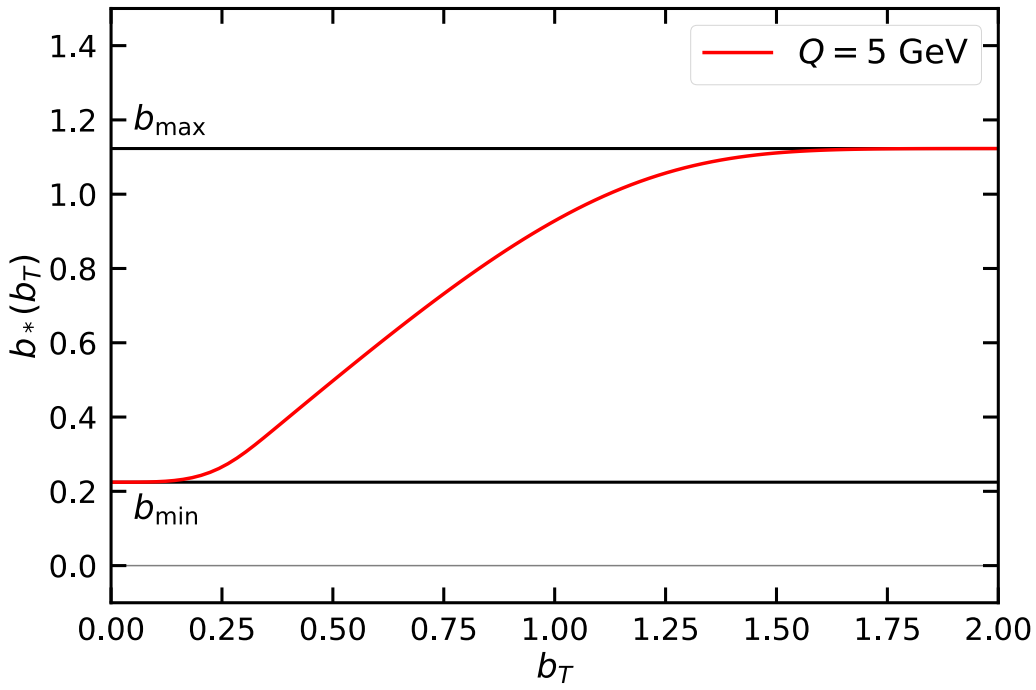

Figure 1.7: Example of the $b_\star$ prescription, Eq. (1.70), at $Q = 5\,\text{GeV}$.

Other definitions for $b_*(b_T)$ are possible; for instance, Collins, Soper and Sterman, in Ref. [61], used

$$b_*(b_T) = \frac{b_T}{\sqrt{1 + \frac{b_T^2}{b_{\max}^2}}}\,, \tag{1.71}$$

with $b_{\max} \sim 0.5\ \text{GeV}^{-1}$. With this in place, we write the TMD $\tilde{f}_1$ as

$$\begin{aligned} \tilde{f}_1(x, b_T; \mu, \zeta) &= \left[\frac{\tilde{f}_1(x, b_T; \mu, \zeta)}{\tilde{f}_1(x, b_*(b_T); \mu, \zeta)}\right] \tilde{f}_1(x, b_*(b_T); \mu, \zeta) \\ &\equiv f_{\text{NP}}(x, b_T, \zeta)\, \tilde{f}_1(x, b_*(b_T); \mu, \zeta)\ . \end{aligned} \tag{1.72}$$

This separation is advantageous because, due to the behaviour of $b_*(b_T)$, $\tilde{f}_1(x, b_*(b_T); \mu, \zeta)$ can be computed in perturbation theory for any value of b_T, while $f_{\text{NP}}(x, b_T, \zeta)$ embodies the non-perturbative dependence that has to be constrained through a fit to experimental data.

However, by means of Eq. (1.72), we can work out some general properties of f_{NP}. First, f_{NP} is independent of the renormalization scale μ, since this dependence cancels in the ratio. More explicitly, choosing $\mu_0 = \mu_b = 2e^{-\gamma_E}/b_T$ and using Eqs. (1.49) and (1.50),

we obtain

$$f_{\rm NP}(x,b_T,\zeta) = \frac{\tilde{f}_1(x,b_T;\mu,\zeta)}{\tilde{f}_1(x,b_*(b_T);\mu,\zeta)} = \exp\left\{ K(\mu_b)\,\ln\frac{\sqrt{\zeta}}{\mu_b} - K(\mu_{b_*})\,\ln\frac{\sqrt{\zeta}}{\mu_{b_*}} + \int_{\mu_b}^{\mu_{b_*}} \frac{d\mu'}{\mu'}\left[\gamma_F\Big(\alpha_S(\mu')\Big) - \gamma_K\Big(\alpha_S(\mu')\Big)\,\ln\frac{\sqrt{\zeta}}{\mu'}\right]\right\} \frac{\tilde{f}_1(x,b_T;\mu_b,\mu_b^2)}{\tilde{f}_1\Big(x,b_*(b_T);\mu_{b_*},\mu_{b_*}^2\Big)}\,, \tag{1.73}$$

with $\mu_{b_*} \equiv \mu_b(b_*(b_T))$. For large b_T, μ_{b_*} saturates to some minimal value $\mu_b(b_{max})$, while μ_b becomes increasingly small. As a consequence of this deviation between μ_{b_*} and μ_b, as well as between $\sqrt{\zeta}$ and μ_b in the exponential, Eq. (1.73) tends to be suppressed, and so does f_{NP}. In the small-b_T region, $b_* \to b_{min}$ as $b_T \to 0$; thus, looking at Eq. (1.69), we can see that μ_{b_*} saturates to Q while μ_b becomes larger and larger. In this limit, we have [62]

$$f_{\rm NP} \xrightarrow[b_T\to 0]{} 1 + \mathcal{O}\left(\frac{1}{Q^p}\right)\,, \tag{1.74}$$

with some positive power p. Since TMD factorization applies at leading power in q_T/Q, we can neglect the power suppressed contribution such that $f_{NP} \to 1$ for $b_T \to 0$. Finally, it is important to stress that the split between perturbative and non-perturbative components of a TMD is prescription-dependent and reflects the chosen treatment to regularise the Landau pole. For any such choice, only the product in Eq. (1.72) is meaningful; it is therefore misleading to regard f_{NP} as a universal, process-independent non-perturbative part of TMDs.

Chapter 2

Azimuthal asymmetries in photon-photon colliders

Currently, our phenomenological knowledge on quark TMD fragmentation functions relies mainly on SIDIS and nearly back-to-back hadron production in e^+e^- annihilation, for which, however, quark flavour separation remains challenging. Moreover, TMD PDFs and FFs always appear coupled in SIDIS, making phenomenology even more complicated, while in e^+e^- collisions, where only fragmentation processes play a role, experimental information is presently relatively scarce. These limitations motivate considering additional processes and observables sensitive to intrinsic parton motion effects, for which TMD factorization is guaranteed, with the aim of improving the knowledge and phenomenology of TMD fragmentation functions.
A new class of processes for which TMD factorization is expected to hold, given the clearness of the initial electromagnetic state and the presence of final state interactions only, is inclusive hadron-pair production in photon-photon collisions. These can be studied at present in ultraperipheral collisions at hadron colliders, like the Large Hadron Collider (LHC) at CERN and the Relativistic Heavy Ion Collider at Brookhaven National Laboratory, although in these experiments the intricate hadronic environment can hinder the study of TMD observables.Photon-photon collisions are also actively investigated as a source of information for Higgs and heavy-boson properties and decays, and light-by-light scattering. In fact, the γ-γ collider operational mode is considered in all major proposals for future circular and linear lepton colliders (for more information on photon-photon physics, see e.g. Refs. [64–68]).
Therefore, we propose to consider photon-photon scattering as a future tool for gaining new complementary and clean information on quark TMD fragmentation functions; two aspects are particularly noteworthy:

- In $\gamma\gamma$ collisions flavour separation would result more effective, as compared to SIDIS or $\ell^+\ell^-$ annihilations, since the contributions of d, s, b quarks should be suppressed by a relative factor 1/16 (coming from their fractional electric charge to the fourth

power) with respect to those of u, c, quarks. This would certainly help in better determining quark TMD FFs and disentangling different flavour contributions.

- While $\ell^+\ell^-$ colliders operate at some fixed energy scale (the centre of mass (c.m.)energy of the two leptons), photon-photon collisions allow to vary the perturbative energy scale (related to the photon virtualities). Thus, one can study the scale dependence of the TMD FFs in the same process and experimental setup.

It is natural to ask about the reachable luminosity in the photon-photon collision mode at lepton colliders, and the attainable c.m. energy. All these aspects must be carefully considered while developing proposals for future lepton colliders and the related detectors. At this stage, we suggest taking into account the possibility of conducting a valuable, complementary analysis of the 3D structure of hadrons and TMDs, together with the main physics cases considered. The main motivation of this work is to stimulate the study of TMD physics at future photon-photon colliders, at the time the nuclear and particle physics communities continue to discuss prospects for future large-scale hadron and lepton colliders.

2.1 Lepton colliders as effective photon photon colliders

As a first illustrative example, we will consider the azimuthal distribution of a pseudoscalar hadron pair, inclusively produced in opposite hemispheres with respect to the final jet thrust axis, in photon-photon collisions, $\ell^+\ell^- \to \gamma^*\gamma \to q\bar{q} \to h_1h_2 + X$, with one deeply virtual and one quasi-real photon. To this end, we will adopt the TMD approach at leading order and leading twist, complemented by the helicity formalism, which allows us to follow step by step, in the physical process, the role of the spin and polarization state of the particles involved.
In what follows, we describe the formalism adopted and outline the kinematics of the process. Next, a detailed derivation of the differential cross section and the measurable azimuthal asymmetries is presented, alongside a discussion of their physical content. Any additional technical details on the kinematics, the virtual photon helicity density matrix and the hard-scattering helicity amplitudes are presented in the appendices.

2.1.1 Kinematics and Formalism

In this section, we provide the main analytic expressions and kinematical details required to derive the differential cross section for the process

$$\ell^+(l_+) + \ell^-(l_-) \to \ell^+(l'_+) + h_1(P_1) + h_2(P_2) + X\,, \tag{2.1}$$

where the four-momenta of the particles involved are shown within brackets. At leading order in the electromagnetic and strong coupling constants, α and α_S respectively, the dominant channel of this reaction is

$$\gamma_1^*(q_1) + \gamma_2(q_2) \to q(K_q) + \bar{q}(K_{\bar{q}}) \to h_1(P_1) + h_2(P_2) + X\,, \tag{2.2}$$

that is the production of a quark-antiquark pair by two-photon fusion, and their subsequent fragmentation into two light unpolarised or scalar mesons (we mainly have in mind pion and kaon mesons here). In Eq. (2.1) we are considering the single-tagged configuration for a leptonic circular collider ($\ell = e, \mu$) where, for instance, the final antilepton ℓ'^+ with four-momentum l'_+ is detected and the virtuality $q_1^2 = (l_+ - l'_+)^2 \equiv -Q_1^2$ of γ_1 is known, while the final lepton ℓ'^- is undetected and γ_2 can be effectively considered as (quasi)real, $q_2^2 \simeq 0$, and described by a collinear Weizsäcker-Williams distribution inside the parent beam lepton [69, 70]. For completeness, we will also consider the case in which the lepton beams can be longitudinally polarized. Furthermore, we note that the two final hadrons are produced almost back to back (in the partonic c.m. frame), with a large transverse momentum with respect to the $\gamma^*\gamma$ axis. Intrinsic transverse momentum effects in the fragmentation process, encoded in the quark TMD fragmentation functions, lead to an observable non-collinearity of the two final hadrons around the q-$\bar{q}$ axis. This in turn manifests itself as azimuthal correlations in the two-hadron angular distribution around the jet thrust axis.

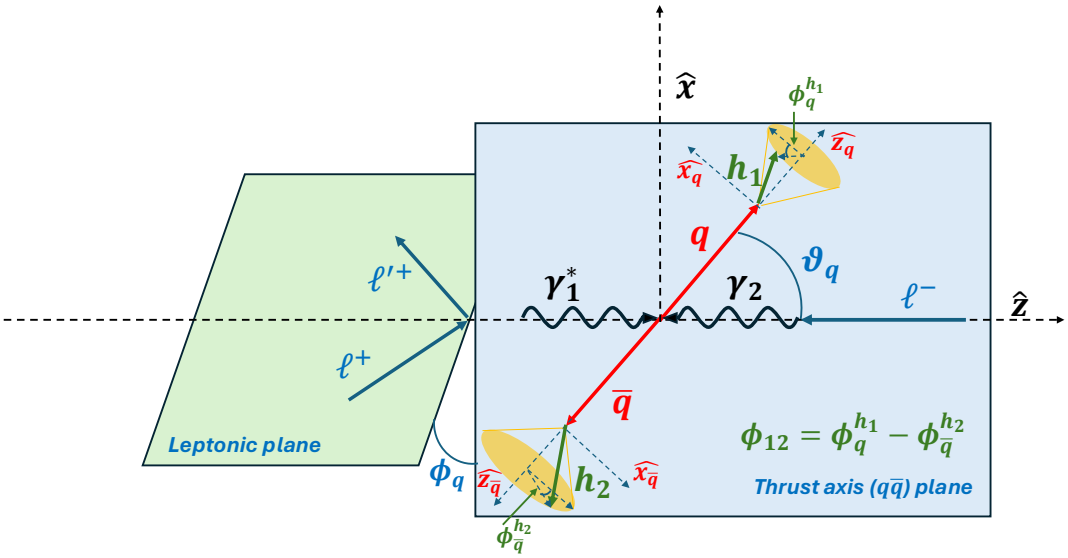

Figure 2.1: Kinematics of the process $\ell^+(l_+)\,\ell^-(l_-) \to \ell^+(l'_+)\,h_1(P_1)\,h_2(P_2) + X$ in the two-photon center-of-mass frame.

Before going into more details, some comments are in order:

a) As mentioned in the introduction, we adopt here a TMD factorization approach within the helicity formalism. The simple electromagnetic initial state should guarantee the validity of the approach as in $\ell^+\ell^-$ SIA processes. Moreover, it has been proven that TMD fragmentation functions are universal and process independent (see e.g. Refs. [71–73]), so that we can consider the process in Eq. (2.1) as a useful additional tool for TMD FF phenomenology.

b) From the theoretical point of view, the two-hadron azimuthal distribution around the jet thrust axis is the cleanest possible observable to consider; from the experimental point of view, however, it requires a good determination of the thrust axis that can be difficult to achieve. In fact, experimental results for SIA processes are often presented for the azimuthal distribution of one final hadron around the direction of motion of the second one. In this thesis, mainly devoted to illustrate a first application of the TMD approach in photon-photon collisions, we keep on working in the thrust-axis configuration. The formalism adopted here has been already worked out also for the second kinematical configuration, and could be easily implemented in our case, see Ref. [23] and references therein for more details.

c) TMD evolution with the energy scale has been formulated within the Collins-Soper-Sterman approach [16, 46, 61, 74] and the soft collinear effective theory, see e.g. Refs. [75, 76]. In this work we present results in a simplified framework valid at a fixed energy scale. Full implementation of scale evolution of TMD FFs, crucial when experimental data will become available, has been already performed, using our same framework, for the $e^+e^- \to h_1\, h_2 + X$ process in Refs. [77, 78] and can be directly applied to the process under study. While making the analytical expressions of the quantities considered more involved, it does not modify the general structure of the azimuthal modulations.

d) A possible competing contribution to our observable comes from the gluon distribution $f_{g/\ell}(\xi)$ inside the second lepton, coupled to the hard process $\gamma^*\, g \to\, q\, \bar{q}$. However, this contribution should be suppressed with respect to the photon one, since one needs first to produce a $q\bar{q}$ pair by a primary photon inside the lepton to generate a gluon. This is only partially compensated by the order $\alpha\, \alpha_S(Q^2)$ of the cross section for the hard $\gamma^*\, g \to q\, \bar{q}$ process, as compared to the $\gamma^*\, \gamma \to q\, \bar{q}$ one of order α^2. Moreover, in principle this contribution can be distinguished experimentally by the presence of additional hadronic production along the second lepton beam, which is suppressed in photon-photon scattering. Anyway, the γ-g contribution could be easily added to the γ-γ one by simply adapting the results presented below, implementing the required changes in the couplings and replacing the photon distribution in the second lepton, $f_{\gamma/\ell}$, by the gluon one. In this case the results are

very similar to those discussed in the literature for the SIDIS case, see e.g. Ref. [79] and references therein. In fact, we have verified that, with due changes, our results agree with those of Ref. [79] for the common parts.

Concerning the kinematics of the process, different c.m. frames enter into play: the lepton-beam $\ell^+\ell^-$ c.m. frame, the $\gamma_1^*\,\ell^-$ (analogous to the $\gamma^* p$ frame commonly adopted in SIDIS) and the $\gamma_1^*\,\gamma_2$ ones. We will summarize in this section the derivation of the differential cross section of the process under investigation. The azimuthal distributions of the two final hadrons around the final jet axis, which in our lowest-order (in the strong coupling constant) analysis coincides with the $q\bar{q}$ axis, will be discussed in the following section. Useful kinematical relations in the different c.m. frames, required for the calculations, are collected and discussed in Appendix A. To summarize what has been said so far, we will adopt a leading order and leading twist TMD factorization approach within the helicity formalism, which clearly describes, for each step of the process, the polarization state of the particles involved and their role in the measured azimuthal distributions. Given the simplicity of the initial (electromagnetic) state, the process under consideration is on an equal footing with direct lepton-antilepton annihilation, for which TMD factorization has been fully proven. Therefore, we are confident that the same approach can be applied to photon-photon collisions. Within the above described framework, the differential cross section for the process in Eq. (2.1) can be written as follows:

$$\begin{aligned}
\mathrm{d}\sigma^{\ell^+\ell^-\to\ell'^+\,h_1\,h_2\,X} = {} & \frac{1}{4\,(l_+\cdot l_-)}\,\frac{\mathrm{d}^3\boldsymbol{l}'_+}{2(2\pi)^3\,l'^0_+}\,\frac{\mathrm{d}^3\boldsymbol{K}_q}{2(2\pi)^3 K_q^0}\,\frac{\mathrm{d}^3\boldsymbol{K}_{\bar{q}}}{2(2\pi)^3 K_{\bar{q}}^0}\,(2\pi)^4\,\delta^{(4)}(q_1+q_2-K_q-K_{\bar{q}}) \\
& \times \sum_q \sum_{\{\lambda_i\}} \tilde{\rho}_{\lambda_1,\lambda'_1}(\gamma_1^*)\,\rho_{\lambda_2,\lambda'_2}(\gamma_2)\,f_{\gamma/\ell^-,\mathcal{P}^{\ell^-}_{\hat{z}_-}}(\xi)\,\frac{\mathrm{d}\xi}{\xi}\,\hat{H}_{\lambda_q,\lambda_{\bar{q}};\lambda_1,\lambda_2}\,\hat{H}^*_{\lambda'_q,\lambda'_{\bar{q}};\lambda'_1,\lambda'_2} \\
& \times \hat{D}^{h_1}_{\lambda_q,\lambda'_q}(z_1,\boldsymbol{p}_{\perp 1})\,\mathrm{d}z_1\,\mathrm{d}^2\boldsymbol{p}_{\perp 1}\,\hat{D}^{h_2}_{\lambda_{\bar{q}},\lambda'_{\bar{q}}}(z_2,\boldsymbol{p}_{\perp 2})\,\mathrm{d}z_2\,\mathrm{d}^2\boldsymbol{p}_{\perp 2}\,.
\end{aligned} \tag{2.3}$$

In this equation, the first line contains the kinematical terms related to the initial flux factor, the ℓ'^+ Lorentz-invariant phase space factor (LIPS), which will be expressed in the $\ell^+\ell^-$ c.m. frame, the LIPS for the quark and the antiquark produced in the $\gamma_1^*\gamma_2$ annihilation, as well as the Dirac δ imposing momentum conservation in the hard process. The last two lines refer to the dynamical kernel of the cross section, including the hard-scattering amplitudes and the parton hadronisation process into the two final hadrons, through the TMD fragmentation functions. According to the factorization approach, in a reference frame where the initial photons move collinearly and in opposite directions, this kernel is given in terms of the distributions of the initial photons inside the parent leptons, the hard-scattering amplitudes for the process $\gamma_1^*\,\gamma_2 \to q\,\bar{q}$, and the fragmentation functions of the final quark and antiquark (q, $\bar{q}$) into the observed hadrons (h_1, h_2).
Let us illustrate all the ingredients entering this expression in more detail:

1. The first sum over (light) quark flavours extends to $q = u, \bar{u}, d, \bar{d}, s, \bar{s}$; it can be generalized to include heavy (c, b) flavours.

2. In the second sum $\{\lambda_i\}$ stays for a sum over all involved helicity indices;

3. $\tilde{\rho}(\gamma_1^*)$ and $\rho(\gamma_2)$ are, respectively, the helicity density matrices of the virtual photon γ_1^* and the quasi-real one, γ_2, whose expression will be given in the following.

4. $f_{\gamma/\ell,\mathcal{P}_{\hat{z}}^\ell}(\xi)$ is the Weizsächer-Williams distribution for the quasi-real photon inside the initial unpolarised ($\mathcal{P}_{\hat{z}}^\ell = 0$) or longitudinally polarized ($\mathcal{P}_{\hat{z}}^\ell = \pm 1$) ℓ^- lepton and ξ the corresponding light-cone momentum fraction.

5. The $\hat{H}_{\lambda_q,\lambda_{\bar{q}};\lambda_1,\lambda_2}$'s are the helicity scattering amplitudes for the hard partonic process $\gamma_1^*(\lambda_1) + \gamma_2(\lambda_2) \to q(\lambda_q) + \bar{q}(\lambda_{\bar{q}})$.

6. Finally, the $\hat{D}^h_{\lambda_q,\lambda'_q}(z, \boldsymbol{p}_\perp)$'s are the transverse momentum dependent fragmentation functions encoding the soft fragmentation process of quark q into the final hadron h carrying a light-cone momentum fraction z of the parent quark momentum and an intrinsic transverse momentum $\boldsymbol{p}_\perp$ with respect to its direction of motion.

In order to simplify the notation, an energy scale dependence of the parton distribution and fragmentation functions is implied. Let us now summarize, referring to Appendix A for more details, some useful standard manipulations on the kinematical factors in the first line of Eq. (2.3). We will adopt the usual invariant variables for deep inelastic scattering,

$$s = (l_+ + l_-)^2 = 2l_+ \cdot l_- \,, \quad x_B = \frac{Q^2}{2q_1 \cdot l_-} \,, \quad y = \frac{q_1 \cdot l_-}{l_+ \cdot l_-} \,, \tag{2.4}$$

with $Q^2 = -q_1^2 = x_B\, y\, s$. Notice that we will neglect lepton, quark, and hadron masses in the following. From Eq. (2.4) it is easy to derive the flux factor in Eq. (2.3), $4\, l_+ \cdot l_- = 2s$. The Lorentz-invariant phase space for the final tagged positron can be written, in the ℓ^+-ℓ^- c.m. frame, as follows:

$$\frac{\mathrm{d}^3 \boldsymbol{l}'_+}{2(2\pi)^3\, l'^0_+} = \frac{1}{16\pi^2}\, s\, y\, \mathrm{d}x_B\, \mathrm{d}y \,, \tag{2.5}$$

where the angular dependence has been integrated over. This can be seen explicitly by looking, e.g. ,at the expression of l'_+ in Eq. (A.1) and evaluating from there the Jacobian for the change of variables $\mathrm{d}(l'_+)^1 \mathrm{d}(l'_+)^2 \mathrm{d}(l'_+)^3 = |J|\, \mathrm{d}x_B\, \mathrm{d}y\, \mathrm{d}\phi_\ell$. Concerning the four-dimensional Dirac δ in Eq. (2.3), we can write

$$\delta^{(4)}(q_1 + q_2 - K_q - K_{\bar{q}}) = \delta(q_1^+ + q_2^+ - K_q^+ - K_{\bar{q}}^+)\, \delta(q_1^- + q_2^- - K_q^- - K_{\bar{q}}^-)\, \delta^{(2)}(-\boldsymbol{K}_{q\,T} - \boldsymbol{K}_{\bar{q}\,T}) \,, \tag{2.6}$$

where we have switched temporarily to light-cone four-vector components, $a^\mu = (a^+, a^-, \boldsymbol{a}_T)$, with $a^\pm = (a^0 \pm a^3)/\sqrt{2}$. The 2-dimensional Dirac delta on the transverse momenta fixes $\boldsymbol{K}_{q\,T} \equiv \boldsymbol{K}_T = -\boldsymbol{K}_{\bar{q}\,T}$. Moreover, by using the results of Appendix A, we find:

$$\delta(q_1^+ + q_2^+ - K_q^+ - K_{\bar{q}}^+)\, \delta(q_1^- + q_2^- - K_q^- - K_{\bar{q}}^-) = \frac{2}{ys}\, \delta(1 - \zeta_q - \zeta_{\bar{q}})\, \delta\left(\xi - x_B - \frac{\boldsymbol{K}_T^2}{\zeta_q \zeta_{\bar{q}} y s}\right) \,, \tag{2.7}$$

where the additional invariants $\zeta_{q,\bar{q}}$ are defined as

$$\zeta_q = \frac{K_q \cdot l_-}{q_1 \cdot l_-}\,, \qquad \zeta_{\bar{q}} = \frac{K_{\bar{q}} \cdot l_-}{q_1 \cdot l_-}\,, \tag{2.8}$$

see Appendix A for more details. The LIPS for the final quark-antiquark pair can be further manipulated:

$$\frac{\mathrm{d}^3\boldsymbol{K}_q}{2(2\pi)^3 K_q^0}\,\frac{\mathrm{d}^3\boldsymbol{K}_{\bar{q}}}{2(2\pi)^3 K_{\bar{q}}^0}\,\delta^{(2)}(-\boldsymbol{K}_{q\,T} - \boldsymbol{K}_{\bar{q}\,T}) \;=\; \frac{1}{4(2\pi)^6}\,\frac{\mathrm{d}K_q^3}{K_q^0}\,\mathrm{d}^2\boldsymbol{K}_T\,\frac{\mathrm{d}K_{\bar{q}}^3}{K_{\bar{q}}^0}\,. \tag{2.9}$$

By using again the results of Appendix A we find that

$$\frac{\mathrm{d}K_q^3}{K_q^0} = \mathrm{d}\eta_q = \frac{\mathrm{d}\zeta_q}{\zeta_q}\,, \tag{2.10}$$

where η_q is the quark pseudorapidity, and similarly for $K_{\bar{q}}$. Furthermore, $\mathrm{d}^2\boldsymbol{K}_T = K_T\,\mathrm{d}K_T\,\mathrm{d}\phi_q = (1/2)\,\mathrm{d}\boldsymbol{K}_T^2\,\mathrm{d}\phi_q$. Inserting all these results into Eq. (2.3) and collecting the constant factors, we finally get

$$\begin{aligned}
&\frac{\mathrm{d}\sigma^{\ell^+\ell^-\to\ell'^+\,h_1\,h_2\,X}}{\mathrm{d}x_B\,\mathrm{d}y\,\mathrm{d}\zeta\,\mathrm{d}\boldsymbol{K}_T^2\,\mathrm{d}\phi_q\,\mathrm{d}\xi\,\mathrm{d}z_1\,\mathrm{d}^2\boldsymbol{p}_{\perp 1}\,\mathrm{d}z_2\,\mathrm{d}^2\boldsymbol{p}_{\perp 2}} = \\
&\frac{1}{2^9\,\pi^4}\,\frac{1}{\zeta(1-\zeta)\,\xi\,s} \\
&\times \sum_q \sum_{\{\lambda_i\}} \tilde{\rho}_{\lambda_1,\lambda_1'}(\gamma_1^*)\,\rho_{\lambda_2,\lambda_2'}(\gamma_2)\,f_{\gamma/\ell^-,\mathcal{P}^{\ell^-}_{\hat{z}_-}}(\xi)\,\hat{H}_{\lambda_q,\lambda_{\bar{q}};\lambda_1,\lambda_2}\,\hat{H}^*_{\lambda_q',\lambda_{\bar{q}}';\lambda_1',\lambda_2'} \\
&\times \hat{D}^{h_1}_{\lambda_q,\lambda_q'}(z_1,\boldsymbol{p}_{\perp 1})\,\hat{D}^{h_2}_{\lambda_{\bar{q}},\lambda_{\bar{q}}'}(z_2,\boldsymbol{p}_{\perp 2})\,\delta\left(\xi - x_B - \frac{\boldsymbol{K}_T^2}{\zeta(1-\zeta)ys}\right)\,,
\end{aligned}$$

where $\zeta_{\bar{q}} = \zeta$, $\zeta_q = 1-\zeta$, and the remaining Dirac δ can be used either to fix ξ in terms of $\boldsymbol{K}_T^2$ or vice versa. The various ingredients of the dynamical kernel in the above equation are described below. The expression of the helicity density matrix for the tagged virtual photon γ_1^* in the deeply inelastic scattering regime, $\rho_{\lambda_1,\lambda_1'}(\gamma_1^*)$, properly normalized to unity, has been derived and discussed in detail, e.g., in Refs. [64, 80, 81]. For completeness, we summarize its derivation in Appendix B. Its expression in terms of the deeply inelastic scattering invariants, in the photon helicity frame, where the photon moves along the $+\hat{z}$ axis and the leptonic ℓ^+-ℓ'^+ plane spans an azimuthal angle ϕ_ℓ with respect to the $\hat{x}$-$\hat{z}$

plane, reads

$$\rho(\gamma_1^*) = \frac{1}{2(2-y)^2} \times \begin{pmatrix} 1+(1-y)^2+\mathcal{P}^{\ell^+}_{\hat{z}_+}\, y(2-y) & -e^{-i\phi_\ell}\sqrt{2(1-y)}\left[(2-y)+\mathcal{P}^{\ell^+}_{\hat{z}_+}\, y\right] & -e^{-i2\phi_\ell}\,2(1-y) \\ -e^{i\phi_\ell}\sqrt{2(1-y)}\left[(2-y)+\mathcal{P}^{\ell^+}_{\hat{z}_+}\, y\right] & 4(1-y) & e^{-i\phi_\ell}\sqrt{2(1-y)}\left[(2-y)-\mathcal{P}^{\ell^+}_{\hat{z}_+}\, y\right] \\ -e^{i2\phi_\ell}\,2(1-y) & e^{i\phi_\ell}\sqrt{2(1-y)}\left[(2-y)-\mathcal{P}^{\ell^+}_{\hat{z}_+}\, y\right] & 1+(1-y)^2-\mathcal{P}^{\ell^+}_{\hat{z}_+}\, y(2-y) \end{pmatrix}, \tag{2.11}$$

where $\mathcal{P}^{\ell^+}_{\hat{z}_+} = 0, \pm 1$ for unpolarised or longitudinally polarized initial leptons ℓ^+, respectively, and, without loss of generality, in the following we will take $\phi_\ell = 0$. Notice that the normalized helicity density matrix ($\rho = \tilde{\rho}/\mathrm{Tr}[\tilde{\rho}]$, so that $\mathrm{Tr}[\rho] = 1$) in Eq. (2.11) has to be used in normalized observables related to $\mathrm{d}\sigma/\sigma$, while in the differential cross section $d\sigma$, Eq. (2.11), one has to reinstate the appropriate normalization factor, using $\tilde{\rho} = \rho\,\mathrm{Tr}[\tilde{\rho}]$, where

$$\mathrm{Tr}[\tilde{\rho}] \;=\; \frac{2\,e^2\,(2-y)^2}{Q^2\,y^2} \;\equiv\; \frac{2\,e^2\,(2-y)^2}{x_B\,y^3\,s}\,. \tag{2.12}$$

Concerning the untagged quasi-real photon γ_2, since it can only have $\lambda_2 = \pm 1$ helicities, its helicity density matrix can be effectively written as a 2×2 matrix,

$$\rho(\gamma_2) = \frac{1}{2}\begin{pmatrix} 1+\mathcal{P}^{\gamma_2}_{\hat{z}_2} & 0 \\ 0 & 1-\mathcal{P}^{\gamma_2}_{\hat{z}_2} \end{pmatrix}, \tag{2.13}$$

where $\mathcal{P}^{\gamma_2}_{\hat{z}_2}$ is the longitudinal component of the γ_2 polarization (pseudo)vector along its direction of motion, $\mathcal{P}^{\gamma_2}_{\hat{z}_2} = \pm 1$. Notice that in our partonic reference frame γ_1^* and γ_2 move back to back along the $\hat{z}$ axis, so that $\hat{z}_2 = \hat{z}_- = -\hat{z}_1 \equiv -\hat{z}$. As a consequence of Eq. (2.13), only two distinct combinations play a role in Eq. (2.11),

$$\begin{aligned} \left[\,\rho_{++}(\gamma_2)+\rho_{--}(\gamma_2)\,\right] f_{\gamma/\ell^-,\mathcal{P}^{\ell^-}_{\hat{z}_-}}(\xi) \;&=\; f_{\gamma,+/\ell^-,\mathcal{P}^{\ell^-}_{\hat{z}_-}}(\xi) + f_{\gamma,-/\ell^-,\mathcal{P}^{\ell^-}_{\hat{z}_-}}(\xi) \;=\; f_{\gamma/\ell}(\xi)\,, \\ \left[\,\rho_{++}(\gamma_2)-\rho_{--}(\gamma_2)\,\right] f_{\gamma/\ell^-,\mathcal{P}^{\ell^-}_{\hat{z}_-}}(\xi) \;&=\; \mathcal{P}^{\gamma_2}_{\hat{z}_2}\, f_{\gamma/\ell^-,\mathcal{P}^{\ell^-}_{\hat{z}_-}}(\xi) \\ &=\; f_{\gamma,+/\ell^-,\mathcal{P}^{\ell^-}_{\hat{z}_-}}(\xi) \;-\; f_{\gamma,-/\ell^-,\mathcal{P}^{\ell^-}_{\hat{z}_-}}(\xi) \;=\; \mathcal{P}^{\ell^-}_{\hat{z}_-}\,\Delta_L f_{\gamma/\ell}(\xi)\,, \end{aligned} \tag{2.14}$$

where $f_{\gamma/\ell}(\xi) = f_{\gamma,\pm/\ell^-,\pm} + f_{\gamma,\mp/\ell^-,\pm}$ and $\Delta_L f_{\gamma/\ell}(\xi) = f_{\gamma,\pm/\ell^-,\pm} - f_{\gamma,\mp/\ell^-,\pm}$ are, respectively, the unpolarised and longitudinally polarized Weizsäker-Williams parton distributions for γ_2 inside lepton ℓ^-.

The next ingredient in the dynamical kernel of Eq. (2.11) are the helicity amplitudes $\hat{H}_{\lambda_q,\lambda_{\bar{q}};\lambda_1,\lambda_2}$ for the hard-scattering process $\gamma_1^*(q_1,\lambda_1)+\gamma_2(q_2,\lambda_2)\to q(K_q,\lambda_q)+\bar{q}(K_{\bar{q}},\lambda_{\bar{q}})$. Since we are considering the production of light quarks, neglecting their masses, due to helicity conservation in the photon-quark vertices, the only non-vanishing amplitudes have opposite values of the quark and antiquark helicities, which helps in simplifying the expression of the kernel in Eq. (2.11). Moreover, using parity conservation, one can see that there are only six independent amplitudes. We list here all the non-vanishing helicity amplitudes for real photon γ_2 and massless quarks, in terms of Q^2, the virtuality of photon 1, the partonic Mandelstam invariants $\hat{s}$, $\hat{t}$, $\hat{u}$ and the azimuthal angle ϕ_q between the q-$\bar{q}$ plane and the leptonic plane for the virtual photon 1 (assumed to be, without loss of generality, the $\hat{x}$-$\hat{z}$ plane). We also give their expression in terms of the invariants x_B, ξ and ζ, that will be used to evaluate the $A_{U,L}$ and $B_{U,L}$ factors in Eqs. (2.23) and (2.24) respectively, in the sequel.

$$
\begin{aligned}
\hat{H}_{+-;1,1} &= -\hat{H}_{-+;-1,-1} = -2\sqrt{3}\,e^2\,e_q^2\,\frac{Q^2}{\hat{s}+Q^2}\sqrt{\frac{\hat{u}}{\hat{t}}} = -2\sqrt{3}\,e^2\,e_q^2\,\frac{x_B}{\xi}\sqrt{\frac{1-\zeta}{\zeta}}\,,\\
\hat{H}_{+-;1,-1} &= -\hat{H}^*_{-+;-1,1} = -2\sqrt{3}\,e^2\,e_q^2\,e^{i2\phi_q}\,\frac{\hat{s}}{\hat{s}+Q^2}\sqrt{\frac{\hat{u}}{\hat{t}}} = -2\sqrt{3}\,e^2\,e_q^2\,e^{i2\phi_q}\,\frac{\xi-x_B}{\xi}\sqrt{\frac{1-\zeta}{\zeta}}\,,\\
\hat{H}_{+-;-1,1} &= -\hat{H}^*_{-+;1,-1} = 2\sqrt{3}\,e^2\,e_q^2\,e^{-i2\phi_q}\,\frac{\hat{s}}{\hat{s}+Q^2}\sqrt{\frac{\hat{t}}{\hat{u}}} = \sqrt{3}\,e^2\,e_q^2\,e^{-i2\phi_q}\,\frac{\xi-x_B}{\xi}\sqrt{\frac{\zeta}{1-\zeta}}\,,\\
\hat{H}_{+-;-1,-1} &= -\hat{H}_{-+;1,1} = 2\sqrt{3}\,e^2\,e_q^2\,\frac{Q^2}{\hat{s}+Q^2}\sqrt{\frac{\hat{t}}{\hat{u}}} = 2\sqrt{3}\,e^2\,e_q^2\,\frac{x_B}{\xi}\sqrt{\frac{\zeta}{1-\zeta}}\,,\\
\hat{H}_{+-;0,\pm1} &= -\hat{H}_{-+;0,\pm1} = \pm 2\sqrt{6}\,e^2\,e_q^2\,e^{\mp i\phi_q}\,\frac{\sqrt{\hat{s}}Q}{\hat{s}+Q^2} = \pm 2\sqrt{6}\,e^2\,e_q^2\,e^{\mp i\phi_q}\,\frac{\sqrt{x_B(\xi-x_B)}}{\xi}\,.
\end{aligned}
\tag{2.15}
$$

The last step of the scattering process consists in the independent fragmentation of the quark and the antiquark (produced exactly back to back in their c.m. frame in the leading order approach considered here, along the jet thrust-axis direction) in the final observed hadrons. This non-perturbative process is embodied into the transverse momentum dependent fragmentation functions $D^{h_1}_{\lambda_q,\lambda'_q}(z_1,\boldsymbol{p}_{\perp 1})$ for $q\to h_1+X$ (and analogously for the antiquark fragmentation). As a result of the explicit account of intrinsic transverse motion effects, the two observed hadrons are no longer exactly back to back in the partonic c.m. frame. This generates possible azimuthal asymmetries in their distribution around the jet axis, which are the main subject of this study.

TMD fragmentation functions into unpolarised (or spinless) and spin-$\frac{1}{2}$ hadrons within the helicity formalism have been discussed in detail in Refs. [23, 45]. Here we only summarize some relations useful for the evaluation of the kernel. TMD FFs for the

process $a(s_a) \to h + X$, where a is a quark or an antiquark, can be written as

$$\hat{D}^{h/a}_{\lambda_a,\lambda'_a}(z,\boldsymbol{p}_\perp) = \sum_{\lambda_h} \sum\!\!\!\!\!\!\int_{X,\lambda_X} \hat{\mathcal{D}}_{\lambda_h,\lambda_X;\lambda_a}(z,\boldsymbol{p}_\perp)\hat{\mathcal{D}}^*_{\lambda_h,\lambda_X;\lambda'_a}(z,\boldsymbol{p}_\perp)\,, \tag{2.16}$$

where the $\hat{\mathcal{D}}_{\lambda_h,\lambda_X;\lambda_a}(z,\boldsymbol{p}_\perp)$'s are soft, non-perturbative helicity amplitudes for the process $a(\lambda_a) \to h(\lambda_h) + X(\lambda_X)$ and the symbol $\sum\!\!\!\!\!\!\int_{X,\lambda_X}$ stands for the helicity sum and phase space integration for the final unobserved remnants, collectively named X, in the fragmentation process. Using parity symmetry of strong interactions it is easy to see that for quark fragmentation into spinless or unpolarised final hadrons there are only two independent, leading twist TMD FFs: the unpolarised one,

$$\hat{D}^{h/a}_{++}(z,\boldsymbol{p}_\perp) = \hat{D}^{h/a}_{--}(z,\boldsymbol{p}_\perp) = D^h_a(z,p_\perp)\,, \tag{2.17}$$

where $p_\perp = |\boldsymbol{p}_\perp|$, and the Collins fragmentation function [36], describing the fragmentation of a transversely polarized quark into an unpolarised hadron,

$$\hat{D}^{h/a}_{+-}(z,\boldsymbol{p}_\perp) = D^{h/a}_{+-}(z,p_\perp)e^{i\phi^h_a}\,, \tag{2.18}$$

where ϕ^h_a is the azimuthal angle of the hadron h momentum in the fragmenting parton helicity frame. It is also easy to see that

$$\hat{D}^{h/a}_{-+}(z,\boldsymbol{p}_\perp) = -\left[\hat{D}^{h/a}_{+-}(z,\boldsymbol{p}_\perp)\right]^* = -D^{h/a}_{+-}(z,p_\perp)e^{-i\phi^h_a}\,. \tag{2.19}$$

Common notations adopted in the literature for the $p_\perp$-dependent term of the quark Collins FF are:

$$\Delta^N D^h_{a\uparrow}(z,p_\perp) = \frac{2p_\perp}{zm_h}\,H_1^{\perp,a}(z,p_\perp) = -i2D^{h/a}_{+-}(z,p_\perp)\,, \tag{2.20}$$

with m_h the mass of hadron h, while the $\uparrow$ arrow specifies that the quark a is transversely polarized with respect to the plane containing the quark itself and the hadron. Notice also that

$$\int \mathrm{d}^2\boldsymbol{p}_\perp\, D^h_a(z,p_\perp) = D^h_a(z)\,, \tag{2.21}$$

the usual collinear unpolarised fragmentation function. Moreover, for future use, we also define the lowest transverse moment of the Collins function,

$$\begin{aligned}\int \mathrm{d}^2\boldsymbol{p}_\perp\,\Delta^N D^h_{a\uparrow}(z,p_\perp) &\equiv \int \mathrm{d}^2\boldsymbol{p}_\perp\,\frac{2p_\perp}{zm_h}\,H_1^{\perp,a}(z,p_\perp) = 2\pi\int \mathrm{d}p_\perp\,p_\perp\,\Delta^N D^h_{a\uparrow}(z,p_\perp)\\ &= \Delta^N D^h_{a\uparrow}(z) = 4\,H_1^{\perp(1/2)a}(z)\,.\end{aligned}$$

2.1.2 Cross section and azimuthal asymmetries

Inserting Eqs. (2.11)–(2.20) into Eq. (2.11) and using symmetry considerations, after some lengthy but straightforward calculations, one finally finds the explicit expression of the differential cross section (in the sequel we will use $\mathcal{P}_\pm$ for $\mathcal{P}^{\ell^\pm}_{\hat{z}_\pm}$ for shortness),

$$\frac{\mathrm{d}\sigma^{\ell^+\ell^-\to\ell'^+\,h_1\,h_2\,X}\,(\mathcal{P}_+,\,\mathcal{P}_-)}{\mathrm{d}x_B\,\mathrm{d}y\,\mathrm{d}\zeta\,\mathrm{d}\phi_q\,\mathrm{d}\xi\,\mathrm{d}z_1\,\mathrm{d}^2\boldsymbol{p}_{\perp 1}\,\mathrm{d}z_2\,\mathrm{d}^2\boldsymbol{p}_{\perp 2}} = \frac{3\,\alpha^3}{4\,\pi}\,\frac{1}{x_B\,y^2\,\xi^3\,s}\sum_q e_q^4$$

$$
\begin{aligned}
&\times \Big\{ \Big[A_U + \mathcal{P}_+\mathcal{P}_- \, A_L + \Big(A_U^{\cos\phi_q} + \mathcal{P}_+\mathcal{P}_- \, A_L^{\cos\phi_q} \Big) \cos\phi_q + A_U^{\cos 2\phi_q} \cos 2\phi_q \Big] \; D_q^{h_1}(z_1, p_{\perp 1}) D_{\bar{q}}^{h_2}(z_2, p_{\perp 2}) \\
&\quad + \Big[\Big(B_U^{\cos\phi_{12}} + \mathcal{P}_+\mathcal{P}_- \, B_L^{\cos\phi_{12}} \Big) \cos\phi_{12} + \Big(B_U^{\cos(\phi_q - \phi_{12})} + \mathcal{P}_+\mathcal{P}_- \, B_L^{\cos(\phi_q - \phi_{12})} \Big) \cos(\phi_q - \phi_{12}) \\
&\quad + \Big(B_U^{\cos(\phi_q + \phi_{12})} + \mathcal{P}_+\mathcal{P}_- \, B_L^{\cos(\phi_q + \phi_{12})} \Big) \cos(\phi_q + \phi_{12}) + B_U^{\cos(2\phi_q - \phi_{12})} \cos(2\phi_q - \phi_{12}) \\
&\quad + B_U^{\cos(2\phi_q + \phi_{12})} \cos(2\phi_q + \phi_{12}) \Big] \; \Delta^N D_{q^\uparrow}^{h_1}(z_1, p_{\perp 1}) \Delta^N D_{\bar{q}^\uparrow}^{h_2}(z_2, p_{\perp 2}) \Big\} \, , \qquad (2.22)
\end{aligned}
$$

where we have used the remaining Dirac δ in Eq. (2.11)) to fix $\boldsymbol{K}_T^2 = \zeta(1-\zeta)(\xi - x_B) ys = \zeta(1-\zeta)\hat{s}$. In Eq. (2.22)), ϕ_q is the azimuthal angle of the scattering plane of the process $\gamma_1^* \gamma_2 \to q\bar{q}$ with respect to the leptonic plane ℓ^+-ℓ'^+ for the tagged photon. Moreover, we have introduced the angle $\phi_{12} = \phi_q^{h_1} - \phi_{\bar{q}}^{h_2}$, where, as can be seen from Eq. (2.18), $\phi_q^{h_1}$ ($\phi_{\bar{q}}^{h_2}$) is the azimuthal angle of hadron $h_1(h_2)$ around the direction of motion of the parent quark(antiquark). The subscripts U and L in the A, B coefficients refer to configurations where both lepton beams are unpolarised, that is $\mathcal{P}_+ = \mathcal{P}_- = 0$, or longitudinally polarized, $\mathcal{P}_+ = \pm 1$ and $\mathcal{P}_- = \pm 1$, respectively. Using also the results of Eq. (2.15), the A coefficients read

$$
\begin{aligned}
A_U &= 2 \left\{ [\, 1 + (1-y)^2 \,] \, [\, x_B^2 + (\xi - x_B)^2 \,] \, \frac{1 - 2\zeta(1-\zeta)}{\zeta(1-\zeta)} \; + \; 16 \, (1-y) \, x_B (\xi - x_B) \right\} f_{\gamma/\ell}(\xi) \, , \\
A_U^{\cos\phi_q} &= -\, 8 \, (2-y) \sqrt{1-y} \, (\xi - 2x_B) \sqrt{x_B(\xi - x_B)} \, \frac{1 - 2\zeta}{\sqrt{\zeta(1-\zeta)}} \, f_{\gamma/\ell}(\xi) \, , \\
A_U^{\cos 2\phi_q} &= 16 \, (1-y) \, x_B (\xi - x_B) \, f_{\gamma/\ell}(\xi) \, , \\
A_L &= -\, 2y(2-y) \, \xi (\xi - 2x_B) \, \frac{1 - 2\zeta(1-\zeta)}{\zeta(1-\zeta)} \, \Delta_L f_{\gamma/\ell}(\xi) \, , \\
A_L^{\cos\phi_q} &= \; 8 \, y \sqrt{1-y} \, \xi \sqrt{x_B(\xi - x_B)} \, \frac{1 - 2\zeta}{\sqrt{\zeta(1-\zeta)}} \, \Delta_L f_{\gamma/\ell}(\xi) \, . \qquad (2.23)
\end{aligned}
$$

Similarly, for the B terms we obtain

$$
\begin{aligned}
B_U^{\cos\phi_{12}} &= \Big\{ [1 + (1-y)^2] \, [\, x_B^2 + (\xi - x_B)^2 \,] \; - \; 8 \, (1-y) \, x_B (\xi - x_B) \Big\} \, f_{\gamma/\ell}(\xi) \, , \\
B_U^{\cos(\phi_q - \phi_{12})} &= -\, 2 \, (2-y) \sqrt{1-y} \, (\xi - 2x_B) \sqrt{x_B(\xi - x_B)} \sqrt{\frac{\zeta}{1-\zeta}} \; f_{\gamma/\ell}(\xi) \, , \\
B_U^{\cos(\phi_q + \phi_{12})} &= \; 2 \, (2-y) \sqrt{1-y} \, (\xi - 2x_B) \sqrt{x_B(\xi - x_B)} \sqrt{\frac{1-\zeta}{\zeta}} \; f_{\gamma/\ell}(\xi) \, , \\
B_U^{\cos(2\phi_q - \phi_{12})} &= \; 2 \, (1-y) \, x_B (\xi - x_B) \, \frac{\zeta}{1-\zeta} \; f_{\gamma/\ell}(\xi) \\
B_U^{\cos(2\phi_q + \phi_{12})} &= \; 2 \, (1-y) \, x_B (\xi - x_B) \, \frac{1-\zeta}{\zeta} \; f_{\gamma/\ell}(\xi) \, , \\
B_L^{\cos\phi_{12}} &= -\, y \, (2-y) \, \xi (\xi - 2x_B) \; \Delta_L f_{\gamma/\ell}(\xi) \, , \\
B_L^{\cos(\phi_q - \phi_{12})} &= \; 2 \, y \sqrt{1-y} \, \xi \sqrt{x_B(\xi - x_B)} \sqrt{\frac{\zeta}{1-\zeta}} \; \Delta_L f_{\gamma/\ell}(\xi) \, , \\
B_L^{\cos(\phi_q + \phi_{12})} &= -\, 2 \, y \sqrt{1-y} \, \xi \sqrt{x_B(\xi - x_B)} \sqrt{\frac{1-\zeta}{\zeta}} \; \Delta_L f_{\gamma/\ell}(\xi) \, . \qquad (2.24)
\end{aligned}
$$

In the above equations, we have given all the expressions in terms of the variables x_B, y, ζ, and ξ in which the cross section is differential. Using the results of Appendix A one can easily find the same quantities in terms of the partonic Mandelstam variables. To collect more statistics one can first perform the change of variables $(\phi_q^{h_1}, \phi_{\bar{q}}^{h_2}) \to (\phi_q^{h_1}, \phi_q^{h_1} - \phi_{\bar{q}}^{h_2} \equiv \phi_{12})$, then integrate Eq. (2.22) over the azimuthal angle $\phi_q^{h_1}$ and the moduli of the intrinsic transverse momenta, $p_{\perp 1}$, and $p_{\perp 2}$. By using Eqs. (2.21) and (2.22), one finally gets

$$
\begin{aligned}
&\frac{\mathrm{d}\sigma^{\ell^+\ell^-\to\ell'^+\,h_1\,h_2\,X}\,(\mathcal{P}_+,\,\mathcal{P}_-)}{\mathrm{d}x_B\,\mathrm{d}y\,\mathrm{d}\zeta\,\mathrm{d}\phi_q\,\mathrm{d}\xi\,\mathrm{d}z_1\,\mathrm{d}z_2\,\mathrm{d}\phi_{12}} = \frac{3\,\alpha^3}{8\,\pi^2}\,\frac{1}{x_B\,y^2\,\xi^3\,s}\,\sum_q e_q^4 \\
&\times\Big\{\Big[A_U + \mathcal{P}_+\mathcal{P}_-\,A_L + \Big(A_U^{\cos\phi_q} + \mathcal{P}_+\mathcal{P}_-\,A_L^{\cos\phi_q}\Big)\cos\phi_q + A_U^{\cos 2\phi_q}\cos 2\phi_q\Big]\,D_q^{h_1}(z_1)\,D_{\bar{q}}^{h_2}(z_2) \\
&\quad + \Big[\Big(B_U^{\cos\phi_{12}} + \mathcal{P}_+\mathcal{P}_-\,B_L^{\cos\phi_{12}}\Big)\cos\phi_{12} + \Big(B_U^{\cos(\phi_q-\phi_{12})} + \mathcal{P}_+\mathcal{P}_-\,B_L^{\cos(\phi_q-\phi_{12})}\Big)\cos(\phi_q-\phi_{12}) \\
&\quad + \Big(B_U^{\cos(\phi_q+\phi_{12})} + \mathcal{P}_+\mathcal{P}_-\,B_L^{\cos(\phi_q+\phi_{12})}\Big)\cos(\phi_q+\phi_{12}) + B_U^{\cos(2\phi_q-\phi_{12})}\cos(2\phi_q-\phi_{12}) \\
&\quad + B_U^{\cos(2\phi_q+\phi_{12})}\cos(2\phi_q+\phi_{12})\Big]\,\Delta^N D_{q^\uparrow}^{h_1}(z_1)\,\Delta^N D_{\bar{q}^\uparrow}^{h_2}(z_2)\Big\}\,. \qquad (2.25)
\end{aligned}
$$

From Eqs. (2.22), (2.25), and using the shorthand notation $\mathrm{d}\sigma(\mathcal{P}_+,\,\mathcal{P}_-)$ for the differential cross section, we see that

$$
\begin{aligned}
\mathrm{d}\sigma(0,0) &= \mathrm{d}\sigma(1,0) = \mathrm{d}\sigma(0,1) = \mathrm{d}\sigma^{\mathrm{unp}}\,, \\
\mathrm{d}\sigma(1,1) &= \mathrm{d}\sigma(-1,-1)\,, \qquad (2.26) \\
\mathrm{d}\sigma(1,-1) &= \mathrm{d}\sigma(-1,1)\,.
\end{aligned}
$$

Additionally,

$$
\begin{aligned}
\mathrm{d}\sigma^{\mathrm{unp}} &= \frac{1}{4}\Big[\mathrm{d}\sigma(1,1) + \mathrm{d}\sigma(1,-1) + \mathrm{d}\sigma(-1,1) + \mathrm{d}\sigma(-1,-1)\Big] \\
&= \frac{1}{2}\Big[\mathrm{d}\sigma(1,1) + \mathrm{d}\sigma(1,-1)\Big]\,, \qquad (2.27) \\
\Delta_L\sigma &= \mathrm{d}\sigma(1,1) - \mathrm{d}\sigma(1,-1) = \mathrm{d}\sigma(-1,-1) - \mathrm{d}\sigma(-1,+1)\,. \qquad (2.28)
\end{aligned}
$$

We can therefore define the longitudinal spin asymmetry

$$
A_{LL} = \frac{\mathrm{d}\sigma(1,1) - \mathrm{d}\sigma(1,-1)}{\mathrm{d}\sigma(1,1) + \mathrm{d}\sigma(1,-1)} = \frac{\Delta_L\sigma}{2\,\mathrm{d}\sigma^{\mathrm{unp}}}\,. \qquad (2.29)
$$

To isolate the factors associated with the different azimuthal modulations appearing in Eqs. (2.22), (2.25), and (2.29), it is common to define appropriate azimuthal moments of the unpolarised cross section, $\mathrm{d}\sigma^{\mathrm{unp}}$, and the longitudinal spin asymmetry A_{LL}. In our case their general form can be given as follows:

$$
\langle\,\mathrm{d}\sigma^{\mathrm{unp}}|\,n_q; m_{12}\,\rangle = 2\,\frac{\int\,\mathrm{d}\phi_q\,\mathrm{d}\phi_{12}\,\mathrm{d}\sigma^{\mathrm{unp}}(\phi_q,\phi_{12})\,\cos[n_q\phi_q + m_{12}\phi_{12}]}{\int\,\mathrm{d}\phi_q\,\mathrm{d}\phi_{12}\,\mathrm{d}\sigma^{\mathrm{unp}}(\phi_q,\phi_{12})}\,, \qquad (2.30)
$$

and

$$
\langle\,A_{LL}|\,n_q; m_{12}\,\rangle = 2\,\frac{\int\,\mathrm{d}\phi_q\,\mathrm{d}\phi_{12}\,A_{LL}\,\mathrm{d}\sigma^{\mathrm{unp}}(\phi_q,\phi_{12})\cos[n_q\phi_q + m_{12}\phi_{12}]}{\int\,\mathrm{d}\phi_q\,\mathrm{d}\phi_{12}\,\mathrm{d}\sigma^{\mathrm{unp}}(\phi_q,\phi_{12})}\,, \qquad (2.31)
$$

n_q	m_{12}	$\left\langle \mathrm{d}\sigma^{\mathrm{unp}} \middle\vert n_q; m_{12} \right\rangle$	$\left\langle A_{LL} \middle\vert n_q; m_{12} \right\rangle$
0	0	–	$\dfrac{A_L}{A_U}$
±1	0	$\dfrac{A_U^{\cos\phi_q}}{A_U}$	$\dfrac{A_L^{\cos\phi_q}}{A_U}$
±2	0	$\dfrac{A_U^{\cos 2\phi_q}}{A_U}$	0
0	±1	$\dfrac{B_U^{\cos\phi_{12}}}{A_U} \dfrac{\sum_q e_q^4\, \Delta^N D_{q^\uparrow}^{h_1}\, \Delta^N D_{\bar{q}^\uparrow}^{h_2}}{\sum_q e_q^4\, D_q^{h_1}\, D_{\bar{q}}^{h_2}}$	$\dfrac{B_L^{\cos\phi_{12}}}{A_U} \dfrac{\sum_q e_q^4\, \Delta^N D_{q^\uparrow}^{h_1}\, \Delta^N D_{\bar{q}^\uparrow}^{h_2}}{\sum_q e_q^4\, D_q^{h_1}\, D_{\bar{q}}^{h_2}}$
1	±1	$\dfrac{B_U^{\cos(\phi_q\pm\phi_{12})}}{A_U} \dfrac{\sum_q e_q^4\, \Delta^N D_{q^\uparrow}^{h_1}\, \Delta^N D_{\bar{q}^\uparrow}^{h_2}}{\sum_q e_q^4\, D_q^{h_1}\, D_{\bar{q}}^{h_2}}$	$\dfrac{B_L^{\cos(\phi_q\pm\phi_{12})}}{A_U} \dfrac{\sum_q e_q^4\, \Delta^N D_{q^\uparrow}^{h_1}\, \Delta^N D_{\bar{q}^\uparrow}^{h_2}}{\sum_q e_q^4\, D_q^{h_1}\, D_{\bar{q}}^{h_2}}$
-1	∓1	$''$	$''$
2	±1	$\dfrac{B_U^{\cos(2\phi_q\pm\phi_{12})}}{A_U} \dfrac{\sum_q e_q^4\, \Delta^N D_{q^\uparrow}^{h_1}\, \Delta^N D_{\bar{q}^\uparrow}^{h_2}}{\sum_q e_q^4\, D_q^{h_1}\, D_{\bar{q}}^{h_2}}$	0
-2	∓1	$''$	$''$

Table 2.1: Summary of the relevant azimuthal moments of the unpolarised cross section, $\mathrm{d}\sigma^{\mathrm{unp}}$, and of the longitudinal azimuthal asymmetry, A_{LL}, according to Eqs. (2.30) and (2.31).

where $n_q = 0, 1, 2$ and $m_{12} = 0, \pm1$. Notice that in the case of Eq. (2.30) the trivial case $n_q = m_{12} = 0$ will not be considered anymore. The relevant azimuthal moments are summarized in Table 2.1.

For clarity, in Table 2.1 we have simplified all the overall prefactors appearing in Eqs. (2.22) and (2.25); this is correct if we are considering the fully differential cross section, without any integration over the kinematical variables x_B, y, and ξ; however, if we want to integrate over some of the variables in order to gather further statistics, we must explicitly reinstate the corresponding prefactors in the numerator and denominator of the moments. The azimuthal moments in the first three rows of Table 2.1 do not depend (at fixed z_1 and z_2) on the fragmentation functions, therefore they do not provide any information on the Collins FF. However, they can be useful in testing the approach as far as the initial state of the process is concerned. The azimuthal moments in the rest of Table 2.1 are the ones carrying information on the Collins FF. The complete prefactor ratios multiplying the ratio of products of (Collins and unpolarised) fragmentation functions can be separately integrated over some (or even all) of the other variables (x_B, y, ζ, ξ). In doing so, the kinematical constraints described in Appendix A must be taken into

account in order to stay in the regime of validity of the approach.

Similar reasoning applies also to the more differential expression of the cross section in Eq. (2.22), where the dependence on the moduli of the hadron transverse momenta with respect to the parent quarks(antiquarks) is still explicit.

Let us also recall that the two angles entering the azimuthal moments, ϕ_q and ϕ_{12}, are measured around different, well-distinct, (light-cone) directions, the first one being the azimuthal angle of the q-$\bar{q}$ plane (relative to the leptonic plane) around the direction of motion of the two colliding photons in their c.m. frame, while the second one is the difference among the azimuthal angles of the two final hadrons around the parent quark(antiquark) direction of motion (coinciding with the jet thrust-axis in our leading order approach).

From the phenomenological point of view, it is important to stress that the ratio of combinations of Collins and unpolarised fragmentation functions appearing in Table 2.1 is the same one involved in the e^+e^- SIA process, $e^+e^- \to h_1\, h_2 + X$, with the important difference that the fractional charge relative weight among different flavours is 16:1:1 in our case and 4:1:1 in the SIA case, respectively for u, d, s flavours. Therefore, the analysis of the process considered here would contribute to better disentangle the flavour dependence of the Collins FF, especially for u quarks. In fact, this is one of the main motivations for considering this observable in future photon-photon colliders. A second important benefit, once the already available full TMD scale evolution scheme will be implemented, is to study the scale dependence of the TMD Collins FF within the same process and experimental setup by varying the virtuality of the DIS photon.

2.1.3 Preliminary Results

[1] In this section we will present some preliminary estimates for the azimuthal moments of the cross section and the double longitudinal asymmetry displayed in Table 2.1 for the two-pion production case. In order to collect more statistics, we will present results for the azimuthal moments for like-charged ($\pi^+\pi^+ + \pi^-\pi^-$) and unlike-charged ($\pi^+\pi^- + \pi^-\pi^+$) pion pairs, at different fixed values of Q^2, as a function of z_2 in bins of z_1 (similarly to what is done for Belle data in SIA e^+e^- annihilations). All the other variables will be properly integrated over the allowed kinematical range. Let us notice first that the integration over the variable ζ in the coefficients $A_{U,L}$, Eq. (2.23), and $B_{U,L}$, Eq. (2.24), can be performed analytically. Since the allowed kinematic range for ζ, Eq. (A.22), is symmetric, two of the coefficients, $A_{U,L}^{\cos\phi_q}$, that are antisymmetric in ζ, will vanish once integrated over the full range. Therefore, for these two cases, we integrate only over half the allowed range. Accordingly, the same is due for A_U (which is clearly symmetric in ζ) when evaluating the corresponding azimuthal moments. At fixed Q^2 and x_B, $y = Q^2/(x_B\, s)$ is also fixed. The remaining integrations on x_B, ξ and z_1 (in the chosen bin) are performed numerically.

[1] We would like to thank Dr. Carlo Flore for his collaboration on this section.

The evaluation of the coefficients $A_{U,L}$, $B_{U,L}$ requires an explicit expression of the unpolarised and longitudinally polarized WW photon distributions. We will adopt the results of Refs. [82, 83]:

$$f_{\gamma/\ell}(\xi) \;=\; \frac{\alpha}{2\pi}\left[\frac{1+(1-\xi)^2}{\xi}\,\ln\!\left(\frac{Q^2_{\rm max}}{Q^2_{\rm min}}\right) + 2m_e^2\,\xi\left(\frac{1}{Q^2_{\rm max}}-\frac{1}{Q^2_{\rm min}}\right)\right], \tag{2.32}$$

$$\Delta_L f_{\gamma/\ell}(\xi) = \frac{\alpha}{2\pi}\left[\frac{1-(1-\xi)^2}{\xi}\,\ln\left(\frac{Q^2_{\rm max}}{Q^2_{\rm min}}\right) + 2m_e^2\,\xi^2\left(\frac{1}{Q^2_{\rm max}}-\frac{1}{Q^2_{\rm min}}\right)\right], \tag{2.33}$$

where

$$Q^2_{\rm min} \;=\; \frac{m_e^2\,\xi^2}{1-\xi}, \qquad\qquad Q^2_{\rm max} \;=\; \frac{s}{4}\,\theta_c^2\,(1-\xi) + Q^2_{\rm min}\,. \tag{2.34}$$

Here θ_c is the maximum deflection angle of the photon from the flight direction of the emitting lepton in the cm frame, and depends on the experimental setup. As an example, in Table 2.2 we report the expected values of a few relevant parameters of interest for some of the proposed future lepton colliders (see Ref. [84] for more details).

Facility	$\sqrt{s}$ [GeV]	θ_c [mrad]	$\int \mathrm{d}t\,\mathcal{L}$ [ab^{-1}/year]
FCC-ee	92	30	17
CEPC	92	33	15
ILC	500	14	0.3
CLIC	3000	20	0.6

Table 2.2: Summary of some selected tentative parameters for proposed future lepton colliders [84].

To proceed we also need a parametrisation of the collinear unpolarised pion fragmentation functions and of the first $p_\perp$-moment of the Collins TMD FFs. To this end we will adopt the recent parametrization proposed in Ref. [85], obtained by fitting available results for the pion Collins asymmetry coming from SIDIS and e^+e^- SIA data.

The unpolarized TMD fragmentation function is parametrized with a simple factorized Gaussian ansatz:

$$D_q^h(z,p_\perp) \;=\; D_q^h(z)\,\frac{e^{-\,p_\perp^2/\langle\,p_\perp^2\,\rangle}}{\pi\,\langle\,p_\perp^2\,\rangle}\,, \tag{2.35}$$

where $\langle\,p_\perp^2\,\rangle \;=\; 0.12$ GeV^2, as extracted from a fit to HERMES multiplicities [86], and for the collinear FFs the set by de Florian, Sassot and Stratmann (DSS) has been adopted [87].

The Collins FF has been taken proportional to the corresponding TMD FF times a factorized, Gaussian-like $p_\perp$-dependent factor:

$$\Delta^N D_{q^\uparrow}^h(z,p_\perp) \;=\; \mathcal{N}_q^C(z)\,\frac{p_\perp}{M_C}\,2\sqrt{2\,e}\,e^{-p_\perp^2/M_C^2}\,D_q^h(z,p_\perp)\,, \tag{2.36}$$

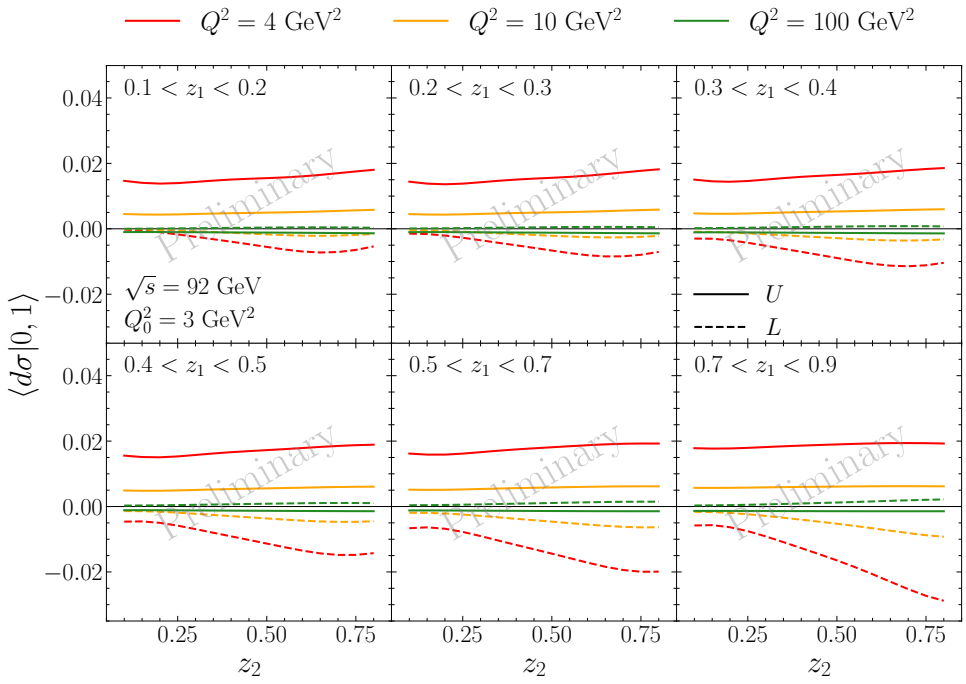

Figure 2.2: Preliminary estimates of the azimuthal moment $\langle \mathrm{d}\sigma^{\mathrm{unp}} \,|\, 0,1 \rangle$ for unlike-charged (U) and like-charged (L) combinations of pion pairs for the kinematical setup of FCC-ee, Table 2.2, at several fixed values of Q^2, as a function of z_2 and in bins of z_1.

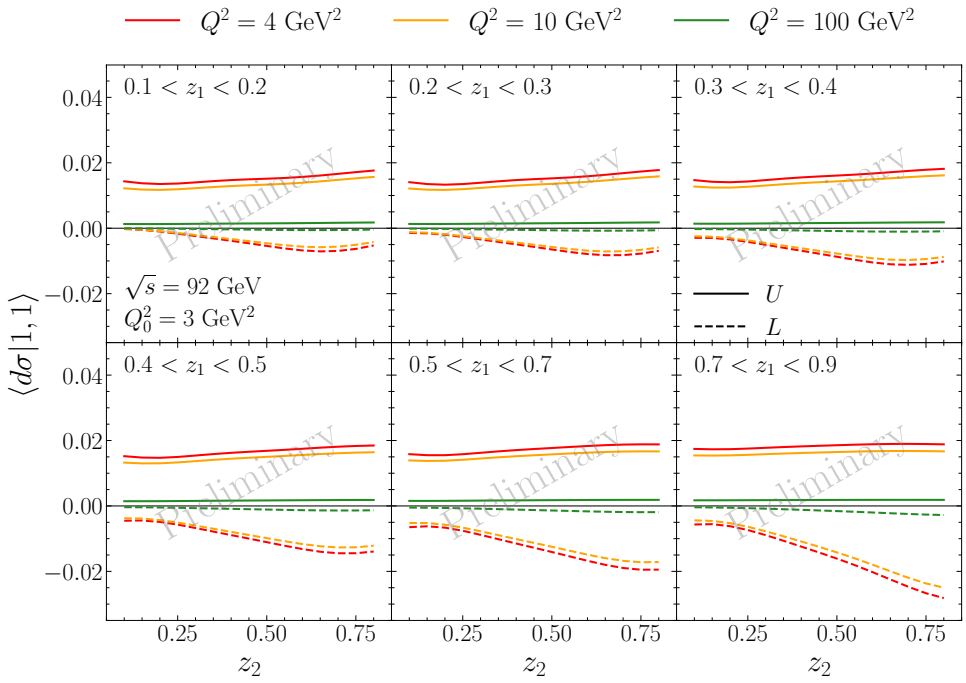

Figure 2.3: Preliminary estimates of the azimuthal moment $\langle \mathrm{d}\sigma^{\mathrm{unp}} \,|\, 1,1 \rangle$ for unlike-charged (U) and like-charged (L) combinations of pion pairs for the kinematical setup of FCC-ee, Table 2.2, at several fixed values of Q^2, as a function of z_2 and in bins of z_1.

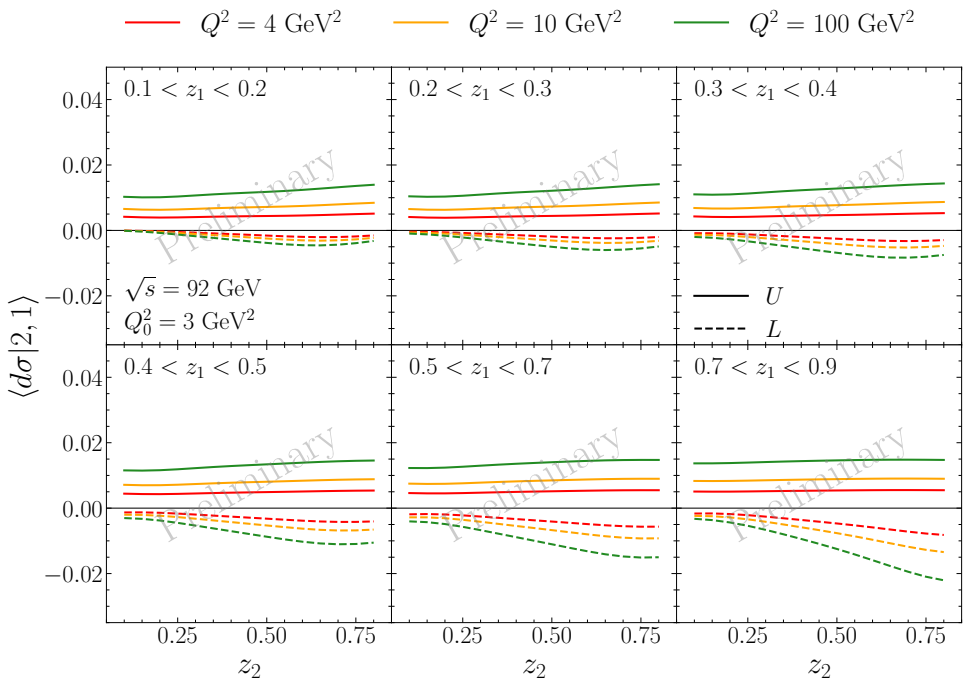

Figure 2.4: Preliminary estimates of the azimuthal moment $\langle \, \mathrm{d}\sigma^{\mathrm{unp}} \, | \, 2, 1 \, \rangle$ for unlike-charged (U) and like-charged (L) combinations of pion pairs for the kinematical setup of FCC-ee, Table 2.2, at several fixed values of Q^2, as a function of z_2 and in bins of z_1.

where the flavour q is limited to the favoured (e.g. $D_u^{\pi^+}$) and unfavoured (e.g. $D_d^{\pi^+}$) cases, M_C is a free parameter with mass dimension, $\mathcal{N}^C_{\mathrm{fav}}(z) = \mathcal{N}^C_{\mathrm{fav}}\, z^\gamma$, $\mathcal{N}^C_{\mathrm{unf}}(z) = \mathcal{N}^C_{\mathrm{unf}}$. See Refs. [85, 86] and references therein for more details on the fit procedure, the value of the fit parameters and their statistical uncertainties.

Scale evolution is taken into account through a simplified scheme, applying DGLAP evolution to the collinear components of the TMD FFs. As said, the implementation of the proper TMD evolution within the Collins-Soper-Sterman approach is already available for two-hadron production in e^+e^- SIA processes and can be applied also to this case. This is left as a future development in view of more detailed phenomenological analyses. Notice in any case that, based on the present phenomenological information coming from SIDIS, e^+e^- annihilations and DY processes, scale evolution effects appear to be mild for spin and azimuthal asymmetries.

In Figs. 2.2-2.4 we present, for the tentative FCC-ee kinematical setup of Table 2.2, estimates for some of the azimuthal moments of the unpolarised differential cross section $\mathrm{d}\sigma^{\mathrm{unp}}/\mathrm{d}Q^2\, \mathrm{d}z_1\, dz_2$, at different fixed values of the tagged photon virtuality Q^2, as a function of z_2 and in bins of z_1, integrated over the other variables in the allowed range.

In this preliminary analysis we present only the central-value curves of our estimates, postponing to future more extensive studies a detailed investigation on the statistical uncertainties of our results and the determination of statistical error bands.

In Figs. 2.5-2.6 we present similar preliminary results for two azimuthal moments,

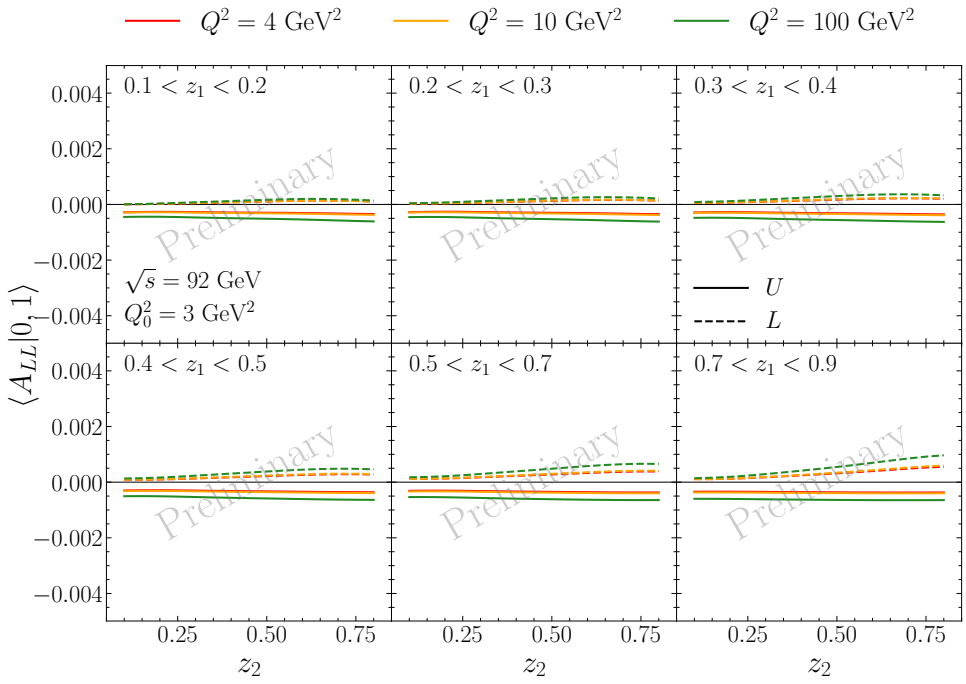

Figure 2.5: Preliminary estimates of the azimuthal moment $\langle A_{LL} \,|\, 0, 1 \rangle$ for unlike-charged (U) and like-charged (L) combinations of pion pairs for the kinematical setup of FCC-ee, Table 2.2, at several fixed values of Q^2, as a function of z_2 and in bins of z_1.

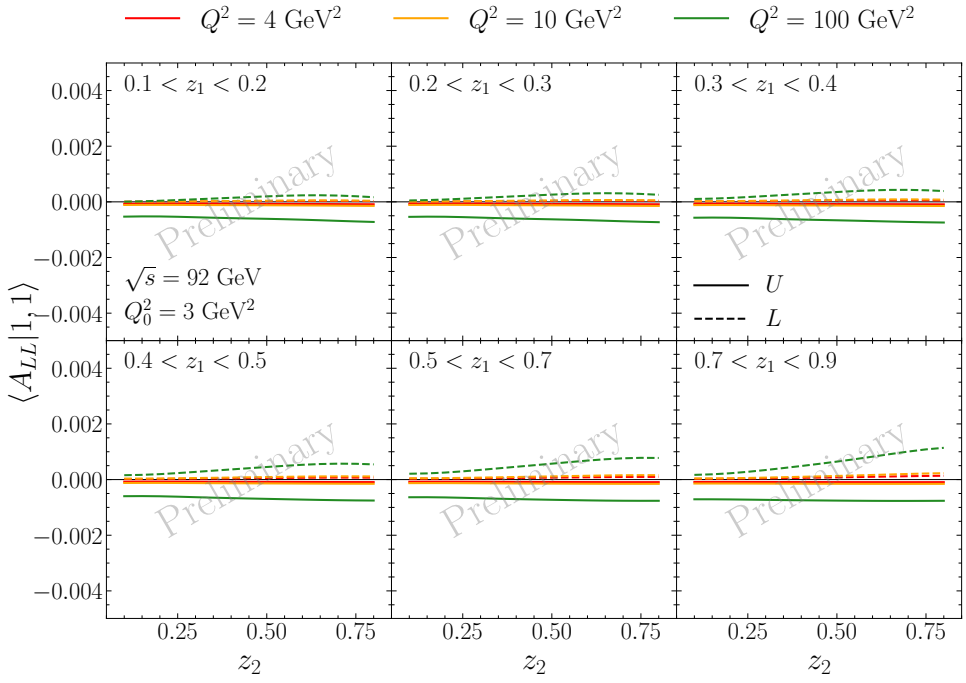

Figure 2.6: Preliminary estimates of the azimuthal moment $\langle A_{LL} \,|\, 1, 1 \rangle$ for unlike-charged (U) and like-charged (L) combinations of pion pairs for the kinematical setup of FCC-ee, Table 2.2, at several fixed values of Q^2, as a function of z_2 and in bins of z_1.

$\langle A_{LL} \,|\, 0,1 \rangle$ and $\langle A_{LL} \,|\, 1,1 \rangle$, of the double longitudinal spin asymmetry A_{LL}.

As a general comment, in these kinematical setup the azimuthal moments of the unpolarised cross section seem to be small but, at least in some case, of the order of a few percent in size, that might be at reach of future experiments. Concerning A_{LL}, the two moments considered are of the order of a few per mille in size and therefore unlikely to be measurable.

Notice that the size of the moments depends not only on the ratio of weighted combinations of Collins and unpolarised fragmentation functions, but also on the prefactor, related to ratios of the corresponding $A_{U,L}$, $B_{U,L}$ coefficients. The size of these prefactors depend crucially on the considered range of values of the variables Q^2, x_B, ξ. A complete careful study of the allowed variable phase-space is therefore mandatory in order to possibly maximize the size of the azimuthal moments and to properly determine the potential role of these observables in improving our phenomenological knowledge of the TMD fragmentation functions. At the same time one has also to verify that the unpolarised cross section is not excessively suppressed in these phase-space regions. This more in-depth study is currently in progress and will hopefully be completed soon.

2.2 Hadron-pair production in two quasi-real photon collisions

In this section, adopting the same formalism as in the previous ones, we will discuss the production of two unpolarized, almost back-to-back hadrons in quasi-real photon-photon collisions at lepton colliders. At variance with the previous case, therefore, here both final leptons are undetected. The derivation of the cross section and the azimuthal asymmetries around the thrust-axis will follow the same lines as in the $\gamma^*\gamma$ case, therefore we will restrict ourself to the essential steps of the calculation.

For completeness, a similar derivation in the case of ultraperipheral heavy-ion collisions at hadron colliders (LHC, RHIC), adopting a more general (and common in the literature) scheme involving hadronic correlators and Sudakov decompositions for the kinematics will be discussed in Sec. 2.3.

The process under consideration is the following:

$$\ell^+(l_+)\,\ell^-(l_-) \;\to\; \gamma_1(q_1^2=0)\,\gamma_2(q_2^2=0) \;\to\; q(K_q)\,\bar{q}(K_{\bar{q}}) \;\to\; h_1(P_1)\,h_2(P_2) \,+\, X\,. \quad (2.37)$$

Again, the invariant differential cross section for the process can be written as follows:

$$\begin{aligned}\mathrm{d}\sigma^{\ell^+\ell^-\to h_1\,h_2\,X} = {}& \frac{1}{4\,(l_+\cdot l_-)}\,\frac{\mathrm{d}^3\boldsymbol{K}_q}{2(2\pi)^3 K_q^0}\,\frac{\mathrm{d}^3\boldsymbol{K}_{\bar{q}}}{2(2\pi)^3 K_{\bar{q}}^0}\,(2\pi)^4\,\delta^{(4)}(q_1+q_2-K_q-K_{\bar{q}}) \\ & \times \sum_q \sum_{\{\lambda_i\}} \rho_{\lambda_1,\lambda_1'}(\gamma_1)\,\rho_{\lambda_2,\lambda_2'}(\gamma_2)\,f_{\gamma_1/\ell^+,\mathcal{P}^{\ell^+}_{\hat{z}_+}}(\xi_1)\,\frac{\mathrm{d}\xi_1}{\xi_1}\,f_{\gamma_2/\ell^-,\mathcal{P}^{\ell^-}_{\hat{z}_-}}(\xi_2)\,\frac{\mathrm{d}\xi_2}{\xi_2}\end{aligned}$$

$$\times\, \hat{H}_{\lambda_q,\lambda_{\bar{q}};\lambda_1,\lambda_2}\, \hat{H}^*_{\lambda'_q,\lambda'_{\bar{q}};\lambda'_1,\lambda'_2}\, \hat{D}^{h_1}_{\lambda_q,\lambda'_q}(z_1,\boldsymbol{p}_{\perp 1})\, \mathrm{d}z_1 \mathrm{d}^2\boldsymbol{p}_{\perp 1}\, \hat{D}^{h_2}_{\lambda_{\bar{q}},\lambda'_{\bar{q}}}(z_2,\boldsymbol{p}_{\perp 2})\, \mathrm{d}z_2 \mathrm{d}^2\boldsymbol{p}_{\perp 2}\,, \tag{2.38}$$

where the meaning of all factors has been already illustrated in the previous sections. The first line includes all kinematical factors, the initial flux and the Lorentz invariant phase-space factors for the two observed jets (that in our leading order approach are identified with the final quark and antiquark in the hard partonic process). The second and third lines include all dynamical factors and will be denoted as the Kernel of Eq. (2.38) in the sequel.

In the leptonic center of mass reference frame, we have:

$$\begin{aligned} l_+ &= \frac{\sqrt{s}}{2}\,(1,0,0,1)\,, \qquad l_- = \frac{\sqrt{s}}{2}\,(1,0,0,-1) \\ q_1 &= \xi_1\,\frac{\sqrt{s}}{2}\,(1,0,0,1)\,, \qquad q_2 = \xi_2\,\frac{\sqrt{s}}{2}\,(1,0,0,-1) \\ q_1+q_2 &= \frac{\sqrt{s}}{2}\,(\xi_1+\xi_2,0,0,\xi_1-\xi_2) \\ K_{q,\bar{q}} &= K_T\,(\cosh\eta_{q,\bar{q}},\pm\cos\phi_q,\pm\sin\phi_q,\sinh\eta_{q,\bar{q}})\,, \end{aligned} \tag{2.39}$$

where ϕ_q is the azimuthal angle of the plane containing the thrust axis with respect to the xz-plane of the chosen cm frame. Moreover, $K_T = |\boldsymbol{K}_T|$, with $\boldsymbol{K}_T = K_T\,(\cos\phi_q,\sin\phi_q)$.

From Eq. (2.39) we see that the total energy in the partonic center of mass reference frame is $\sqrt{\hat{s}} = \xi_1\,\xi_2\,s$. Moreover, in this frame,

$$\begin{aligned} q_1 &= \frac{\sqrt{\hat{s}}}{2}\,(1,0,0,1)\,, \qquad q_2 = \frac{\sqrt{\hat{s}}}{2}\,(1,0,0,-1) \\ K_{q,\bar{q}} &= K_T(\cosh\hat{\eta},\pm\cos\phi_q,\pm\sin\phi_q,\pm\sinh\hat{\eta})\,, \end{aligned} \tag{2.40}$$

since in this frame $\eta_q \equiv \hat{\eta} = -\eta_{\bar{q}}$.

Let us now consider the kinematic factors in the first line of Eq. (2.38). The flux factor $4\,(l_+\cdot l_-) = s/2$. Working in the leptonic cm frame, the four-dimensional Dirac delta can be easily decomposed as follows:

$$\begin{aligned} \delta^{(4)}(q_1+q_2-K_q-K_{\bar{q}}) &= \frac{2}{s}\,\delta\Big(\xi_1 - \frac{K_T}{\sqrt{s}}\left(e^{\eta_q}+e^{\eta_{\bar{q}}}\right)\Big) \\ \times\,\delta\Big(\xi_2 - \frac{K_T}{\sqrt{s}}\left(e^{-\eta_q}+e^{-\eta_{\bar{q}}}\right)\Big)\,&\delta^{(2)}\Big(-\boldsymbol{K}_{q\,T}-\boldsymbol{K}_{\bar{q}\,T}\Big)\,. \end{aligned} \tag{2.41}$$

Therefore, in this case the light-cone fractions $\xi_{1,2}$ of the quasi-real photons are fixed once we know the transverse momentum K_T and the (pseudo)rapidities $\eta_{q,\bar{q}}$ of the two jets originating from the $q,\bar{q}$ fragmentation. Precisely,

$$\bar{\xi}_1 = \frac{K_T}{\sqrt{s}}\left(e^{\eta_q}+e^{\eta_{\bar{q}}}\right), \qquad \bar{\xi}_2 = \frac{K_T}{\sqrt{s}}\left(e^{-\eta_q}+e^{-\eta_{\bar{q}}}\right). \tag{2.42}$$

Clearly, the remaining two-dimensional Dirac delta in Eq. (2.41) gives

$$\boldsymbol{K}_{qT} \,=\, \boldsymbol{K}_T \,=\, -\boldsymbol{K}_{\bar{q}T}\,, \tag{2.43}$$

as it was anticipated in Eqs. (2.39), (2.40).

Let us consider now the factor

$$\begin{aligned}
&\frac{\mathrm{d}^3\boldsymbol{K}_q}{2(2\pi)^3\,K_q^0}\,\frac{\mathrm{d}^3\boldsymbol{K}_{\bar{q}}}{2(2\pi)^3 K_{\bar{q}}^0}\,\delta^{(2)}\Big(-\boldsymbol{K}_{qT}-\boldsymbol{K}_{\bar{q}T}\Big) \\
&=\,\frac{1}{2^8\,\pi^6}\,\frac{\mathrm{d}K_q^3\,\mathrm{d}^2\boldsymbol{K}_{qT}}{K_q^0}\,\frac{\mathrm{d}K_{\bar{q}}^3\,\mathrm{d}^2\boldsymbol{K}_{\bar{q}T}}{K_{\bar{q}}^0}\,\delta^{(2)}\Big(-\boldsymbol{K}_{qT}-\boldsymbol{K}_{\bar{q}T}\Big) &(2.44)\\
&=\,\frac{1}{2^8\,\pi^6}\,\mathrm{d}^2\boldsymbol{K}_T\,\mathrm{d}\eta_q\,\mathrm{d}\eta_{\bar{q}}\,, &(2.45)
\end{aligned}$$

where we have used Eq. (2.40) to set $\mathrm{d}K_{q,\bar{q}}^3/K_{q,\bar{q}}^0 \,=\, \mathrm{d}\eta_{q,\bar{q}}$.

The expression of the differential cross section (2.38) can therefore be written as:

$$\begin{aligned}
\mathrm{d}\sigma^{\ell^+\ell^-\to h_1\,h_2\,X} \,&=\, \frac{1}{2\,s}\,\frac{2}{s}\,\delta\Big(\,\xi_1\,-\,\frac{K_T}{\sqrt{s}}\,\Big(e^{\eta_q}\,+\,e^{\eta_{\bar{q}}}\Big)\Big)\,\delta\Big(\,\xi_2\,-\,\frac{K_T}{\sqrt{s}}\,\Big(e^{-\eta_q}\,+\,e^{-\eta_{\bar{q}}}\Big)\Big) \\
&\times\,(2\pi)^4\,\frac{1}{2^8\,\pi^6}\,\mathrm{d}^2\boldsymbol{K}_T\,\mathrm{d}\eta_q\,\mathrm{d}\eta_{\bar{q}}\,\frac{\mathrm{d}\xi_1}{\xi_1}\,\frac{\mathrm{d}\xi_2}{\xi_2}\,\times\,\text{Kernel} \\
&=\,\frac{1}{16\,\pi^2\,s^2}\,\frac{1}{\bar{\xi}_1\,\bar{\xi}_2}\,\mathrm{d}^2\boldsymbol{K}_T\,\mathrm{d}\eta_q\,\mathrm{d}\eta_{\bar{q}}\,\times\,\text{Kernel}\,. &(2.46)
\end{aligned}$$

Furthermore, from Eq. (2.42),

$$\frac{1}{\bar{\xi}_1\,\bar{\xi}_2} \,=\, \frac{s}{K_T^2}\,\frac{1}{2\,[\,1+\cosh(\eta_q\,-\,\eta_{\bar{q}})\,]}\,, \tag{2.47}$$

so that

$$\frac{\mathrm{d}\sigma^{\ell^+\ell^-\to h_1\,h_2\,X}}{\mathrm{d}^2\boldsymbol{K}_T\,\mathrm{d}\eta_q\,\mathrm{d}\eta_{\bar{q}}} \,=\, \frac{1}{32\,\pi^2\,s\,K_T^2}\,\frac{1}{1+\cosh(\eta_q\,-\,\eta_{\bar{q}})}\,\times\,\text{Kernel}\,. \tag{2.48}$$

Let us now consider all the factors in the dynamical Kernel, as defined in the last two lines of Eq. (2.38). Since they were already discussed in details in the previous sections, we will only briefly recall the main steps of the calculation here.

The normalized helicity density matrix of the two quasi-real photons reduces to

$$\rho(\gamma_i) = \frac{1}{2}\begin{pmatrix} 1+\mathcal{P}_{\hat{z}_i}^{\gamma_i} & 0 \\ 0 & 1-\mathcal{P}_{\hat{z}_i}^{\gamma_i} \end{pmatrix}. \tag{2.49}$$

Due to parity conservation, only two combinations of the photon WW distribution inside the initial leptons may appear in the Kernel:

$$\Big[\,\rho_{++}(\gamma_i)\,+\,\rho_{--}(\gamma_i)\,\Big]\,f_{\gamma_i/\ell^\pm,\mathcal{P}_\pm}(\bar{\xi}_i)$$

$$= f_{\gamma_i,+/\ell^\pm,\mathcal{P}_\pm}(\bar{\xi}_i) + f_{\gamma_i,-/\ell^\pm,\mathcal{P}_\pm}(\bar{\xi}_i) \equiv f_{\gamma_i/\ell^\pm}(\bar{\xi}_i)\,, \tag{2.50}$$

and

$$\begin{aligned}&\Big[\rho_{++}(\gamma_i) - \rho_{--}(\gamma_i)\Big] f_{\gamma_i/\ell^\pm,\mathcal{P}_\pm}(\bar{\xi}_i)\\ &= f_{\gamma_i,+/\ell^\pm,\mathcal{P}_\pm}(\bar{\xi}_i) - f_{\gamma_i,-/\ell^\pm,\mathcal{P}_\pm}(\bar{\xi}_i) \equiv \mathcal{P}_\pm\,\Delta_L f_{\gamma_i/\ell^\pm}(\bar{\xi}_i)\,,\end{aligned} \tag{2.51}$$

where as done previously we use the shorthand notation $\mathcal{P}_\pm \equiv \mathcal{P}^{\ell^\pm}_{\hat{z}_\pm}$ for the longitudinal component of the lepton polarization vectors (in their proper helicity reference frame), with $\mathcal{P}_i = 0, \pm 1$.

Concerning the helicity amplitudes for the hard partonic scattering,

$$\gamma_1(q_1,\lambda_1)\,\gamma_2(q_2,\lambda_2) \to q(K_q,\lambda_q)\,\bar{q}(K_{\bar{q}},\lambda_{\bar{q}})\,, \tag{2.52}$$

they can be directly recovered from the ones for the $\gamma^*\gamma$ case, Eq. (2.15), by simply taking the limit $Q^2 = -q_1^2 \to 0$. As a result, only four amplitudes are non vanishing (in the massless limit considered here) and due to parity conservation only two of them are independent:

$$\begin{aligned}\hat{H}_{+-;1,-1} &= -\hat{H}^*_{-+;-1,1} = -2\sqrt{3}\,e^2\,e_q^2\,e^{i2\phi_q}\,e^{(\eta_q-\eta_{\bar{q}})/2}\\ \hat{H}_{+-;-1,1} &= -\hat{H}^*_{-+;1,-1} = 2\sqrt{3}\,e^2\,e_q^2\,e^{-i2\phi_q}\,e^{-(\eta_q-\eta_{\bar{q}})/2}\,.\end{aligned} \tag{2.53}$$

Regarding the fragmentation sector, as in the previous case for (pseudo)scalar or unpolarized hadrons only two terms contribute to the kernel, involving respectively the product of the unpolarized fragmentation functions, $D_q^{h_1}(z_1,p_{\perp 1})\,D_{\bar{q}}^{h_2}(z_2,p_{\perp 2})$, and that of the Collins FFs, $\Delta^N D_{q^\uparrow}^{h_1}(z_1,p_{\perp 1})\,\Delta^N D_{\bar{q}^\uparrow}^{h_2}(z_2,p_{\perp 2})$, for the final quarks and antiquarks.

Inserting all these ingredients into Eq. (2.54), after some calculations, we finally get:

$$\begin{aligned}\frac{\mathrm{d}\sigma^{\ell^+\ell^-\to h_1\,h_2\,X}(\mathcal{P}_+,\mathcal{P}_-)}{\mathrm{d}^2\boldsymbol{K}_T\,\mathrm{d}\eta_q\,\mathrm{d}\eta_{\bar{q}}\,\mathrm{d}z_1\,\mathrm{d}^2\boldsymbol{p}_{\perp 1}\,\mathrm{d}z_2\,\mathrm{d}^2\boldsymbol{p}_{\perp 2}} &= \frac{6\,\alpha^2}{s\,K_T^2}\,\frac{1}{1+\cosh(\eta_q-\eta_{\bar{q}})}\sum_q e_q^4\\ &\times\Big\{f_{\gamma/\ell}(\bar{\xi}_1)\,f_{\gamma/\ell}(\bar{\xi}_2) - \mathcal{P}_+\,\mathcal{P}_-\,\Delta_L f_{\gamma/\ell}(\bar{\xi}_1)\,\Delta_L f_{\gamma/\ell}(\bar{\xi}_2)\Big\}\\ &\times\Big\{\cosh(\eta_q-\eta_{\bar{q}})\,D_q^{h_1}(z_1,p_{\perp 1})\,D_{\bar{q}}^{h_2}(z_2,p_{\perp 2})\\ &+\frac{1}{4}\cos(\phi_q^{h_1}-\phi_{\bar{q}}^{h_2})\,\Delta^N D_{q^\uparrow}^{h_1}(z_1,p_{\perp 1})\,\Delta^N D_{\bar{q}^\uparrow}^{h_2}(z_2,p_{\perp 2})\Big\}\,.\end{aligned} \tag{2.54}$$

We recall that $\phi_q^{h_1}$ and $\phi_{\bar{q}}^{h_2}$ are respectively the azimuthal angles of the two hadrons around the direction of motion of the parent quark/antiquark as measured in their helicity reference frame.

Notice that, at variance with the more complex $\gamma^*\gamma$ case, here the unpolarized and longitudinally polarized WW distributions multiply the same factors related to the fragmentation functions, therefore their contributions are simply additive.

By introducing again the variables

$$\zeta_q \equiv \zeta = \frac{1}{1+e^{\eta_q-\eta_{\bar{q}}}} \qquad \zeta_{\bar{q}} = 1-\zeta = \frac{1}{1+e^{-(\eta_q-\eta_{\bar{q}})}}\,, \tag{2.55}$$

it is also easy to see that

$$\frac{\cosh(\eta_q - \eta_{\bar{q}})}{1 + \cosh(\eta_q - \eta_{\bar{q}})} = \zeta^2 + (1-\zeta)^2\,,$$
$$\frac{1}{1 + \cosh(\eta_q - \eta_{\bar{q}})} = 2\,\zeta\,(1-\zeta)\,. \tag{2.56}$$

Therefore, Eq. (2.54) agrees, with the obvious changes in the notation, with Eq. (2.93) for the case of heavy-ion ultraperipheral collisions. Notice that there the azimuthal angles $\phi_{1,2}$ are both measured around the chosen light-cone direction, while in our case, as said, $\phi_q^{h_1}$, $\phi_{\bar{q}}^{h_2}$ are each measured around the $\hat{z}$ axis of the parent parton helicity frame, therefore, $\phi_q^{h_1} = \phi_1$, $\phi_{\bar{q}}^{h_2} = 2\,\pi - \phi_2$.

Since $K_T = |\boldsymbol{K}_T|$ plays the role of the hard scale for this process, to guarantee the validity of the TMD approach we require that $K_T \geq K_0 \gg \Lambda_{\rm QCD}$, where K_0 is a convenient reference hard scale. Therefore, the allowed range of values for K_T is

$$K_0 \leq K_T \leq \frac{\sqrt{s}}{2}\,, \tag{2.57}$$

with $K_T = \sqrt{s}/2$ corresponding to the limit $\eta_q = \eta_{\bar{q}} = 0$ and $\bar{\xi}_1 = \bar{\xi}_2 = 1$. Furthermore, one can see that at fixed s and K_T, it must be

$$\log\left\{\frac{1}{2}\left[\frac{\sqrt{s}}{K_T} - \sqrt{\frac{s}{K_T^2} - 4}\right]\right\} \leq \eta_q \leq \log\left\{\frac{1}{2}\left[\frac{\sqrt{s}}{K_T} + \sqrt{\frac{s}{K_T^2} - 4}\right]\right\}. \tag{2.58}$$

Notice that $\sqrt{s}/K_T \geq 2$,because of Eq. (2.57). Finally, at fixed η_q within the range (2.58), one has

$$-\log\left(\frac{\sqrt{s}}{K_T} - e^{-\eta_q}\right) \leq \eta_{\bar{q}} \leq \log\left(\frac{\sqrt{s}}{K_T} - e^{\eta_q}\right). \tag{2.59}$$

The allowed phase space for η_q and $\eta_{\bar{q}}$ is clearly symmetric.

To collect more statistics, we can first consider that

$$\mathrm{d}^2\boldsymbol{K}_T = K_T\,\mathrm{d}K_T\,\mathrm{d}\phi_q = (1/2)\,\mathrm{d}K_T^2\,\mathrm{d}\phi_q\,.$$

Using the fact that the differential cross section (2.54) is independent of ϕ_q, we can integrate over it and simply get an additional 2π factor on the right-hand side. Moreover, using Eqs. (2.21) and (2.22), and performing the substitution $(\phi_q^{h_1}, \phi_{\bar{q}}^{h_2}) \to (\phi_q^{h_1}, \phi_q^{h_1} - \phi_{\bar{q}}^{h_2} \equiv \phi_{12})$ we can write

$$\int \mathrm{d}^2\boldsymbol{p}_{\perp 1} \int \mathrm{d}^2\boldsymbol{p}_{\perp 1}\, D_q^{h_1}(z_1, p_{\perp 1})\, D_{\bar{q}}^{h_2}(z_2, p_{\perp 2}) = D_q^{h_1}(z_1)\, D_{\bar{q}}^{h_2}(z_2)\,,$$
$$\int \mathrm{d}^2\boldsymbol{p}_{\perp 1} \int \mathrm{d}^2\boldsymbol{p}_{\perp 1}\, \Delta^N D_{q^\uparrow}^{h_1}(z_1, p_{\perp 1})\, \Delta^N D_{\bar{q}^\uparrow}^{h_2}(z_2, p_{\perp 2})$$
$$= \frac{1}{2\pi}\, \Delta^N D_{q^\uparrow}^{h_1}(z_1)\, \Delta^N D_{\bar{q}^\uparrow}^{h_2}(z_2)\, \mathrm{d}\phi_{12}\,. \tag{2.60}$$

Inserting these results into Eq. (2.54) we therefore get the less differential cross section

$$\begin{aligned}\frac{\mathrm{d}\sigma^{\ell^+\ell^-\to h_1\,h_2\,X}(\mathcal{P}_+,\mathcal{P}_-)}{\mathrm{d}\boldsymbol{K}_T^2\,\mathrm{d}\eta_q\,\mathrm{d}\eta_{\bar q}\,\mathrm{d}z_1\,\mathrm{d}z_2\,\mathrm{d}\phi_{12}} &= \frac{3\,\alpha^2}{s\,\boldsymbol{K}_T^2}\,\frac{1}{1+\cosh(\eta_q\,-\,\eta_{\bar q})}\,\sum_q e_q^4 \\ &\times\Big\{\,f_{\gamma/\ell}(\bar\xi_1)\,f_{\gamma/\ell}(\bar\xi_2)\;-\;\mathcal{P}_+\,\mathcal{P}_-\,\Delta_L f_{\gamma/\ell}(\bar\xi_1)\,\Delta_L f_{\gamma/\ell}(\bar\xi_2)\,\Big\} \\ &\times\Big\{\,\cosh(\eta_q\,-\,\eta_{\bar q})\,D_q^{h_1}(z_1)\,D_{\bar q}^{h_2}(z_2) \\ &+\;\frac{1}{4}\,\cos\phi_{12}\,\Delta^N D_{q^\uparrow}^{h_1}(z_1)\,\Delta^N D_{\bar q^\uparrow}^{h_2}(z_2)\,\Big\}. \end{aligned} \tag{2.61}$$

Using again as shortand notation for the differential cross section $\mathrm{d}\sigma(\mathcal{P}_+,\mathcal{P}_-)$, we can write

$$\begin{aligned}\mathrm{d}\sigma^{\mathrm{unp}} &= \frac{1}{2}\,\big[\,\mathrm{d}\sigma(+,+)\;+\;\mathrm{d}\sigma(+,-)\big]\,, \\ \mathrm{d}\Delta_L\sigma &= \mathrm{d}\sigma(+,+)\;-\;\mathrm{d}\sigma(+,-)\,, \end{aligned} \tag{2.62}$$

and define the double longitudinal spin asymmetry

$$A_{LL} \;=\; \frac{\mathrm{d}\sigma(+,+)\;-\;\mathrm{d}\sigma(+,-)}{\mathrm{d}\sigma(+,+)\;+\;\mathrm{d}\sigma(+,-)} \;=\; \frac{\mathrm{d}\Delta_L\sigma}{2\,\mathrm{d}\sigma^{\mathrm{unp}}}\,. \tag{2.63}$$

We can also define, as usual, the azimuthal moments of the differential cross section $\mathrm{d}\sigma^{\mathrm{unp}}$ and the double longitudinal spin asymmetry A_{LL}:

$$\begin{aligned}\langle\,\mathrm{d}\sigma^{\mathrm{unp}}\,|\,\cos\phi_{12}\,\rangle &= 2\,\frac{\int\mathrm{d}\phi_{12}\;\cos\phi_{12}\,\mathrm{d}\sigma^{\mathrm{unp}}}{\int\mathrm{d}\phi_{12}\,\mathrm{d}\sigma^{\mathrm{unp}}} \\ &= \frac{1}{4\,\cosh(\eta_q\,-\,\eta_{\bar q})}\,\frac{\sum_q\,e_q^4\,\Delta^N D_{q^\uparrow}^{h_1}(z_1)\,\Delta^N D_{\bar q^\uparrow}^{h_2}(z_2)}{\sum_q\,e_q^4\,D_q^{h_1}(z_1)\,D_{\bar q}^{h_2}(z_2)}\,, \end{aligned}$$

$$\begin{aligned}\langle\,A_{LL}\,|\,\cos\phi_{12}\,\rangle &= 2\,\frac{\int\mathrm{d}\phi_{12}\;\cos\phi_{12}\,A_{LL}\,\mathrm{d}\sigma^{\mathrm{unp}}}{\int\mathrm{d}\phi_{12}\,\mathrm{d}\sigma^{\mathrm{unp}}} \\ &= -\,\frac{1}{4\,\cosh(\eta_q\,-\,\eta_{\bar q})}\,\frac{\Delta_L f_{\gamma/\ell}(\bar\xi_1)\,\Delta_L f_{\gamma/\ell}(\bar\xi_2)}{f_{\gamma/\ell}(\bar\xi_1)\,f_{\gamma/\ell}(\bar\xi_2)}\,\frac{\sum_q\,e_q^4\,\Delta^N D_{q^\uparrow}^{h_1}(z_1)\,\Delta^N D_{\bar q^\uparrow}^{h_2}(z_2)}{\sum_q\,e_q^4\,D_q^{h_1}(z_1)\,D_{\bar q}^{h_2}(z_2)}\,. \end{aligned} \tag{2.64}$$

Notice that these expressions of the azimuthal moments are obtained by simplifying all common factors within the numerator and denominator. This procedure is only justified if we are working at fixed kinematical variables K_T, $\eta_{q,\bar q}$. In case we want to integrate over some definite range one or more of these variables we first need to reinstate all appropriate factors in the numerator and denominator of the moments. In fact, $\bar\xi_{1,2}$ depend on K_T and $\eta_{q,\bar q}$. Moreover both the WW photon distributions and the q, $\bar q$ fragmentation functions depend, through TMD evolution which is always understood here, on the hard scale of the process, K_T. Although from available phenomenology TMD evolution seems to play

a mild role as far as concerns spin and azimuthal asymmetries, this still needs further study and must be taken into proper account in future phenomenological analyses.

Finally, let us remark that all the above discussion on the azimuthal asymmetries and moments, based on Eq. (2.61), can be clearly repeated also for the more differential cross section (2.54), where the intrinsic transverse momenta of the two hadrons w.r.t. their parent partons have not been integrated out.

2.3 Cross section for inclusive hadron-pair production in UPCs

In this appendix we calculate the differential cross section for the process

$$\mathcal{N}(\mathcal{P}_1) + \mathcal{N}(\mathcal{P}_2) \to h_1(P_1) + h_2(P_2) + X\,, \tag{2.65}$$

where the four momenta of the particles are given within brackets, and the hadron pair in the final state is produced in an ultraperipheral collision (UPC) of two highly charged nuclei. We focus on the specific kinematic configuration where the hadrons are almost back to back in the plane perpendicular to the direction of the initial nuclei. The final state X consists mostly of the same two nuclei, as the energy carried away by the photons is small. It is however possible for the nuclei to mutually excite each other through photon exchange, leading to subsequent emission of one or more neutrons along both beam directions.

According to the Equivalent Photon Approximation (EPA), first considered by Fermi, von Weizsäcker and Williams [69, 70, 88], an ultra-relativistic nucleus with atomic number A and charge Z can be seen as a flux of photons, described by the distribution $f_{\gamma/A}(\xi)$ [89]

$$f_{\gamma/A}(\xi) = \frac{Z^2\alpha}{\pi}\,\frac{1}{\xi}\left[2x_i\,K_0(x_i)K_1(x_i)\;-\;x_i^2(K_0^2(x_i)-K_1^2(x_i))\right], \tag{2.66}$$

where ξ is the momentum of a charged nucleon, inside the nucleus, carried by the photon. The above expression involves an integration between $b_{\min}$ and infinity over the impact parameter b, which is the distance between the two colliding nuclei transverse to the beam axis. In Eq. (2.66), $x_i = \xi\, M_N\, b_{\min}$, with M_N being the nucleon mass, whereas K_0, K_1 are the modified Bessel functions of the second kind of zero and first order, related respectively to the emission of longitudinally and transversely polarized photons. The transverse polarization dominates for ultrarelativistic particles ($\gamma \gg 1$).

The dominant hadron-pair production channel is the photon-photon fusion subprocess

$$\gamma(q_1) + \gamma(q_2) \to q(K_q) \;+\; \bar{q}(K_{\bar{q}}) \to h_1(P_1) \;+\; h_2(P_2) \;+\; X\,. \tag{2.67}$$

In the following we calculate the cross section within a manifestly covariant formalism, using two different methods to define the azimuthal angles: one based on the reconstruction

of the thrust axis, described in Appendix 2.3.1, and the other based on a reference frame similar to the Gottfried-Jackson frame of the Drell-Yan process, also known as hadron frame, discussed in Appendix 2.3.2.

2.3.1 Thrust-axis method

We start by performing a Sudakov decomposition of all the particle momenta in terms of the two light-like vectors n_1 and n_2, which are essentially defined by the nucleon momenta $\mathcal{P}_{1N}$ and $\mathcal{P}_{2N}$, such that $n_1 \cdot n_2 = 1$. Hence we have

$$\begin{aligned}
\mathcal{P}_{1N}^{\mu} &= \mathcal{P}_{1N}^{+}\, n_1^{\mu} + \frac{\mathcal{P}_{1N}^{2}}{2\,\mathcal{P}_{1N}^{+}}\, n_2^{\mu} \approx \mathcal{P}_{1N}^{+}\, n_1^{\mu}\,, \\
\mathcal{P}_{2N}^{\mu} &= \frac{\mathcal{P}_{2N}^{2}}{2\mathcal{P}_{2N}^{-}}\, n_1^{\mu} + \mathcal{P}_{2N}^{-} n_1^{\mu} \approx \mathcal{P}_{2N}^{-}\, n_2^{\mu}\,.
\end{aligned} \tag{2.68}$$

Assuming that the photons are emitted collinearly to their parent nuclei, the other momenta entering the scattering process $\gamma\gamma \to q\bar{q}$ can be written as

$$\begin{aligned}
q_1^{\mu} &= \xi_1\, \mathcal{P}_{1N}^{+}\, n_1^{\mu}\,, \\
q_2^{\mu} &= \xi_2\, \mathcal{P}_{2N}^{-}\, n_2^{\mu}\,, \\
K_q^{\mu} &= K_q^{+} n_1^{\mu} \;+\; \frac{\boldsymbol{K}_{qT}^{2}}{2K_q^{+}}\, n_2^{\mu} \;+\; K_{qT}^{\mu}\,, \\
K_{\bar{q}}^{\mu} &= \frac{\boldsymbol{K}_{\bar{q}T}^{2}}{2K_{\bar{q}}^{-}}\, n_1^{\mu} \;+\; K_{\bar{q}}^{-}\, n_2^{\mu} \;+\; K_{\bar{q}T}^{\mu}\,.
\end{aligned} \tag{2.69}$$

We assume that at sufficiently high energies the cross section factorizes as follows

$$\begin{aligned}
\mathrm{d}\sigma = \frac{1}{8 s_{NN}} \int \frac{\mathrm{d}\xi_1}{\xi_1} \frac{\mathrm{d}\xi_2}{\xi_2} \frac{\mathrm{d}^3 K_q}{(2\pi)^3\, 2E_q} \frac{\mathrm{d}^3 K_{\bar{q}}}{(2\pi)^3\, 2E_{\bar{q}}} \frac{\mathrm{d}^3 P_1}{E_1} \frac{\mathrm{d}^3 P_2}{E_2}\, (2\pi)^4\, \delta^4(q_1{+}q_2{-}K_q{-}K_{\bar{q}}) \\
\times\, g_{T\mu\alpha}\, g_{T\nu\beta}\, f_{\gamma/A}(\xi_1)\, f_{\gamma/A}(\xi_2)\, H^{\mu\nu}_{\gamma\gamma\to q\bar{q}} \otimes H^{*\alpha\beta}_{\gamma\gamma\to q\bar{q}} \otimes \Delta(z_1, k_{q\perp}) \otimes \overline{\Delta}(z_2, k_{\bar{q}\perp})\,,
\end{aligned} \tag{2.70}$$

where we have summed over the polarization states of the incoming photons by means of the symmetric transverse projector

$$g_T^{\mu\nu} = g^{\mu\nu} - n_1^{\mu}\, n_2^{\nu} - n_1^{\nu}\, n_2^{\mu}\,. \tag{2.71}$$

Moreover, in Eq. (2.70), $H_{\gamma\gamma\to q\bar{q}}$ is the amplitude for the hard partonic subprocess $\gamma\gamma \to q\bar{q}$, the convolutions $\otimes$ denote appropriate traces over the Dirac indices, while Δ and $\overline{\Delta}$ are the fragmentation correlators defined in Eq. (1.24), describing respectively the quark and antiquark transition to a hadron. The momentum conserving delta-function can be decomposed as follows

$$\delta^4(q_1{+}q_2{-}K_q{-}K_{\bar{q}}) = \delta(x_1\mathcal{P}_{1N}^{+} - K_q^{+} - K_{\bar{q}}^{+})\, \delta(x_2\mathcal{P}_{2N}^{+} - K_q^{+} - K_{\bar{q}}^{-})\, \delta^2(K_{qT} + K_{\bar{q}T})$$

$$= \frac{2}{s_{NN}}\,\delta\left(x_1 - \frac{K_q^+}{\mathcal{P}_{1N}^+} - \frac{\boldsymbol{K}_{\bar{q}T}^2}{2K_{\bar{q}}^-\mathcal{P}_{1N}^+}\right)\,\delta\left(x_2 - \frac{K_{\bar{q}}^-}{\mathcal{P}_{2N}^-} - \frac{\boldsymbol{K}_{\bar{q}T}^2}{2K_{\bar{q}}^+\mathcal{P}_{2N}^-}\right) \times \delta^2(K_{qT} + K_{\bar{q}T})\,. \tag{2.72}$$

In the center-of-mass frame of the two nucleons emitting the photons, where

$$\mathcal{P}_{1N}^+ = \mathcal{P}_{2N}^- = \sqrt{\frac{s_{NN}}{2}}\,, \tag{2.73}$$

we can introduce the rapidities of the final quark and antiquark, in terms of which we can write

$$K_q^+ = \frac{|\boldsymbol{K}_{qT}|}{\sqrt{2}}\,e^{\eta_q}\,, \qquad K_{\bar{q}}^- = \frac{|\boldsymbol{K}_{\bar{q}T}|}{\sqrt{2}}\,e^{-\eta_{\bar{q}}}\,. \tag{2.74}$$

Our final results can be expressed as a function of the following energy fractions of the final (anti)quarks

$$\zeta_q = \frac{K_q\cdot q_1}{q_1\cdot q_2} = \frac{1}{1+e^{\eta_q-\eta_{\bar{q}}}}\,, \qquad \zeta_{\bar{q}} = \frac{K_{\bar{q}}\cdot q_1}{q_1\cdot q_2} = \frac{1}{1+e^{\eta_{\bar{q}}-\eta_q}}\,. \tag{2.75}$$

Due to momentum conservation, $q_1+q_2 = K_q + K_{\bar{q}}$, we have $\zeta_q+\zeta_{\bar{q}}=1$, so that we can define $\zeta\equiv\zeta_q$ and therefore $\zeta_{\bar{q}} = 1-\zeta$. Hence Eqs. (2.69) can be rewritten as

$$q_1^\mu = \xi_1\sqrt{\frac{s_{NN}}{2}}\,n_1^\mu\,, \tag{2.76}$$

$$q_2^\mu = \xi_2\sqrt{\frac{s_{NN}}{2}}\,n_2^\mu\,, \tag{2.77}$$

$$K_q^\mu = \frac{\boldsymbol{K}_T^2}{\zeta}\,\frac{1}{\xi_2\sqrt{2\,s_{NN}}}\,n_1^\mu + \zeta\,\xi_2\sqrt{\frac{s_{NN}}{2}}\,n_2^\mu + K_T^\mu\,, \tag{2.78}$$

$$K_{\bar{q}}^\mu = \frac{\boldsymbol{K}_T^2}{(1-\zeta)}\,\frac{1}{\xi_2\sqrt{2\,s_{NN}}}\,n_1^\mu + (1-\zeta)\,\xi_2\sqrt{\frac{s_{NN}}{2}}\,n_2^\mu - K_T^\mu\,, \tag{2.79}$$

with $\boldsymbol{K}_T \equiv \boldsymbol{K}_{qT} = -\boldsymbol{K}_{\bar{q}T}$. The partonic Mandelstam variables are written in terms of ζ and $|\boldsymbol{K}_T|$ according to

$$\begin{aligned}\hat{s} &= (q_1+q_2)^2 = \frac{\boldsymbol{K}_T^2}{\zeta\,(1-\zeta)}\,,\\ \hat{t} &= (q_1-K_q)^2 = -\frac{\boldsymbol{K}_T^2}{1-\zeta}\,,\\ \hat{u} &= (q_1-K_{\bar{q}})^2 = -\frac{\boldsymbol{K}_T^2}{\zeta}\,,\end{aligned} \tag{2.80}$$

from which we obtain that $q_1+q_2 = K_1+K_2$ implies that $\boldsymbol{K}_T^2 = \hat{s}\,\zeta\,(1-\zeta) = \xi_1\,\xi_2\,s_{NN}\,\zeta\,(1-\zeta)$. Thus the previous expressions can be rewritten in their final form as

$$\begin{aligned}q_1^\mu &= \xi_1\,\sqrt{\frac{s_{NN}}{2}}\,n_1^\mu\,,\\ q_2^\mu &= \xi_2\,\sqrt{\frac{s_{NN}}{2}}\,n_2^\mu\,,\end{aligned} \tag{2.81}$$

$$K_q^\mu = (1-\zeta)\,\xi_1\sqrt{\frac{s_{NN}}{2}}\,n_1^\mu \,+\, \zeta\,\xi_2\sqrt{\frac{s_{NN}}{2}}\,n_2^\mu \,+\, \sqrt{\zeta\,(1-\zeta)\,\hat{s}}\;\hat{K}_T^\mu\,,$$
$$K_{\bar{q}}^\mu = \zeta\,\xi_1\sqrt{\frac{s_{NN}}{2}}\,n_1^\mu \,+\, (1-\zeta)\,\xi_2\sqrt{\frac{s_{NN}}{2}}\,n_2^\mu \,-\, \sqrt{\zeta\,(1-\zeta)\,\hat{s}}\;\hat{K}_T^\mu\,. \tag{2.82}$$

Concerning the momenta of the two final hadrons, P_1 and P_2, we can use the quark and antiquark momenta as light-like vectors to perform the further decomposition:

$$P_1^\mu = z_1\,K_q^\mu \,+\, \frac{M_1^2+\boldsymbol{p}_{1\perp}^2}{2z_1(K_q\cdot K_{\bar{q}})}\,K_{\bar{q}}^\mu \,+\, p_{1\perp}^\mu \approx z_1 K_q^\mu \,+\, p_{1\perp}^\mu\,,$$
$$P_2^\mu = \frac{M_2^2+\boldsymbol{p}_{2\perp}^2}{2z_2(K_{\bar{q}}\cdot K_q)}\,K_q^\mu \,+\, z_2\,K_{\bar{q}}^\mu \,+\, p_{2\perp}^\mu \approx z_2\,K_{\bar{q}}^\mu \,+\, p_{2\perp}^\mu\,. \tag{2.83}$$

The corresponding phase-space element can thus be expressed as

$$\frac{\mathrm{d}^3P_1}{E_1}\frac{\mathrm{d}^3P_2}{E_2} = \frac{\mathrm{d}(P_1\cdot K_{\bar{q}})}{P_1\cdot K_{\bar{q}}}\,\mathrm{d}^2p_{1\perp}\,\frac{\mathrm{d}(P_2\cdot K_q)}{P_2\cdot K_q}\,\mathrm{d}^2p_{2\perp} = \frac{\mathrm{d}z_1}{z_1}\,\frac{\mathrm{d}z_2}{z_2}\,\mathrm{d}^2p_{1\perp}\,\mathrm{d}^2p_{2\perp}\,. \tag{2.84}$$

Similarly, for the outgoing quark-antiquark pair,

$$\frac{\mathrm{d}^3K_q}{(2\pi)^3\,2E_q}\,\frac{\mathrm{d}^3K_{\bar{q}}}{(2\pi)^3\,2E_{\bar{q}}} = \frac{1}{4}\,\frac{1}{(2\pi)^6}\,\frac{\mathrm{d}K_q^+}{K_q^+}\,\frac{\mathrm{d}K_{\bar{q}}^+}{K_{\bar{q}}^+}\,\mathrm{d}^2K_{qT}\,\mathrm{d}^2K_{\bar{q}T} = \frac{1}{4}\,\frac{1}{(2\pi)^6}\,\mathrm{d}\eta_q\,\mathrm{d}\eta_{\bar{q}}\,\mathrm{d}^2K_{qT}\,\mathrm{d}^2K_{\bar{q}T}\,. \tag{2.85}$$

By substituting Eqs. (2.72), (2.84) and (2.85) into Eq. (2.70), we obtain

$$\frac{\mathrm{d}\sigma}{\mathrm{d}\eta_q\,\mathrm{d}\eta_{\bar{q}}\,\mathrm{d}^2K_T\,\mathrm{d}z_1\,\mathrm{d}z_2\,\mathrm{d}^2p_{1\perp}\,\mathrm{d}^2p_{2\perp}} = \frac{1}{16\,s_{NN}^2}\,\frac{1}{(2\pi)^2}\,\frac{1}{\xi_1\,\xi_2\,z_1\,z_2}\,g_{T\mu\alpha}\,g_{T\nu\beta}\,f_{\gamma/A}(\xi_1)\,f_{\gamma/A}(\xi_2)$$
$$\times\, H^{\mu\nu}_{\gamma\gamma\to q\bar{q}}\otimes H^{*\alpha\beta}_{\gamma\gamma\to q\bar{q}}\otimes\Delta(z_1,k_{\bar{q}\perp})\otimes\overline{\Delta}(z_2,k_{\bar{q}\perp})\,, \tag{2.86}$$

with the momentum fractions ξ_1 and ξ_2 given by, in the nucleon-nucleon c.m. frame,

$$\xi_1 = \frac{|\boldsymbol{K}_T|}{\sqrt{s_{NN}}}\,(e^{\eta_q}+e^{\eta_{\bar{q}}}) = \frac{|\boldsymbol{K}_T|}{\sqrt{s_{NN}}}\,\frac{1}{1-\zeta}\,e^{\eta_q}\,,$$
$$\xi_2 = \frac{|\boldsymbol{K}_T|}{\sqrt{s_{NN}}}\,(e^{-\eta_q}+e^{-\eta_{\bar{q}}}) = \frac{|\boldsymbol{K}_T|}{\sqrt{s_{NN}}}\,\frac{1}{\zeta}\,e^{-\eta_q}\,. \tag{2.87}$$

The transverse momentum dependent (anti)quark fragmentation correlators for unpolarized hadrons are usually parametrized by using an alternative Sudakov decomposition in which P_1 and P_2 have no transverse momenta. The quark and antiquark momenta therefore read

$$K_q^\mu = \frac{1}{z_1}\,P_1^\mu + z_1\,\frac{\boldsymbol{k}_{q\perp}^2}{2\,(P_1\cdot P_2)}\,P_2^\mu + k_{q\perp}^\mu \approx \frac{1}{z_1}\,P_1^\mu + k_{q\perp}^\mu\,,$$
$$K_{\bar{q}}^\mu = \frac{1}{z_2}\,P_2^\mu + z_2\,\frac{\boldsymbol{k}_{\bar{q}\perp}^2}{2\,(P_1\cdot P_2)}\,P_1^\mu + k_{\bar{q}\perp}^\mu \approx \frac{1}{z_2}\,P_2^\mu + k_{\bar{q}\perp}^\mu\,. \tag{2.88}$$

The relation between the transverse vectors $(k^\mu_{q\perp}, k^\mu_{\bar{q}\perp})$ and $(p^\mu_{1\perp}, p^\mu_{1\perp})$, defined in the two different reference frames considered, can be found by noticing that, from the above equations and from Eqs. (2.83):

$$\begin{aligned} k^\mu_{q\perp} &\approx K^\mu_q - \frac{1}{z_1} P^\mu_1 \approx K^\mu_q - \frac{1}{z_1}\left(z_1 K^\mu_q + p^\mu_{1\perp}\right) = -\frac{1}{z_1} p^\mu_{1\perp}\,, \\ k^\mu_{\bar{q}\perp} &\approx K^\mu_{\bar{q}} - \frac{1}{z_2} P^\mu_2 \approx K^\mu_{\bar{q}} - \frac{1}{z_2}\left(z_2 K^\mu_{\bar{q}} + p^\mu_{2\perp}\right) = -\frac{1}{z_2} p^\mu_{2\perp}\,. \end{aligned} \tag{2.89}$$

The quark and antiquark fragmentation correlators are thus given by [90]

$$\begin{aligned} \Delta(z_1, k_{q\perp}) &= D_1(z_1, z_1^2\, k^2_{q\perp})\, \not{P}_1 \;+\; i\, H_1^\perp(z_1, z_1^2\, k^2_{q\perp})\, \frac{[\not{k}_{q\perp}\,, \not{P}_1\,]}{2M_1}\,, \\ \overline{\Delta}(z_2, k_{\bar{q}\perp}) &= \overline{D}_1(z_2, z_2^2\, k^2_{\bar{q}\perp})\, \not{P}_2 \;+\; i\, \overline{H}_1^\perp(z_2, z_2^2\, k^2_{\bar{q}\perp})\, \frac{[\not{k}_{\bar{q}\perp}\,, \not{P}_2\,]}{2M_2}\,, \end{aligned} \tag{2.90}$$

where D_1 is the unpolarized fragmentation function and $H_1^\perp$ is the Collins function.

It is useful to decompose all the momenta in terms of a new set of light-like vectors κ_1 and κ_2, such that $\kappa_1 \cdot \kappa_2 = 1$ and K_q and $K_{\bar{q}}$ have no transverse momenta,

$$\begin{aligned} q^\mu_1 &= \sqrt{\frac{\hat{s}}{2}}\,(1-\zeta)\,\kappa^\mu_1 \;+\; \sqrt{\frac{\hat{s}}{2}}\,\zeta\,\kappa^\mu_2 \;+\; \sqrt{\zeta(1-\zeta)\,\hat{s}}\,\hat{q}^\mu_\perp\,, \\ q^\mu_2 &= \sqrt{\frac{\hat{s}}{2}}\,\zeta\,\kappa^\mu_1 \;+\; \sqrt{\frac{\hat{s}}{2}}\,(1-\zeta)\,\kappa^\mu_2 \;-\; \sqrt{\zeta(1-\zeta)\,\hat{s}}\,\hat{q}^\mu_\perp\,, \\ K^\mu_q &= \sqrt{\frac{\hat{s}}{2}}\,\kappa^\mu_1\,, \\ K^\mu_{\bar{q}} &= \sqrt{\frac{\hat{s}}{2}}\,\kappa^\mu_2\,, \\ P^\mu_1 &= z_1\sqrt{\frac{\hat{s}}{2}}\,\kappa^\mu_1 \;+\; \frac{\sqrt{2}}{2}\,\frac{z_1\,\boldsymbol{k}^2_{q\perp}}{\sqrt{\hat{s}}}\,\kappa^\mu_2 - z_1\,k^\mu_{q\perp}\,, \\ P^\mu_2 &= \frac{\sqrt{2}}{2}\,\frac{z_2\,\boldsymbol{k}^2_{q\perp}}{\sqrt{\hat{s}}}\,\kappa^\mu_1 \;+\; z_2\sqrt{\frac{\hat{s}}{2}}\,\kappa^\mu_2 \;-\; z_2\,k^\mu_{q\perp}\,. \end{aligned} \tag{2.91}$$

Using the shorthand notation

$$\mathrm{d}\sigma \equiv \frac{\mathrm{d}\sigma}{\mathrm{d}\eta_q\,\mathrm{d}\eta_{\bar{q}}\,\mathrm{d}^2K_T\,\mathrm{d}z_1\,\mathrm{d}z_2\,\mathrm{d}^2p_{1\perp}\,\mathrm{d}^2p_{2\perp}}\,, \tag{2.92}$$

we can write the cross section in its final form as follows

$$\begin{aligned} \mathrm{d}\sigma = \frac{6\,\alpha^2}{s_{NN}\,\boldsymbol{K}_T^2} \sum_q e_q^4\, f_{\gamma/A}(\xi_1)\, f_{\gamma/A}(\xi_2) \Big\{ &\left[\zeta^2 + (1-\zeta)^2\right] D_1^q(z_1, p^2_{1\perp})\, \overline{D}_1^q(z_2, p^2_{2\perp}) \\ &+ 2\,\zeta(1-\zeta)\,\frac{|\boldsymbol{p}_{1\perp}|\,|\boldsymbol{p}_{2\perp}|}{M_1 M_2\, z_1\, z_2}\,\cos(\phi_1+\phi_2)\, H_{1T}^{\perp\,q}(z_1, p^2_{1\perp})\, \overline{H}_{1T}^{\perp\,q}(z_2, p^2_{2\perp}) \Big\}\,, \end{aligned} \tag{2.93}$$

where we have assumed that the two photons lie in a plane with azimuthal angle $\phi = 0$, while ϕ_1 and ϕ_2 are the azimuthal angles of P_1 and P_2, respectively.

2.3.2 Gottfried-Jackson frame

A second way of defining the azimuthal asymmetries is based on the integration over all thrust axis directions, leaving only one azimuthal angle. This angle is defined as the angle between the planes spanned by the momentum of hadron h_2 and the lepton momenta, and the transverse momentum of hadron h_1 with respect to hadron h_2. The cross section in its most differential form can be written as

$$\begin{aligned}\mathrm{d}\sigma = \frac{1}{8 s_{NN}} \int \frac{\mathrm{d}\xi_1}{\xi_1} \frac{\mathrm{d}\xi_2}{\xi_2} \frac{\mathrm{d}z}{z} \frac{\mathrm{d}\bar{z}}{\bar{z}} \, \mathrm{d}^2 k_{qT} \, \mathrm{d}^2 k_{\bar{q}T} \, \frac{\mathrm{d}^3 P_1}{(2\pi)^3 \, 2E_1} \frac{\mathrm{d}^3 P_2}{(2\pi)^3 \, 2E_2} \, (2\pi)^4 \, \delta^4(q_1 + q_2 - K_q - K_{\bar{q}}) \\ \times g_{T\mu\alpha} \, g_{T\nu\beta} \, f_{\gamma/A}(\xi_1) \, f_{\gamma/A}(\xi_2) \sum_q H^{\mu\nu}_{\gamma\gamma\to q\bar{q}} \otimes H^{*\alpha\beta}_{\gamma\gamma\to q\bar{q}} \otimes \Delta(z, k_{qT}) \otimes \overline{\Delta}(\bar{z}, k_{\bar{q}T}) \, .\end{aligned} \tag{2.94}$$

It is convenient to introduce the sum of the momenta of the incoming photons:

$$q^\mu \equiv q_1^\mu \, + \, q_2^\mu \, , \tag{2.95}$$

with $\hat{s} = (q_1 + q_2)^2 > 0$. If we define

$$y = \frac{P_2 \cdot q_1}{P_2 \cdot q} \, , \tag{2.96}$$

in the center-of-mass frame of the two incoming photons, neglecting hadron masses and terms of the order $\mathcal{O}(1/s_{NN})$ and assuming that P_2 has no transverse momentum, we can write

$$\begin{aligned} q_1^\mu &= \sqrt{\frac{\hat{s}}{2}} \, y \, \ell_1^\mu \, + \, \sqrt{\frac{\hat{s}}{2}} \, (1-y) \, \ell_2^\mu \, + \, \sqrt{y(1-y) \, \hat{s}} \, \hat{q}_\perp^\mu \, , \\ q_2^\mu &= \sqrt{\frac{\hat{s}}{2}} \, (1-y) \, \ell_1^\mu \, + \, \sqrt{\frac{\hat{s}}{2}} \, y \, \ell_2^\mu \, - \, \sqrt{y(1-y) \, \hat{s}} \, \hat{q}_\perp^\mu \, , \\ q^\mu \equiv q_1^\mu + q_2^\mu &= \sqrt{\frac{\hat{s}}{2}} \, \ell_1^\mu \, + \, \sqrt{\frac{\hat{s}}{2}} \, \ell_2^\mu \, , \\ P_1^\mu &= z_1 \sqrt{\frac{\hat{s}}{2}} \, \ell_1^\mu \, + \frac{\boldsymbol{P}_{1\perp}^2}{z_1 \sqrt{2 \, \hat{s}}} \, \ell_2^\mu \, + \, P_{1\perp}^\mu \, , \\ P_2^\mu &= z_2 \sqrt{\frac{\hat{s}}{2}} \, \ell_2^\mu \, . \end{aligned} \tag{2.97}$$

In this frame, the phase space of the final hadrons becomes

$$\begin{aligned}\frac{\mathrm{d}^3 P_1}{E_1} \frac{\mathrm{d}^3 P_2}{E_2} = \frac{\mathrm{d}P_1^+}{P_1^+} \, \mathrm{d}^2 P_{1\perp} \, \frac{1}{2} \, \mathrm{d}\boldsymbol{P}_2^2 \, \mathrm{d}\cos\theta_2 \, \mathrm{d}\phi_2 \, = \frac{\mathrm{d}z_1}{z_1} \, \mathrm{d}^2 P_{1\perp} \, \frac{1}{2} \, \frac{\mathrm{d}}{\mathrm{d}z_2} \left(z_2^2 \, \frac{\hat{s}}{4} \right) \mathrm{d}z_2 \, \mathrm{d}\cos\theta_2 \, \mathrm{d}\phi_2 \\ = \pi \, \frac{\hat{s}}{2} \, z_2 \, \frac{\mathrm{d}z_1}{z_1} \, \mathrm{d}z_2 \, \mathrm{d}^2 P_{1\perp} \, \mathrm{d}\cos\theta_2 \, .\end{aligned} \tag{2.98}$$

On the other hand, if the longitudinal direction is set by the two outgoing hadrons, we can write

$$q_1^\mu = \sqrt{\frac{\hat{s}}{2}} \, y \, n^\mu \, + \, \frac{\boldsymbol{q}_{1T}^2}{\sqrt{2 \, \hat{s}} \, y} \, \bar{n}^\mu \, + \, \sqrt{y(1-y) \, \hat{s}} \, \hat{q}_{1T}^\mu \, ,$$

$$
\begin{aligned}
q_2^\mu &= \sqrt{\frac{\hat{s}}{2}}\,(1-y)\,n^\mu \,+\, \frac{(\boldsymbol{q}_T-\boldsymbol{q}_{1T})^2}{\sqrt{2\,\hat{s}}\,(1-y)}\,\bar{n}^\mu \,+ q_T^\mu \,-\, \sqrt{y(1-y)\,\hat{s}}\,\hat{q}_{1T}^\mu\,,\\
q^\mu \equiv q_1^\mu + q_2^\mu &= \sqrt{\frac{\hat{s}}{2}}\,n^\mu \,+\, \sqrt{\frac{\hat{s}}{2}}\,\bar{n}^\mu \,+ q_T^\mu\,,\\
P_1^\mu &= z_1\sqrt{\frac{\hat{s}}{2}}\,n^\mu\,,\\
P_2^\mu &= z_2\sqrt{\frac{\hat{s}}{2}}\,\overline{n}^\mu\,,\\
K_q^\mu &= \frac{z_1}{z}\sqrt{\frac{\hat{s}}{2}}\,n^\mu \,+\, \frac{z}{z_1}\,\frac{\boldsymbol{k}_{q\perp}^2}{\sqrt{2\,\hat{s}}}\,\bar{n}^\mu \,+\, k_{qT}^\mu \approx \frac{1}{z}\,P_1^\mu + k_{qT}^\mu\,,\\
K_{\bar{q}}^\mu &= \frac{\bar{z}}{z_2}\,\frac{\boldsymbol{k}_{\bar{q}T}^2}{\sqrt{2\,\hat{s}}}\,n^\mu \,+\, \frac{z_2}{\bar{z}}\sqrt{\frac{\hat{s}}{2}}\,\bar{n}^\mu \,+\, k_{\bar{q}T}^\mu \approx \frac{1}{\bar{z}}\,P_2^\mu \,+\, k_{\bar{q}T}^\mu\,.
\end{aligned}
\tag{2.99}
$$

The momentum-conservation delta function can be decomposed as follows,

$$
\begin{aligned}
\delta\left(q - K_q - K_{\bar{q}}\right) &\approx \delta\left(q^+ - K_q^+\right)\delta\left(q^- - K_{\bar{q}}^-\right)\,\delta^2\left(q_T - k_{qT} - k_{\bar{q}T}\right)\\
&= \frac{2}{\hat{s}}\,z_1\,z_2\,\delta(z-z_1)\,\delta(\bar{z}-z_2)\,\delta^2\left(q_T - k_{qT} - k_{\bar{q}T}\right)\,,
\end{aligned}
\tag{2.100}
$$

fixing $z = z_1$ and $\bar{z} = z_2$.

By comparing the two different Sudakov decompositions of P_1 and P_2 in Eqs. (2.99) and (2.97), we find

$$
\begin{aligned}
n^\mu &= \ell_1^\mu + \frac{1}{z_1}\sqrt{\frac{2}{\hat{s}}}\,P_{1\perp}^\mu \,+ \mathcal{O}\left(\frac{\boldsymbol{P}_{1\perp}^2}{\hat{s}}\right)\,,\\
\overline{n}^\mu &= \ell_2^\mu\,.
\end{aligned}
\tag{2.101}
$$

By substituting the above equations in the expression for q^μ in Eqs. (2.99) and identifying it with the corresponding expression in Eq. (2.97), we find

$$
P_{1\perp}^\mu \approx -z_1\,q_T^\mu\,,
\tag{2.102}
$$

and therefore $\mathrm{d}^2P_{1\perp} = z_1^2\,\mathrm{d}^2q_T$. Furthermore,

$$
y = \frac{1+\cos\theta_2}{2}\,,
\tag{2.103}
$$

where θ_2 is the angle of the z-axis with respect to the incoming photon q_1, $\mathrm{d}\cos\theta_2 = 2\mathrm{d}y$. Thus we can write

$$
\frac{\mathrm{d}^3P_1}{E_1}\,\frac{\mathrm{d}^3P_2}{E_2} = \pi\,\hat{s}\,z_1\,z_2\,\mathrm{d}z_1\,\mathrm{d}z_2\,\mathrm{d}y\,\mathrm{d}^2q_T\,,
\tag{2.104}
$$

which implies

$$
\frac{\mathrm{d}\sigma}{\mathrm{d}z_1\,\mathrm{d}z_2\,\mathrm{d}y\,\mathrm{d}^2q_T} = \frac{1}{64\,\pi}\,z_1\,z_2\int \mathrm{d}\xi_1\,\mathrm{d}\xi_2\,\mathrm{d}^2k_{qT}\,\mathrm{d}^2k_{\bar{q}T}\,\frac{1}{\hat{s}}\,\delta^2(q_T - k_{qT} - k_{\bar{q}T})\,g_{T\mu\alpha}\,g_{T\nu\beta}
$$

$$\times\; f_{\gamma/A}(\xi_1)\, f_{\gamma/A}(\xi_2)\, H^{\mu\nu}_{\gamma\gamma\to q\bar{q}} \otimes H^{*\alpha\beta}_{\gamma\gamma\to q\bar{q}} \otimes \Delta(z_1, k_{qT}) \otimes \overline{\Delta}(\bar{z}_2, k_{\bar{q}T})\,, \tag{2.105}$$

and therefore, as a final result we obtain

$$\frac{\mathrm{d}\sigma}{\mathrm{d}z_1\,\mathrm{d}z_2\,\mathrm{d}y\,\mathrm{d}^2q_T} = \frac{6\,\pi\,\alpha^2}{s_{NN}}\,\frac{z_1^2 z_2^2}{y(1-y)}\int\frac{\mathrm{d}\xi_1}{\xi_1}\,\frac{\mathrm{d}\xi_2}{\xi_2}\,f_{\gamma/A}(\xi_1)\,f_{\gamma/A}(\xi_2)\left\{\left[y^2+(1-y)^2\right]\mathcal{C}[D_1\overline{D}_1]\right.$$
$$\left. +\;2\,y(1-y)\cos(2\phi_1)\,\mathcal{C}[w_2\,H_1^{\perp}\overline{H_1}^{\perp}]\right\}, \tag{2.106}$$

where ϕ_1 is the azimuthal angle between $\hat{\boldsymbol{h}} \equiv \hat{\boldsymbol{x}} \equiv \hat{\boldsymbol{P}}_{1\perp}$ and $\hat{\boldsymbol{l}}_{\perp}$. The convolutions of TMD fragmentation functions are defined as

$$\mathcal{C}[w\,D\overline{D}] \equiv \sum_{q,\bar{q}} e_q^4 \int \mathrm{d}^2k_{qT}\,\mathrm{d}^2k_{\bar{q}T}\,\delta^2(q_T - k_{qT} - k_{\bar{q}T})\,w(k_{qT}, k_{\bar{q}T})\,D^q(z_1, z_1^2k_{qT}^2)\,\overline{D}^q(z_2, z_2^2k_{\bar{q}T}^2)\,, \tag{2.107}$$

with

$$w_2(k_{qT}, k_{\bar{q}T}) = \frac{|\boldsymbol{k}_{qT}|\,|\boldsymbol{k}_{\bar{q}T}|}{M_1\,M_2}\,\cos(\phi_q + \phi_{\bar{q}}) = \frac{1}{M_1\,M_2}\,\frac{2(\boldsymbol{q}_T\cdot\boldsymbol{k}_{qT})(\boldsymbol{q}_T\cdot\boldsymbol{k}_{qT}) - \boldsymbol{k}_{qT}\cdot\boldsymbol{k}_{\bar{q}T}}{\boldsymbol{q}_T^2}$$
$$= \frac{1}{M_1\,M_2}\,[2(\hat{\boldsymbol{h}}\cdot\boldsymbol{k}_{qT})(\hat{\boldsymbol{h}}\cdot\boldsymbol{k}_{qT}) - \boldsymbol{k}_{qT}\cdot\boldsymbol{k}_{\bar{q}T}]\,, \tag{2.108}$$

ϕ_q and $\phi_{\bar{q}}$ being the azimuthal angles of $\boldsymbol{k}_{qT}$ and $\boldsymbol{k}_{\bar{q}T}$ with respect to $\hat{\boldsymbol{h}}$, and $\hat{\boldsymbol{h}} = -\boldsymbol{q}_T/|\boldsymbol{q}_T|$.

A Kinematics

For completeness, we collect here the explicit expressions of the four-momenta of the particles involved in the process of interest, in the different reference frames considered. We also summarize several useful kinematical relations.

The lepton-beam or Laboratory cm frame

We first consider the Laboratory, or ℓ^+-ℓ^- cm frame, where the tagged lepton ℓ^+ moves along the $+\hat{z}$ axis and the untagged one, ℓ^-, in the opposite direction; for massless leptons, we have:

$$\begin{aligned}
l_+ &= \frac{\sqrt{s}}{2}\,(\,1,\,0,\,0,\,1\,)\,,\\
l_- &= q_2/\xi \;=\; \frac{\sqrt{s}}{2}\,(\,1,\,0,\,0,\,-1\,)\,,\\
l'_+ &= \frac{\sqrt{s}}{2}\left(\,1-(1-x_B)y,\,2\sqrt{x_B y(1-y)},\,0,\,1-(1+x_B)y\,\right),\\
q_1 &= \frac{\sqrt{s}}{2}\left(\,(1-x_B)y,\,-2\sqrt{x_B y(1-y)},\,0,\,(1+x_B)y\,\right),
\end{aligned} \tag{A.1}$$

where in the second line ξ is the light-cone momentum fraction of the quasi-real photon γ_2 inside the untagged lepton ℓ^-. Without loss of generality, we have chosen the leptonic plane as the x-z plane of our reference frame. If necessary, one can easily reinstate the most general dependence on the azimuthal angle of the leptonic plane, ϕ_ℓ, with respect to the x-z plane of a general arbitrary frame. Let us also remind the definition of the usual kinematical invariants adopted in deep inelastic scattering:

$$\begin{aligned} s = (l_+ + l_-)^2 = 2\, l_+ \cdot l_- \,, \quad Q^2 = -q_1^2 = -(l_+ - l'_+)^2 = 2\, l_+ \cdot l'_+ \,, \\ x_B = \frac{Q^2}{2\, l_- \cdot q_1} \,, \quad y = \frac{l_- \cdot q_1}{l_- \cdot l_+} \,, \quad Q^2 = x_B\, y\, s \,. \end{aligned} \tag{A.2}$$

By defining as K_q and $K_{\bar{q}}$ the four-momenta of the quark and antiquark produced in the two-photon collision ($q = u, \bar{u}, d, \bar{d}, s, \bar{s}$), we can also introduce two additional invariants:

$$\zeta_q = \frac{K_q \cdot l_-}{q_1 \cdot l_-} \,, \qquad \zeta_{\bar{q}} = \frac{K_{\bar{q}} \cdot l_-}{q_1 \cdot l_-} \,. \tag{A.3}$$

Notice that we neglect light quark masses, therefore $K_q^2 = K_{\bar{q}}^2 = 0$.

The virtual photon - untagged lepton γ_1^*-ℓ^- cm frame

This frame is the analogous of the γ^*-nucleon reference frame usually adopted in semi-inclusive deep inelastic scattering processes, with the untagged lepton ℓ^- and the quasi-real photon γ_2 playing respectively the role of the target nucleon and the collinear struck parton. In this frame γ_1^* moves along the $+\hat{z}$ axis, and the untagged lepton, ℓ^-, and γ_2 in the opposite direction. The cm energy, usually named W, is given by

$$W^2 = (q_1 + l_-)^2 = (1 - x_B)\, y\, s = \frac{1 - x_B}{x_B}\, Q^2 \,. \tag{A.4}$$

The four-momenta of the particles involved are:

$$\begin{aligned} l_+ &= \frac{\sqrt{s}}{2} \frac{1}{\sqrt{(1-x_B)y}} \Big(1 - x_B y,\, 2\sqrt{x_B(1-x_B)(1-y)},\, 0,\, 1 - 2x_B + x_B y \Big) \,, \\ l_- &= q_2/\xi \,=\, \frac{\sqrt{s}}{2} \frac{1}{\sqrt{(1-x_B)y}} \,(\, y,\, 0,\, 0,\, -y \,) \,, \\ l'_+ &= \frac{\sqrt{s}}{2} \frac{1}{\sqrt{(1-x_B)y}} \Big(1 - y + x_B y,\, 2\sqrt{x_B(1-x_B)(1-y)},\, 0,\, 1 - y - 2x_B + x_B y \Big) \,, \\ q_1 &= \frac{\sqrt{s}}{2} \frac{1}{\sqrt{(1-x_B)y}} \Big((1 - 2x_B)y,\, 0,\, 0,\, y \Big) \,. \end{aligned} \tag{A.5}$$

The four-momenta of the final quark and antiquark can be written as:

$$\begin{aligned} K_q &= K_T \,(\, \cosh\eta_q,\, \cos\phi_q,\, \sin\phi_q,\, \sinh\eta_q \,) \,, \\ K_{\bar{q}} &= K_T \,(\, \cosh\eta_{\bar{q}},\, -\cos\phi_q,\, -\sin\phi_q,\, \sinh\eta_{\bar{q}} \,) \,, \end{aligned} \tag{A.6}$$

where we have introduced the pseudo-rapidities of the quark and antiquark, η_q and $\eta_{\bar{q}}$, that in the massless limit coincide with their rapidities.

It is easy then to verify that in this frame the invariants $\zeta_{q,\bar{q}}$ introduced in Eq. (A.3) are given by:

$$\zeta_q = \frac{k_T}{W}\, e^{\eta_q}\,, \qquad \zeta_{\bar{q}} = \frac{k_T}{W}\, e^{\eta_{\bar{q}}}\,. \tag{A.7}$$

The virtual photon - quasi-real photon γ_1^*-γ_2 cm frame

This is the cm frame of the hard partonic scattering process $\gamma_1^*\gamma_2 \to q\bar{q}$, again with γ_1^* moving along the $+\hat{z}$ axis and the untagged lepton and γ_2 moving in the opposite direction. The final quark and antiquark are produced back to back in a plane forming an angle ϕ_q with the ℓ^+-ℓ'^+ leptonic plane, that we have assumed to be the $\hat{x}$-$\hat{z}$ plane. This frame is related to the previous one in section A by a Lorentz boost along the $\hat{z}$ axis specified by the Lorentz factors:

$$\beta = \frac{1-\xi}{1-2x_B+\xi}\,, \qquad \gamma = \frac{1-2x_B+\xi}{2\sqrt{(1-x_B)(\xi-x_B)}}\,. \tag{A.8}$$

The squared cm energy in this frame is:

$$\hat{s} = (q_1+q_2)^2 = (\xi-x_B)ys \;= \frac{\xi-x_B}{x_B}\,Q^2\,, \tag{A.9}$$

which also implies the constraint $\xi > x_B$. The four-momenta of the particles involved are:

$$\begin{aligned}
l_+ &= \frac{\sqrt{s}}{2}\,\frac{1}{\sqrt{(\xi-x_B)y}}\left(\xi - x_B y,\, 2\sqrt{x_B(\xi-x_B)(1-y)},\, 0,\, \xi - 2x_B + x_B y\right),\\
l_- &= q_2/\xi \;=\; \frac{\sqrt{s}}{2}\sqrt{\frac{y}{\xi-x_B}}\;(1,\,0,\,0,\,-1)\,,\\
l'_+ &= \frac{\sqrt{s}}{2}\,\frac{1}{\sqrt{(\xi-x_B)y}}\left(\xi - \xi y + x_B y,\, 2\sqrt{x_B(\xi-x_B)(1-y)},\, 0,\, \xi - \xi y - 2x_B + x_B y\right),\\
q_1 &= \frac{\sqrt{s}}{2}\sqrt{\frac{y}{\xi-x_B}}\left(\xi - 2x_B,\, 0,\, 0,\, \xi\right).
\end{aligned} \tag{A.10}$$

As for the final quark-antiquark pair, we can write in general:

$$K_{q,\bar{q}} = \frac{\sqrt{\hat{s}}}{2}\left(1,\, \pm\sin\theta_q\cos\phi_q,\, \pm\sin\theta_q\sin\phi_q,\, \pm\cos\theta_q\right), \tag{A.11}$$

where θ_q and ϕ_q are respectively the polar and azimuthal angle of the quark direction of motion in the γ_1^*-γ_2 cm frame. It is again more convenient to consider the modulus of the q, $\bar{q}$ transverse momentum, K_T, and their pseudorapidities $\hat{\eta}_{q,\bar{q}}$. In fact, the first one is invariant, while the second ones are simply additive under boosts along the $\hat{z}$ axis. In the γ_1^*-γ_2 frame (which is also the q-$\bar{q}$ cm frame) we clearly have $\hat{\eta}_q = -\hat{\eta}_{\bar{q}} = \hat{\eta}$. We can therefore write the quark and antiquark four-momenta as

$$K_{q,\bar{q}} = K_T\left(\cosh\hat{\eta},\, \pm\cos\phi_q,\, \pm\sin\phi_q,\, \pm\sinh\hat{\eta}\right), \tag{A.12}$$

and the transverse and longitudinal components of the quark three-momentum with respect to the $\hat{z}$ axis are:

$$K_T = \frac{\sqrt{\hat{s}}}{2}\frac{1}{\cosh\hat{\eta}}\,, \quad K_L = \frac{\sqrt{\hat{s}}}{2}\tanh\hat{\eta}\,. \tag{A.13}$$

From this relation we can also see another useful property:

$$\xi = x_B + \frac{4K_T^2\cosh^2\hat{\eta}}{ys}\,. \tag{A.14}$$

Using Eq. (A.8) it is easy to see that, moving back to the γ_1^*-ℓ^- cm frame, by an inverse Lorentz boost with rapidity

$$y_b = \frac{1}{2}\log\left(\frac{\xi - x_B}{1 - x_B}\right) = \log\left(\frac{\sqrt{\hat{s}}}{W}\right), \tag{A.15}$$

the pseudorapidities of the quark and antiquark will become

$$\eta_q = \hat{\eta} - y_b\,, \quad \eta_{\bar{q}} = -\hat{\eta} - y_b\,, \tag{A.16}$$

and

$$\eta_q + \eta_{\bar{q}} = -2y_b = \log\left(\frac{1 - x_B}{\xi - x_B}\right) = \log\left(\frac{W^2}{\hat{s}}\right), \qquad \eta_q - \eta_{\bar{q}} = 2\hat{\eta}\,. \tag{A.17}$$

Following Ref. [79], we can also write the invariant variables $\zeta_{q,\bar{q}}$ introduced in Eq. (A.3) in terms of $\eta_{q,\bar{q}}$:

$$\begin{aligned}
\zeta_{\bar{q}} \equiv \zeta &= \frac{1}{e^{\eta_q - \eta_{\bar{q}}} + 1} = \frac{e^{-\hat{\eta}}}{2\,\cosh\hat{\eta}} = \frac{K_T}{\sqrt{\hat{s}}}\,e^{-\hat{\eta}}\,, \\
\zeta_q \equiv 1 - \zeta &= \frac{1}{e^{\eta_{\bar{q}} - \eta_q} + 1} = \frac{e^{\hat{\eta}}}{2\,\cosh\hat{\eta}} = \frac{K_T}{\sqrt{\hat{s}}}\,e^{\hat{\eta}}\,,
\end{aligned} \tag{A.18}$$

from which it is also clear that $\zeta_q + \zeta_{\bar{q}} = 1$, and in the last equality we have used Eq. (A.13).

Using these results, we can also write

$$K_{q,\bar{q}} = \frac{1}{2}\sqrt{(\xi - x_B)\,y\,s}\,\left(1,\, \pm 2\sqrt{\zeta(1-\zeta)}\,\cos\phi_q,\, \pm 2\sqrt{\zeta(1-\zeta)}\,\sin\phi_q,\, \pm(1 - 2\zeta)\right). \tag{A.19}$$

It is also useful to give the relation between these invariant variables and the Mandelstam invariants in the two-photon cm frame:

$$\hat{s} = (\xi - x_B)ys\,, \qquad \hat{t} = -\zeta\xi ys\,, \qquad \hat{u} = -(1-\zeta)\xi ys\,. \tag{A.20}$$

Let us also remind that there are a few additional kinematical constraints that must be fulfilled in order to guarantee the validity of the formalism adopted: 1) First of all, to stay in the deeply virtual and factorization regime we require $Q^2 \geq Q_0^2 \gg \Lambda^2_{\rm QCD}$, with Q_0^2 an arbitrary fixed hard scale of at least a few GeV^2; 2) Secondly, in order to clearly distinguish the two light-cone directions considered, the $\gamma^*\gamma$ axis and the jet thrust axis,

and keep staying in the validity regime of the factorization approach adopted, we also require $|\boldsymbol{K}_{qT}| = K_T \geq Q_0$. From Eq. (A.18) it is also easy to see that

$$K_T^2 = \zeta(1-\zeta)\hat{s}\,. \tag{A.21}$$

Therefore, putting a lower limit on the value of K_T, as required for the applicability of our factorization scheme, implies a lower cut on $\hat{s}$ and a limited range of allowed values for ζ: Since $\mathrm{Max}[\zeta(1-\zeta)] = 1/4$, $\hat{s} \geq 4\,Q_0^2$ and, at fixed $\hat{s}$,

$$\frac{1}{2}\left\{1-\sqrt{1-\frac{4\,Q_0^2}{\hat{s}}}\right\} \leq \zeta \leq \frac{1}{2}\left\{1+\sqrt{1-\frac{4\,Q_0^2}{\hat{s}}}\right\}. \tag{A.22}$$

For a generic $Q^2 \geq Q_0^2$, requiring that $\hat{s} = (\xi - x_B)Q^2/x_B \geq 4Q_0^2$ implies

$$\xi \geq x_B\left(1+\frac{4Q_0^2}{Q^2}\right). \tag{A.23}$$

Since $\xi \leq 1$, one finds

$$x_B \leq x_B^{\max}(Q^2) = \frac{Q^2}{Q^2+4Q_0^2} < 1\,. \tag{A.24}$$

Given that $x_B^{\min}(Q^2) = Q^2/s$ (for $y = 1$), imposing that $x_B^{\min}(Q^2) \leq x_B^{\max}(Q^2)$, one also finds an upper limit for Q^2, $Q^2 \leq s - 4Q_0^2$. Furthermore,

$$y^{\min}(Q^2) = \frac{Q^2}{x_B^{\max}(Q^2)\,s} = \frac{Q^2+4Q_0^2}{s}\,, \tag{A.25}$$

and, from Eq. (A.23),

$$\xi^{\min}(Q^2) = x_B^{\min}(Q^2)\left(1+\frac{4Q_0^2}{Q^2}\right) = y^{\min}(Q^2)\,. \tag{A.26}$$

Summarizing, then, we have the constraints:

$$\begin{aligned} &Q_0^2 \leq Q^2 \leq s-4Q_0^2\,,\\ &\frac{Q^2}{s} \leq x_B \leq \frac{Q^2}{Q^2+4Q_0^2}\,,\\ &\frac{Q^2+4Q_0^2}{s} \leq y,\,\xi \leq 1\,. \end{aligned} \tag{A.27}$$

B The virtual photon helicity density matrix in DIS processes

The derivation of the virtual photon helicity density matrix was given in detail, although with a notation different from the one adopted in this paper, in Ref. [80]. It was also

briefly discussed, within the same notation adopted here, in Ref. [81]. We therefore believe it can be useful to summarize here the main steps leading to the explicit expression of Eq. (2.11).

Let us start from the helicity amplitudes for a generic process in which a lepton ℓ interacts with a given initial system M by exchanging a single virtual photon, $\ell(l,\lambda_\ell) + M(P_i,\Lambda_i) \to \ell'(l',\lambda_{\ell'}) + M(P_f,\Lambda_f)$. For shortness, $P_{i,f}$, $\Lambda_{i,f}$ represent the full set of initial and final moments and helicities of M. This system can be e.g. a second lepton, like in our case, or a proton/nucleon target like in SIDIS.

The helicity amplitude for this process can be written as follows:

$$\begin{aligned} H_{\lambda_{\ell'},\Lambda_f\,;\lambda_\ell,\Lambda_i} &= e\,\bar{u}_{\lambda_{\ell'}}\,\gamma^\mu\,u_{\lambda_\ell}\left(-i\frac{g_{\mu\nu}}{q^2}\right)M^\nu_{\Lambda_f;\Lambda_i}(P_f,P_i) \\ &= e\,\bar{u}_{\lambda_{\ell'}}\,\gamma^\mu\,u_{\lambda_\ell}\left[-i\frac{g_{\mu\nu}}{q^2}\;+\;\frac{q_\mu q_\nu}{q^4}\right]M^\nu_{\Lambda_f;\Lambda_i}(P_f,P_i) \\ &= e\,\frac{1}{q^2}\bar{u}_{\lambda_{\ell'}}\,\gamma^\mu\,u_{\lambda_\ell}\left[\sum_{\lambda_\gamma}(-1)^{\lambda_\gamma+1}\,\epsilon^*_{\mu,\,\lambda_\gamma}(q)\,\epsilon_{\nu,\,\lambda_\gamma}(q)\right]M^\nu_{\Lambda_f;\Lambda_i}(P_f,P_i)\,, \end{aligned} \tag{B.1}$$

where in the second line we have used Ward identity and in the last line well-known properties of the polarization vectors of a virtual photon.

At the same time, we can separately define the helicity amplitudes for the processes $\ell(l,\lambda_\ell) \to \ell'(l',\lambda_{\ell'}) + \gamma^*(q,\lambda_\gamma)$,

$$\mathcal{H}_{\lambda_{\ell'},\lambda_\gamma;\lambda_\ell} \;=\; e\,\bar{u}_{\lambda_{\ell'}}\,\gamma^\mu\,u_{\lambda_\ell}\,\epsilon^*_{\mu,\,\lambda_\gamma}(q)\,, \tag{B.2}$$

and $\gamma^*(q,\lambda_\gamma) + M(P_i,\Lambda_i) \to M(P_f,\Lambda_f)$,

$$\mathcal{H}_{\Lambda_f;\lambda_\gamma,\Lambda_i} \;=\; \epsilon_{\nu,\,\lambda_\gamma}(q)\,M^\nu_{\Lambda_f;\Lambda_i}(P_f,P_i)\,. \tag{B.3}$$

Let us now consider the differential cross section for the full process $\ell(l,\lambda_\ell)+M(P_i,\Lambda_i) \to \ell'(l',\lambda_{\ell'}) + M(P_f,\Lambda_f)$. Assuming in general that the initial lepton ℓ is in a polarization state described by its helicity density matrix $\rho^{\ell(s_\ell)}_{\lambda_\ell,\lambda'_\ell}$, where s_ℓ specifies the lepton ℓ spin state, and using Eqs. (B.1), (B.2), (B.3), we can write

$$\begin{aligned} \mathrm{d}\sigma \;&\propto\; \sum_{\lambda_\ell,\lambda'_\ell,\lambda_{\ell'}}\;\sum_{\Lambda_i,\Lambda_f}\rho^{\ell(s_\ell)}_{\lambda_\ell,\lambda'_\ell}\,H_{\lambda_{\ell'},\Lambda_f\,;\lambda_\ell,\Lambda_i}\,H^*_{\lambda_{\ell'},\Lambda_f\,;\lambda'_\ell,\Lambda_i} \\ &= \sum_{\lambda_\ell,\lambda'_\ell,\lambda_{\ell'}}\;\sum_{\Lambda_i,\Lambda_f}\rho^{\ell(s_\ell)}_{\lambda_\ell,\lambda'_\ell}\left[\frac{1}{q^2}\sum_{\lambda_\gamma}(-1)^{\lambda_\gamma+1}\,\mathcal{H}_{\lambda_{\ell'},\lambda_\gamma;\lambda_\ell}\,\mathcal{H}_{\Lambda_f;\lambda_\gamma,\Lambda_i}\right] \\ &\times\left[\frac{1}{q^2}\sum_{\lambda'_\gamma}(-1)^{\lambda'_\gamma+1}\,\mathcal{H}^*_{\lambda_{\ell'},\lambda'_\gamma;\lambda'_\ell}\,\mathcal{H}^*_{\Lambda_f;\lambda'_\gamma,\Lambda_i}\right] \\ &= \sum_{\lambda_\gamma,\lambda'_\gamma}\tilde{\rho}_{\lambda_\gamma,\lambda'_\gamma}(\gamma^*)\sum_{\Lambda_i,\Lambda_f}\mathcal{H}_{\Lambda_f,\lambda_\gamma;\Lambda_i}\,\mathcal{H}^*_{\Lambda_f,\lambda'_\gamma;\Lambda_i} \end{aligned} \tag{B.4}$$

where we have defined the (non normalized) helicity density matrix for the virtual photon γ^*,

$$\tilde{\rho}_{\lambda_\gamma,\lambda'_\gamma}(\gamma^*) \;=\; \frac{1}{q^4}\,(-1)^{\lambda_\gamma+\lambda'_\gamma}\sum_{\lambda_\ell,\lambda'_\ell,\lambda_{\ell'}}\rho^{\ell(s_\ell)}_{\lambda_\ell,\lambda'_\ell}\,\mathcal{H}_{\lambda_{\ell'},\lambda_\gamma;\lambda_\ell}\,\mathcal{H}^*_{\lambda_{\ell'},\lambda'_\gamma;\lambda'_\ell}\,. \tag{B.5}$$

This is the expression we were looking for.

The helicity density matrix for the initial lepton can be written in general as

$$\rho^{\ell(s_\ell)}_{\lambda_\ell,\lambda'_\ell} = \frac{1}{2}\left(I + \boldsymbol{\mathcal{P}}^\ell \cdot \boldsymbol{\sigma}\right) = \frac{1}{2}\begin{pmatrix} 1+\mathcal{P}^\ell_{\hat{z}} & \mathcal{P}^\ell_{\hat{x}} + i\mathcal{P}^\ell_{\hat{y}} \\ \mathcal{P}^\ell_{\hat{x}} - i\mathcal{P}^\ell_{\hat{y}} & 1-\mathcal{P}^\ell_{\hat{z}} \end{pmatrix}, \tag{B.6}$$

where $\boldsymbol{\mathcal{P}}^\ell$ is the polarization (pseudo)vector of the lepton. In this paper, we will only consider the case of unpolarized or fully longitudinally polarized lepton beams ($\mathcal{P}^\ell_{\hat{z}} = 0$ or ± 1 respectively), taking $\mathcal{P}^\ell_{\hat{x}} = \mathcal{P}^\ell_{\hat{y}} = 0$.

Inserting Eqs. (B.2), (B.6) into Eq. (B.5) and performing some traces we finally get:

$$\begin{aligned}\tilde{\rho}_{\lambda_\gamma,\lambda'_\gamma}(\gamma^*) = \frac{e^2}{q^4}(-1)^{\lambda_\gamma+\lambda'_\gamma}\Big[&4\,l\cdot\epsilon^*_{\lambda_\gamma}(q)\,l\cdot\epsilon_{\lambda'_\gamma}(q) + q^2\,\epsilon^*_{\lambda_\gamma}(q)\cdot\epsilon_{\lambda'_\gamma}(q) \\ &+2\,i\,\mathcal{P}^\ell_{\hat{z}}\,\epsilon^{\alpha\beta\mu\nu}\,l_\alpha\,\epsilon_{\beta,\lambda_\gamma}(q)\,l_\mu\,\epsilon_{\nu,\lambda'_\gamma}(q)\Big]\,.\end{aligned} \tag{B.7}$$

By assuming that the virtual photon moves along the positive $\hat{z}$ axis of our reference frame, and the leptonic ℓ-ℓ' plane forms an angle ϕ_ℓ with the $\hat{x}$-$\hat{z}$ plane, and using the results of Appendix A in the γ^*-ℓ_2 frame, we get:

$$\begin{aligned} l &= \frac{\sqrt{s}}{2}\frac{1}{\sqrt{(1-x_B)y}} \\ &\left(1-x_By,\, 2\sqrt{x_B(1-x_B)(1-y)}\,\cos\phi_\ell,\, 2\sqrt{x_B(1-x_B)(1-y)}\,\sin\phi_\ell,\, 1-2x_B+x_By\right) \\ q &= \frac{\sqrt{s}}{2}\frac{1}{\sqrt{(1-x_B)\,y}}\left((1-2x_B)y,\,0,\,0,\,y\right). \end{aligned} \tag{B.8}$$

Furthermore, one has

$$\begin{aligned}\epsilon_{\lambda_\gamma=\pm1}(q) &= \frac{1}{\sqrt{2}}\,(\,0,\,-\lambda_\gamma,\,-i,\,0\,) \\ \epsilon_{\lambda_\gamma=0}(q) &= \frac{1}{2}\frac{1}{\sqrt{x_B(1-x_B)}}\,(\,1,0,0,1-2x_B)\,.\end{aligned} \tag{B.9}$$

Inserting these expressions into Eq. (B.7), after some straightforward calculation we finally get the result of Eq. (2.12).

Notice that the normalized helicity density matrix of the virtual photon is entirely given in terms of the DIS invariant y. The only kinematical frame-dependent quantity is the azimuthal angle ϕ_ℓ of the leptonic plane, which is however invariant under boosts along the $\hat{z}$ axis.

Let us finally observe that the virtual photon helicity density matrix is directly related to the usual leptonic tensor $L^{\mu\nu}$.

Chapter 3

Gluon TMDs from Higgs production at the LHC

. Among all hadronic final states, inclusive Higgs production in proton-proton collisions stands out as the cleanest probe of the unpolarised gluon transverse momentum dependent distribution $f_1^g(x, \boldsymbol{k}_\perp)$. The reasons are both conceptual and practical. At the LHC the dominant production mode is gluon fusion, and the observed final state is colour-singlet. Thus, it is possible to avoid colour entanglement issues that can compromise TMD factorization in channels with coloured final states, such as jets or colour octet quarkonia, making the Higgs production one of the simplest channels for which rigorous TMD factorization is available and strongly supported in the literature. In the small-q_T region, precisely where intrinsic and soft transverse momenta dominate, the differential cross section factorises into a hard function and a convolution of two gluon TMDs with the usual soft factor and Collins-Soper evolution; consequently, the shape of the Higgs q_T distribution becomes directly sensitive to f_1^g, with possible modifications from linearly polarised gluons $h_1^{\perp g}$.

On the methodological side, Higgs production benefits from high theoretical precision in the ingredients entering a TMD analysis; in particular, the perturbative treatment of gluon TMDs, including matching/evolution, has been pushed to high orders, with dedicated NNLO studies and applications to the Higgs q_T spectrum, thereby enabling robust extractions with quantified uncertainties.

In order to extract this information from the experimental data, we employ the NangaParbat[1] fitting framework, developed by the MAP Collaboration. This C++ code allows us to perform fits to experimental measurements and generate grids for the resulting TMDs. The framework supports multiple functional forms and evolution options for the TMDs, enabling the selection of physically motivated parametrisations and the assessment of the associated uncertainties. Notably, NangaParbat is modular: the same TMD ingredients can be interfaced with different process modules, ensuring a like-for-like

[1]The NangaParbat code is available at https://github.com/MapCollaboration/NangaParbat.

comparison between theory and data while keeping the treatment of factorisation and evolution consistent across datasets. In the following, we will implement this tool for our analysis.

3.1 Higgs cross section in TMD factorization

We study the inclusive hard scattering process

$$h_1(P_1) + h_2(P_2) \to H(y, q_T, M_H) + X \tag{3.1}$$

in which two hadrons with four-momenta P_1 and P_2 collide to produce a color-singlet Higgs boson of invariant mass $q^2 = M_H^2$, accompanied by an arbitrary and undetected final state X. The hadronic centre of mass energy of the colliding hadrons is denoted by $\sqrt{s}$, and Higgs rapidity y is defined in the laboratory frame of the colliding hadrons.
At the LHC the dominant production channel is gluon fusion, $gg \to H$, mediated by a heavy quark loop, as illustrated in Fig. 1. Since the Yukawa coupling of the Higgs boson to a quark is proportional to the quark mass, the amplitude is dominated by a virtual top loop, while lighter (e.g. b) quark contributions are suppressed.

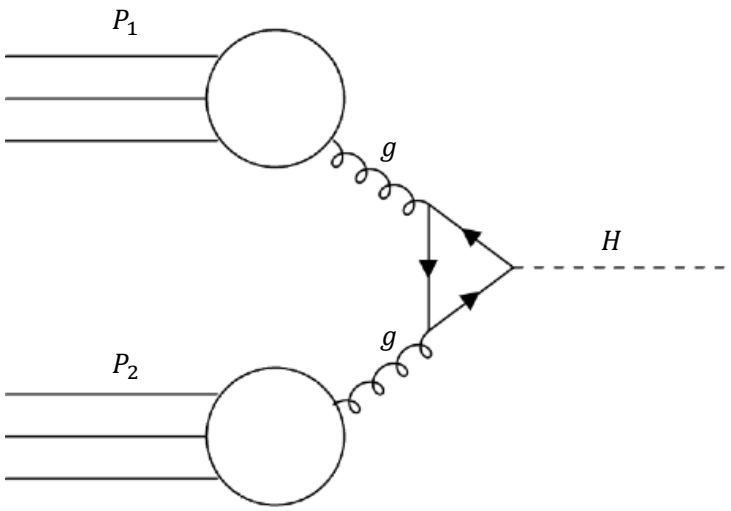

Figure 1: Higgs production through gluon fusion

The matrix element that describes the contribution of the loop is [91]

$$|M(gg \to H)|^2 = \frac{\alpha_S^2(M_H^2) M_H^4 G_F}{288\pi\sqrt{2}} \left| \sum_Q A_Q\left(\frac{4M_Q^2}{M_H^2}\right) \right|^2, \tag{3.2}$$

where $G_F = 1.16639 \times 10^{-5}\,\mathrm{GeV}^{-2}$ is the Fermi constant, $M_Q = M_t$ or M_b denotes the

on-shell pole mass of the top or bottom quark, and the amplitude A_Q is given by

$$A_Q(x) = \frac{3}{2}\, x\Big[1 + (1-x) f(x)\Big],$$
$$f(x) = \begin{cases} \arcsin^2\left(\dfrac{1}{\sqrt{x}}\right), & x \geq 1, \\ -\dfrac{1}{4}\left[\ln\left(\dfrac{1+\sqrt{1-x}}{1-\sqrt{1-x}}\right) - i\pi\right]^2, & x < 1. \end{cases} \tag{3.3}$$

In our analysis, we take the large top mass limit, from which $A_Q \to 1$, reducing the gluon loop to an effective ggH vertex.
Since the process structure closely mirrors Drell-Yan, we employ TMD factorization as in Sec. 1.2, taking care in considering the gluon distribution rather than the quark distribution. In the small transverse momentum region, $q_T \ll M_H$, the differential cross section of the production of a spin-0 Higgs boson can be factorized as

$$\frac{d\sigma}{dQdydq_T} = \frac{\alpha_S^2(Q) Q^2 G_F \mathcal{P}}{288\pi\sqrt{2}\,\hat{s}} H_{ggH}(Q,\mu) \int \frac{d^2\boldsymbol{b}_T}{(2\pi)^2} e^{ib_T\cdot q_T} \\ \times \Big[x_1 \tilde{f}_1^g(x_1, \boldsymbol{b}_T; \mu, \zeta_a)\, x_2 \tilde{f}_1^g(x_2, \boldsymbol{b}_T; \mu, \zeta_b) \;+\; x_1 \tilde{h}_1^g(x_1, \boldsymbol{b}_T; \mu, \zeta_a)\, x_2 \tilde{h}_1^g(x_2, \boldsymbol{b}_T; \mu, \zeta_b)\Big] \tag{3.4}$$

where $\hat{s} = x_1 x_2 s$ is the partonic centre-of-mass energy squared for $gg \to H + X$, and $x_{1(2)} = Q/\sqrt{s} e^{\pm y}$ are the light-cone momentum fractions. $\mathcal{P}$ is the phase-space reduction factor associated with the kinematic cuts on the final state, discussed in Appendix C.[2]

Now we show how the methods developed in Sec. 1.3 enable us to disentangle, within the TMD extraction, the perturbative and non-perturbative contributions. In what follows, we spell out which ingredients can be precomputed in a TMD fit, and which are obtained through the implementation of NangaParbat. We adopt the shorthand notation

$$\overline{F}_g(x, \boldsymbol{b}_T; \mu, \zeta) \equiv x \tilde{f}_1^g(x, \boldsymbol{b}_T; \mu, \zeta)\,, \tag{3.5}$$

which is convenient for the implementation. As reviewed in Sec. 1.2, the scales μ and ζ arise from removing UV and rapidity divergences in the TMD definition; a standard choice is to set them equal to the hard scale, $\mu = \sqrt{\zeta} = Q$.
The computation-intensive part of Eq. (3.4) takes the form

$$I_{ij}(x_1, x_2, q_T; \mu, \zeta) = \int \frac{d^2\mathbf{b}}{4\pi} e^{i\mathbf{b}\cdot\mathbf{q}_T} \overline{F}_i(x_1, \mathbf{b}; \mu, \zeta) \overline{F}_j(x_2, \mathbf{b}; \mu, \zeta)\,. \tag{3.6}$$

where $\overline{F}_{i(j)}$ denote combinations of evolved TMD PDFs. For convenience, the indices i and j do not coincide with the physical gluon label g, but they are related to it by a fixed linear transformation.

[2] For brevity, we will use the shorthand $\sigma_0 \equiv \frac{\alpha_S^2(Q) Q^2 G_F}{288\pi\sqrt{2}\hat{s}}$ throughout.

In general, a two-dimensional integral has to be carried out in Eq. (3.6); however, if $\overline{F_i}$ only depends on the absolute value of $\boldsymbol{b}_T$,$|\boldsymbol{b}_T| = b_T$ as in Eq. (1.42), we can write

$$I_{ij}(x_1, x_2, q_T; \mu, \zeta) = \frac{1}{2}\int_0^\infty db\, b J_0(bq_T)\overline{F}_i(x_1, b; \mu, \zeta)\overline{F}_j(x_2, b; \mu, \zeta)\,. \tag{3.7}$$

As detailed in Sec. 1.3, at small b_T and taking into account correct evolution treatment, the TMD PDF $\overline{F}_i$ can be written as

$$\overline{F}_i(x, b_T; \mu, \zeta) = R(\mu_0, \zeta_0 \to \mu, \zeta; b_T) \sum_{j=g,q(\bar{q})} \Big(C_{ij} \otimes f^j\Big)(x, b_T, \mu_0, \zeta_0)\ , \tag{3.8}$$

where the C_{ij} are the matching functions to the collinear PDFs f_j, while the Sudakov form factor describing the evolution term is collected in $R(\mu_0, \zeta_0 \to \mu, \zeta; b_T)$. Matching and evolution receive non-perturbative contributions that become relevant at large b_T. In order to account for such effects, one usually introduces a phenomenological function f_{NP}. Adopting the b_* prescription (Sec. 1.3.2), we then write:

$$\overline{F}_i(x, b_T; \mu, \zeta) \to \overline{F}_i(x, b_*(b_T); \mu, \zeta) f_{\rm NP}(x, b_T, \zeta)\,. \tag{3.9}$$

Including the non-perturbative function, Eq (3.7) becomes

$$\begin{aligned} I_{ij}(x_1, x_2, q_T; \mu, \zeta) = \int_0^\infty db_T\, J_0(b_T q_T) \Bigg[& \frac{b_T}{2}\overline{F}_i(x_1, b_*(b_T); \mu, \zeta)\overline{F}_j(x_2, b_*(b_T); \mu, \zeta) \\ & \times f_{\rm NP}(x_1, b_T, \zeta) f_{\rm NP}(x_2, b_T, \zeta)\Bigg] \\ = \frac{1}{q_T}\int_0^\infty d\bar{b}_T\, J_0(\bar{b}_T) \Bigg[& \frac{\bar{b}_T}{2q_T}\overline{F}_i\left(x_1, b_*\left(\frac{\bar{b}_T}{q_T}\right); \mu, \zeta\right)\overline{F}_j\left(x_2, , b_*\left(\frac{\bar{b}_T}{q_T}\right); \mu, \zeta\right) \\ & \times f_{\rm NP}\left(x_1, \frac{\bar{b}_T}{q_T}, \zeta\right) f_{\rm NP}\left(x_2, \frac{\bar{b}_T}{q_T}, \zeta\right)\Bigg]\,, \end{aligned} \tag{3.10}$$

which is a Hankel transform that can be efficiently evaluated using the Ogata quadrature [92]. Accordingly, Eq. (3.6) can be computed by the weighted sum

$$\begin{aligned} I_{ij}(x_1, x_2, q_T; \mu, \zeta) \simeq \frac{1}{q_T}\sum_{n=1}^{N} \frac{w_n^{(0)} z_n^{(0)}}{2q_T} & \overline{F}_i\left(x_1, b_*\left(\frac{z_n^{(0)}}{q_T}\right); \mu, \zeta\right)\overline{F}_j\left(x_2, b_*\left(\frac{z_n^{(0)}}{q_T}\right); \mu, \zeta\right) \\ & \times f_{\rm NP}\left(x_1, \frac{z_n^{(0)}}{q_T}, \zeta\right) f_{\rm NP}\left(x_2, \frac{z_n^{(0)}}{q_T}, \zeta\right)\,, \end{aligned} \tag{3.11}$$

where the unscaled coordinates $z_n^{(0)}$ and the weights $w_n^{(0)}$ can be precomputed from the zeros of the Bessel function J_0 and one single parameter (see Ref. [92] for details).[3] Based

[3]The superscript 0 in $z_n^{(0)}$ and $w_n^{(0)}$ indicates that the Hankel transform involves the Bessel function of order zero, J_0. This is useful in the next calculation, where the integration over q_T leads to a similar Hankel transform with J_0 replaced by J_1. The Ogata algorithm applies there as well, with different coordinates and weights.

on the (empirically verified) assumption that the absolute value of each term in the sum in the r.h.s. of Eq. (3.11) decreases monotonically, the truncation N is chosen dynamically so that the $(N+1)$-th term is smaller in absolute value than a user-defined tolerance relative to the sum of the preceding N terms.
As customary in QCD, the most convenient basis for the matching in Eq. (1.51) is the "evolution" basis (i.e. Σ, V, T_3, V_3, etc.). In this basis, the operator matrix C_{ij} is nearly diagonal, with the only exception of crossing terms that couple the gluon and the single Σ distributions. Consequently, this basis is also optimal for the computation of I_{ij}. Since the TMDs entering Eq. (3.4) are written in the "physical" basis, we need to rotate $F_{i(j)}$ from the evolution basis, over which the indices i and j run, into the physical one via an appropriate constant matrix T,

$$\overline{F}_g(x_1, b; \mu, \zeta) = \sum_i T_{gi} F_i(x_1, b; \mu, \zeta)\,. \tag{3.12}$$

Putting all the pieces together, the cross section in Eq. (3.4) can be cast into the compact form

$$\frac{d\sigma}{dQdydq_T} \simeq \sum_{n=1}^{N} w_n^{(0)} \frac{z_n^{(0)}}{q_T} S\left(x_1, x_2, \frac{z_n^{(0)}}{q_T}; \mu, \zeta\right) f_{\rm NP}\left(x_1, \frac{z_n^{(0)}}{q_T}, \zeta\right) f_{\rm NP}\left(x_2, \frac{z_n^{(0)}}{q_T}, \zeta\right)\,. \tag{3.13}$$

Eq. (3.13) enables one to precompute the weights S, so that the differential cross section in Eq. (3.4) can be evaluated as a simple weighted sum over the non-perturbative contribution. Although S appears to depend on five arguments, they are not independent; in practice, S depends on only three variables. The two arbitrary scales μ and ζ are typically chosen proportional to Q (by a constant factor), while x_1 and x_2 are functions of Q and y as specified above. Hence, the full dependence on the kinematics of the final state of Eq. (3.4) is fully characterized by Q, y and q_T.
Despite the efficiency of Eq. (3.13), a direct comparison with experimental results often requires bin-integrated observables, since measured differential distributions are usually reported after integration over finite regions of the final-state phase space. The relevant quantity to compare with data is therefore

$$\frac{d\sigma}{dq_T} = \frac{1}{q_{T,\rm max} - q_{T,\rm min}} \int_{Q_{\rm min}}^{Q_{\rm max}} dQ \int_{y_{\rm min}}^{y_{\rm max}} dy \int_{q_{T,\rm min}}^{q_{T,\rm max}} dq_T \left[\frac{d\sigma}{dQdydq_T}\right]\,, \tag{3.14}$$

where the intervals $[y_{\rm min} : y_{\rm max}]$, $[Q_{\rm min} : Q_{\rm max}]$ and $[q_{T,\rm min} : q_{T,\rm max}]$ define the phase space integration domain, and the integrand is given in Eq. (3.4). Consequently, to confront theory with data, these integrations must be performed. While the integrals over Q and y are computed numerically, the integral over q_T can be carried out (semi)analytically by exploiting a property of the Bessel functions J_n (see Appendix B for more details).

3.2 Experimental data

In this section, we describe the experimental data used in this analysis. We consider the Higgs-boson transverse-momentum (q_T) distribution measured by the ATLAS and CMS experiments in two decay channels: two-photon ($\gamma\gamma$) and four-lepton (4ℓ). Table 1 lists the datasets considered. For each channel and experiment, we import the fiducial binned spectra $d\sigma/dp_T^H$, together with bin edges and central values, from HEPDATA. Throughout, we keep the data at particle (fiducial) level, identifying $p_T^H = p_T^{\gamma\gamma}$ in the diphoton channel and $p_T^H = p_T^{4\ell}$ in the four-lepton channel.
At this stage, our main goal is to assess whether these data are sensitive to TMD effects and, consequently, whether they allow a future extraction of the unpolarised gluon TMD. Since the published spectra are inclusive over production mechanisms, the theory prediction entering the likelihood is the sum of the SM modes (ggF, VBF, VH, $t\bar{t}H$, $b\bar{b}H$) evaluated within the relevant fiducial selections. Sensitivity to the gluon TMD is driven by the gluon-fusion channel (dominant in rate), while sub-leading modes are included with state-of-the-art normalizations. Uncertainties associated with these sub-leading contributions are propagated as theory nuisance parameters.
One channel is the Higgs decay into four leptons, $H \to ZZ^* \to 4\ell$ (electrons, muons, or a combination of both). At tree level, this decay proceeds through the Higgs coupling to two neutral gauge bosons, see Fig. 2. For $m_H \simeq 125$ GeV, at least one Z is off shell, but the four charged leptons in the final state allow a clean reconstruction of the Higgs candidate. The other channel is the diphoton decay, $H \to \gamma\gamma$, see Fig. 3. It is rare in the SM because

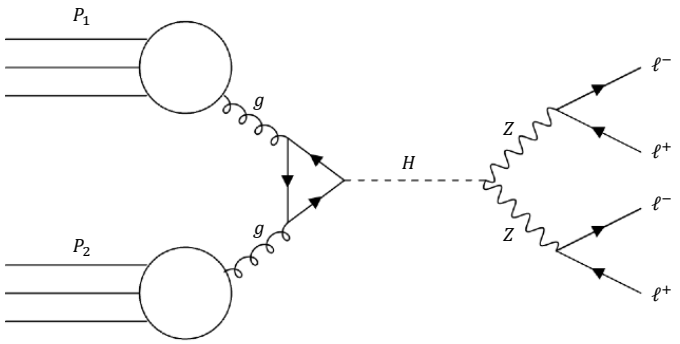

Figure 2: Representative Feynman diagram for Higgs-boson production and decay in the four-lepton channel: gluon–gluon fusion via a heavy-quark loop, followed by $H \to ZZ^{(*)} \to \ell^+\ell^-\,\ell'^+\ell'^-$ with $\ell = e, \mu$.

it occurs via loops of charged particles (primarily the top quark and W bosons), but it offers a striking experimental signature with a narrow peak in the diphoton invariant mass. In addition, we also consider the experimental results obtained by combining these processes, as provided by the ATLAS and CMS experiments, see Refs. [93, 94]. Since our analysis is based on the TMD factorization formula in Eq. (3.4), only data at small

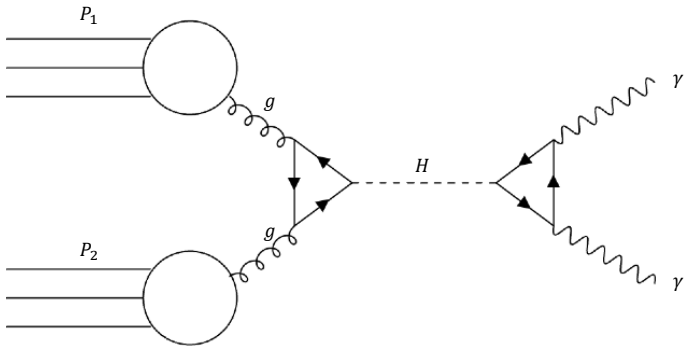

Figure 3: Representative Feynman diagram for Higgs-boson production and decay in the diphoton channel: gluon–gluon fusion via a heavy-quark loop, followed by $H \to \gamma\gamma$.

q_T can be described. Hence, we impose a cut to exclude measurements with large q_T by requiring $q_T/Q \lesssim 0.3$ (numerically, bins below ~ 40 GeV for $m_H \simeq 125$ GeV). The second column in Tab. 1 reports, for each dataset, the number of data points passing this cut; the total number of points included in our analysis is 36.

An important feature of all the datasets listed above is that the cross sections are given within a certain fiducial region, with kinematic cuts on the transverse momentum and pseudorapidity of the particles in the final state. Tables 2 and 3 summarize the cuts implemented for each channel and experiment.

Notice that there are no cuts implemented for the combined data since, to perform the combination, the measurements are extrapolated to the full phase space. Our predictions are corrected by means of the phase-space reduction factor $\mathcal{P}$ introduced in Eq. (3.4), which accounts for these cuts. Details concerning the calculation of $\mathcal{P}$ are given in the Appendix C.

Most of the considered experimental datasets are released with both uncorrelated and correlated uncertainties. As already pointed out in Ref. [103], a proper treatment of the experimental uncertainties is crucial to achieve a reliable extraction of TMDs. In other words, the χ^2, which quantifies the agreement between data and predictions and is minimized during the fit, has to be computed taking into account the nature of the various uncertainties.

In the presence of correlated uncertainties, the χ^2 can be decomposed as [104]

$$\chi^2 = \chi^2_D + \chi^2_\lambda \,, \tag{3.15}$$

where χ^2_D is the uncorrelated (diagonal) contribution, while χ^2_λ is a penalty term that encodes the effect of correlations (see, e.g., Appendix B of Ref. [103]). For the computation of χ^2_D, theoretical predictions are shifted by best-fit nuisance parameters to account for the correlated systematics. The shifted predictions provide a better proxy for visual comparison to experimental data; accordingly, all plots shown below display shifted theory curves.

Experiment	$\mathbf{N_{dat}}$	**Decay**	$\sqrt{s}$ [GeV]	**Lumi**[fb^{-1}]	**Ref.**
CMS RunII	7	$H \to \gamma\gamma$	13000	137	[95]
CMS RunII	3	$H \to 4\ell$	13000	138	[96]
CMS RunI	2	combined	13000	35.9	[93]
CMS 8 TeV	2	$H \to \gamma\gamma$	800	19.7	[97]
ATLAS RunII	7	$H \to \gamma\gamma$	13000	139	[98]
ATLAS RunII	3	$H \to 4\ell$	13000	139	[99]
ATLAS RunI	2	$H \to \gamma\gamma$	13000	36.1	[100]
ATLAS RunI	4	$H \to 4\ell$	13000	36.1	[101]
ATLAS RunI	3	combined	13000	36.1	[94]
ATLAS 8 TeV	2	$H \to \gamma\gamma$	800	20.3	[102]
ATLAS 8 TeV	1	$H \to 4\ell$	800	20.3	[101]
Total	**36**	–	–	–	–

Table 1: Breakdown of the datasets included in this analysis. For each dataset, the table includes information on: the number of data points (N_{dat}) passing the nominal cut on q_T/Q, the decay channel, the centre of mass energy $\sqrt{s}$, and the public reference. For all the data we have fixed the invariant mass at the Higgs mass, $Q = m_H$, and the range of the Higgs rapidity at $|y| < 2.5$. The total number of data points amounts to 36.

An additional key point concerns the choice of the collinear PDFs. To extract f_{NP} in Eq. (1.72), one must fix a specific PDF set; in this work we use the set NNPDF3.1 [105]. Since PDF uncertainties reflect the experimental uncertainty of the dataset used for their extraction, it is natural to regard them as experimental and include them in χ^2 evaluation.

3.3 Preliminary Results

In this section, we present a preliminary consistency test between the experimental measurements of Tab. 1 and our theoretical predictions.
As a first step, we adopt a minimal, x-independent ansatz for the non-perturbative factor f_{NP} in Eq. (1.72). The function f_{NP} accounts for large-b_T behaviour of the TMDs, and, in general, depends on b_T, ζ and x. While the asymptotic dependence on b_T follows from first principles (see Sec. 1.3.2) and the evolution with ζ is determined by the Collins-Soper equation (1.45), the x dependence is a priori unknown. To test the dataset with a simple, x-independent form, we use the DWS parametrisation

$$f_{\rm NP}^{\rm DWS}(b_T, \zeta) = \exp\left[-\frac{1}{2}\left(g_1 + g_2 \ln\frac{\zeta}{2Q_0^2}\right) b_T^2\right]. \tag{3.16}$$

Exp: $H \to 4\ell$	$p_{T,\ell}$ **(GeV)**	$\lvert\eta_\ell\rvert$	**Event selection**	
			$p_{T,\ell}$ **(GeV)**	**Lepton pair mass (GeV)**
CMS Run II 13 TeV	$> 7\ (e), > 5\ (\mu)$	$< 2.5\ (e), < 2.4(\mu)$	$> 20, > 10$	$40 < m_{12} < 120,\ 12 < m_{34} < 120$
ATLAS 8 TeV	$> 7\ (e), > 6\ (\mu)$	$< 2.47(e), < 2.7(\mu)$	$> 20, > 15, > 10$	$50 < m_{12} < 106,\ 12 < m_{34} < 115$
ATLAS Run I 13 TeV	$> 7\ (e), > 5\ (\mu)$	$< 2.47(e), < 2.7(\mu)$	$> 20, > 15, > 10$	$50 < m_{12} < 106,\ 12 < m_{34} < 115$
ATLAS Run II 13 TeV	$> 7\ (e), > 5\ (\mu)$	$< 2.47(e), < 2.7(\mu)$	$> 20, > 15, > 10$	$50 < m_{12} < 106,\ 12 < m_{34} < 115$

Table 2: List of event selection requirements which define the fiducial phase space for the cross-section measurement of the decay channel $H \to 4\ell$.

Exp: $H \to \gamma\gamma$	$p_{T,\gamma_1}/m_{\gamma\gamma}$ (%)	$p_{T,\gamma_2}/m_{\gamma\gamma}$ (%)	$\lvert\eta_\gamma\rvert$
CMS Run II 13 TeV	> 35	> 25	$\lvert\eta_\gamma\rvert < 1.4442\ \vee\ 1.566 < \lvert\eta_\gamma\rvert < 2.5$
CMS Run I 13 TeV	> 35	> 25	$\lvert\eta_\gamma\rvert < 1.4442\ \vee\ 1.566 < \lvert\eta_\gamma\rvert < 2.5$
CMS 8 TeV	> 35	> 25	$\lvert\eta_\gamma\rvert < 1.44\ \vee\ 1.57 < \lvert\eta_\gamma\rvert < 2.5$
ATLAS 8 TeV	> 35	> 25	$\lvert\eta_\gamma\rvert < 1.37\ \vee\ 1.56 < \lvert\eta_\gamma\rvert < 2.37$
ATLAS Run I 13 TeV	> 35	> 25	$\lvert\eta_\gamma\rvert < 1.37\ \vee\ 1.52 < \lvert\eta_\gamma\rvert < 2.37$
ATLAS Run II 13 TeV	> 35	> 25	$\lvert\eta_\gamma\rvert < 1.37\ \vee\ 1.52 < \lvert\eta_\gamma\rvert < 2.37$

Table 3: List of event selection requirements which define the fiducial phase space for the cross-section measurement of the decay channel $H \to \gamma\gamma$

with two parameters, g_1 and g_2, and $Q_0^2 = 1.6\,\mathrm{GeV}^2$, inspired by the work of Davis, Webber, and Stirling, Ref. [106]. As a benchmark, we fix $g_1 = g_2 = 1$ and perform a central-replica fit at N^3LL accuracy, applying the cut $q_T/Q < 0.3$ to stay in the TMD-validity region. Table 4 reports the breakdown of the central-replica χ^2 per dataset, normalised to the corresponding number of points N_{dat}. We quote separately the uncorrelated piece χ^2_D and the correlated penalty χ^2_λ; their sum gives the total χ^2.

The global value $\chi^2 \simeq 2.10$ indicates that our benchmark setup does not yet yield a fully satisfactory description of all datasets. Part of the tension likely stems from limited statistics in some spectra and from residual sensitivity to fiducial selections; nevertheless, several channels are already reasonably captured. In particular, the ATLAS Run II $H \to 4\ell$ measurement shows a good level of agreement, whereas the CMS Run II $H \to 4\ell$ and the ATLAS 8 TeV $H \to \gamma\gamma$ spectra contribute disproportionately to the total χ^2. Overall, the picture for the most recent LHC runs is mixed but encouraging: some distributions are described within uncertainties, while others clearly point to missing flexibility in the present non-perturbative ansatz.

Nevertheless, there is room for improvement in a more refined analysis: we will explore more flexible parametrizations to better capture the data and improve the treatment of uncorrelated uncertainties as well as the implementation of fiducial cuts.

For a visual assessment, Fig. 4 compares data (black dots) and theory (red dots) for the ATLAS and CMS Run II datasets. In each panel, the theoretical points are shifted

Experiment	χ^2_D	χ^2_λ	χ^2
CMS Run II, $H \to \gamma\gamma$	2.147	0	2.147
CMS Run II, $H \to 4\ell$	4.864	0	4.864
CMS 8 TeV, $H \to \gamma\gamma$	0.201	0	0.201
CMS Run I, combined	4.509	0	4.509
ATLAS Run II, $H \to \gamma\gamma$	1.551	0.724	2.275
ATLAS Run II, $H \to 4\ell$	1.440	0.000	1.440
ATLAS Run I, $H \to \gamma\gamma$	0.654	0.034	0.689
ATLAS Run I, $H \to 4\ell$	1.374	0.001	1.375
ATLAS Run I, combined	0.719	0	0.719
ATLAS 8 TeV, $H \to \gamma\gamma$	3.223	0.399	3.622
ATLAS 8 TeV, $H \to 4\ell$	0.001	0	0.001
Total	**1.934**	**0.165**	**2.099**

Table 4: Breakdown of the central–replica fit at N^{3}LL with the selection $q_T/Q < 0.3$. Shown are the uncorrelated (χ^2_D), correlated (χ^2_λ), and total (χ^2) contributions per dataset.

by the best–fit nuisance parameters to account for correlated uncertainties, while the experimental error bars combine uncorrelated components in quadrature. In each panel, the upper part displays the absolute q_T spectrum; the lower one shows the theory/data ratio.

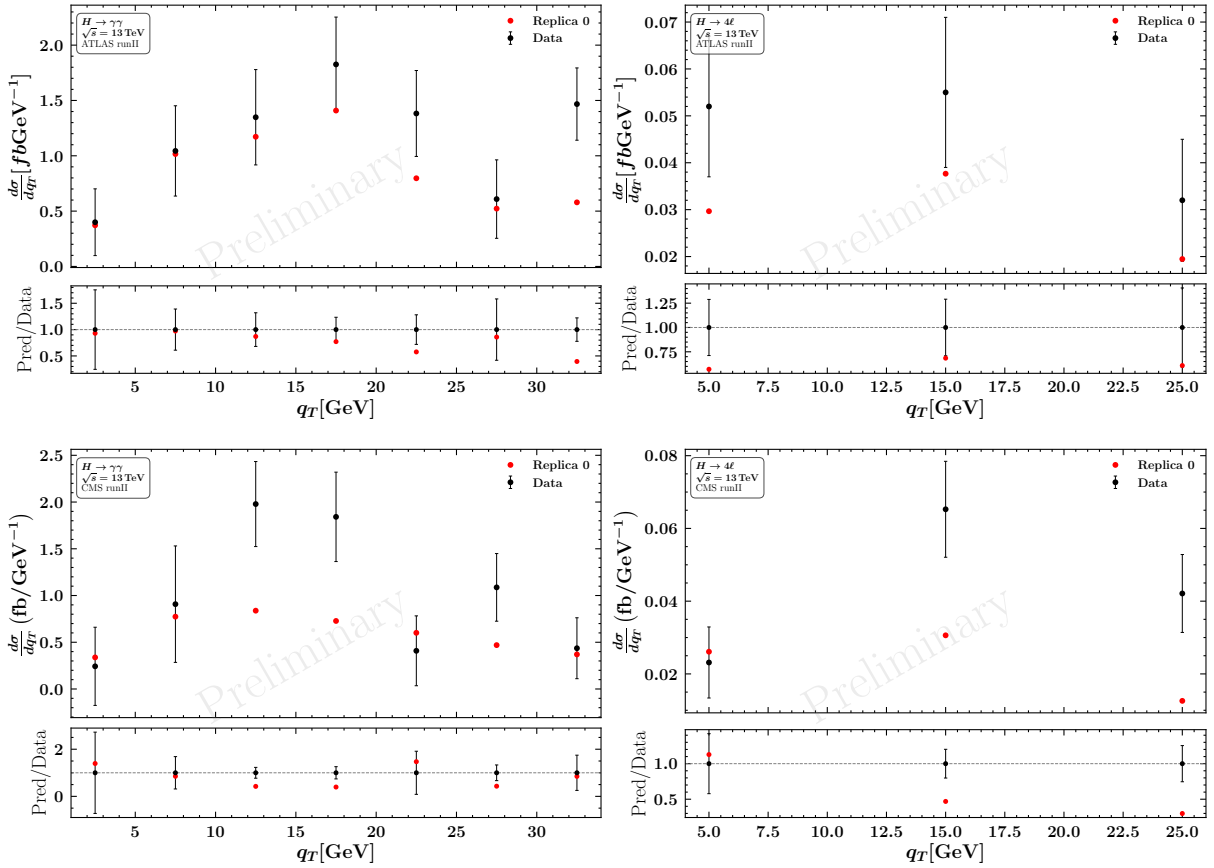

Figure 4: Comparison between ATLAS and CMS Run II measurements and theoretical predictions at N^{3}LL accuracy. Upper panels show the absolute q_T distributions; lower panels show the same distributions normalized to the experimental central values.

A Hard and matching functions

As discussed in Sec. 1.3, a TMD prediction at a given logarithmic accuracy requires two perturbative ingredients: (i) the *hard function* H, encoding short–distance virtual corrections to the partonic hard subprocess, and (ii) the *matching coefficients* $C_{i\leftarrow j}$, which relate TMDs to collinear PDFs in the small–b_T (OPE) regime. Throughout we work in the $\overline{\text{MS}}$ scheme and set $\mu = \sqrt{\zeta} = Q$ unless stated otherwise; color factors are $C_A = N_c$, $C_F = (N_c^2 - 1)/(2N_c)$, $T_R = \frac{1}{2}$, and n_f denotes the number of light flavours.

In what follows we collect the specific expressions needed for the gluon–initiated channel relevant to Higgs production, $gg \to H$, and for the gluon and quark matching coefficients entering the perturbative part of the (unpolarised) gluon TMD.

Hard function

Starting from Eq. (1.54), the hard function at $\mu = Q$ is expanded as

$$H(Q,Q) \;=\; 1 \;+\; \sum_{n=1}^{\infty}\left(\frac{\alpha_s(Q)}{4\pi}\right)^n H^{(n)}\,.$$

For the process $gg \to H$ we use:

$$H_1^{gg\to H} \;=\; 2\left[\,C_A\left(5+\frac{7\pi^2}{6}\right) - 3\,C_F\right], \tag{A.1}$$

$$\begin{aligned} H_2^{gg\to H}(n_f) = \frac{1}{162}\Big[&-135\,C_A + 23827\,C_A^2 - 216\,C_F - 15660\,C_A C_F + 5832\,C_F^2 \\ &+ 2268\,C_A^2\,L_t - 3564\,C_A C_F\,L_t - 4510\,C_A\,n_f - 4428\,C_F\,n_f + 1296\,C_F\,n_f\,L_t \\ &+ 6795\,C_A^2\,\pi^2 - 2268\,C_A C_F\,\pi^2 - 450\,\pi^2\,C_A\,n_f + 333\,\pi^4\,C_A^2 \\ &- 5148\,C_A^2\,\zeta(3) - 1656\,C_A\,n_f\,\zeta(3) + 2592\,C_F\,n_f\,\zeta(3)\Big], \end{aligned} \tag{A.2}$$

where

$$L_t \;\equiv\; 2\,\ln\!\left(\frac{m_H}{m_t}\right), \tag{A.3}$$

and $\zeta(3)$ denotes Apéry's constant (the Riemann zeta function $\zeta(s)$ evaluated at $s=3$).

Matching coefficients

The small–b_T matching relates the gluon (and quark) TMDs to collinear PDFs via Eq. (1.51):

$$\tilde{f}_i(x,b_T;\mu,\zeta) = \sum_j \Big(C_{i\leftarrow j}\otimes f_j\Big)(x,\mu)\,,$$

with perturbative coefficients expanded as (Eq. (1.55))

$$C_{i\leftarrow j} = \sum_{n\geq 0}\left(\frac{\alpha_s}{4\pi}\right)^n C_{i\leftarrow j}^{(n,0)} + \cdots$$

where the superscript $(n,0)$ denotes the non–logarithmic part at order α_s^n in our convention.

LO. At leading order one has

$$C_{q\leftarrow q}^{(0,0)}(x) \;=\; C_{g\leftarrow g}^{(0,0)}(x) \;=\; \delta(1-x)\,, \tag{A.4}$$

while all other flavour transitions vanish.

NLO. At $\mathcal{O}(\alpha_s)$ the non–vanishing coefficients read

$$C_{q\leftarrow q}^{(1,0)}(x) = C_F\left[2(1-x) \;-\; \delta(1-x)\,\frac{\pi^2}{6}\right], \tag{A.5}$$

$$C_{q\leftarrow g}^{(1,0)}(x) = 4\,T_R\,x\,(1-x), \tag{A.6}$$

$$C_{g\leftarrow q}^{(1,0)}(x) = 2\,C_F\,x, \tag{A.7}$$

$$C_{g\leftarrow g}^{(1,0)}(x) = -\,C_A\,\delta(1-x)\,\frac{\pi^2}{6}, \tag{A.8}$$

$$C_{q\leftarrow q'}^{(1,0)}(x) = C_{q\leftarrow \bar{q}}^{(1,0)}(x) \;=\; 0\,. \tag{A.9}$$

For the gluon TMD entering $gg \to H$, the relevant channels at this order are $C_{g\leftarrow g}^{(1,0)}$ and $C_{g\leftarrow q}^{(1,0)}$. Higher–order matching coefficients and the associated logarithmic terms needed at our target accuracy are taken from Refs. [50, 107] and implemented consistently with the evolution discussed in Sec. 1.3.

B Numerical integration

B.1 Integrating over q_T

The bin integration over q_T can be carried out analytically by using the identity for Bessel functions

$$\frac{d}{dx}\left[x^m J_m(x)\right] = x^m J_{m-1}(x)\,, \tag{B.1}$$

which yields

$$\int dx\, x J_0(x) = x J_1(x) \quad \Rightarrow \quad \int_{x_1}^{x_2} dx\, x J_0(x) = x_2 J_1(x_2) - x_1 J_1(x_1)\,. \tag{B.2}$$

Note that the differential cross section in Eq. (3.4) has the schematic form

$$\frac{d\sigma}{dQdydq_T} \propto \int_0^\infty db\, q_T J_0(b_T q_T)\ldots \tag{B.3}$$

where the ellipsis denotes terms independent of q_T. Hence, applying Eq. (B.2) we obtain

$$\begin{aligned}&\int_{q_{T,\min}}^{q_{T,\max}} dq_T \left[\frac{d\sigma}{dQdydq_T}\right] \propto \int_0^\infty db_T \int_{q_{T,\min}}^{q_{T,\max}} dq_T\, q_T J_0(b_T q_T)\cdots = \\ &\int_0^\infty \frac{db_T}{b_T^2} \int_{b_T q_{T,\min}}^{b_T q_{T,\max}} dx\, x J_0(x)\cdots = \int_0^\infty \frac{db_T}{b_T}\left[q_{T,\max} J_1(b_T q_{T,\max}) - q_{T,\min} J_1(b_T q_{T,\min})\right]\ldots .\end{aligned} \tag{B.4}$$

Defining

$$K(q_T) \equiv \int dq_T \left[\frac{d\sigma}{dQdydq_T}\right] \tag{B.5}$$

i.e., the indefinite integral over q_T of the cross section in Eq. (3.4), we then have

$$\int_{q_{T,\min}}^{q_{T,\max}} dq_T \left[\frac{d\sigma}{dQdydq_T}\right] = K(Q,y,q_{T,\max}) - K(Q,y,q_{T,\min})\,, \tag{B.6}$$

with

$$K(Q,y,q_T) = \frac{\sigma_0}{2} H(Q,\mu) \int_0^\infty db\, J_1(bq_T) \overline{F}_g(x_1,b_T;\mu,\zeta) \overline{F}_g(x_2,b_T;\mu,\zeta) \\ \times\ f_{\mathrm{NP}}(x_1,b_T,\zeta) f_{\mathrm{NP}}(x_2,b_T,\zeta)\,, \tag{B.7}$$

which can be evaluated via the Ogata quadrature as

$$K(Q,y,q_T) \simeq \sum_{n=1}^{N} w_n^{(1)} S\left(x_1,x_2,\frac{z_n^{(1)}}{q_T};\mu,\zeta\right) f_{\mathrm{NP}}\left(x_1,\frac{z_n^{(1)}}{q_T},\zeta\right) f_{\mathrm{NP}}\left(x_2,\frac{z_n^{(1)}}{q_T},\zeta\right). \tag{B.8}$$

The unscaled coordinates $z_n^{(1)}$ and the weights $w_n^{(1)}$ can again be precomputed and stored from the zeros of the Bessel function J_1. Eq. (B.6) thus reduces the q_T bin integration to a calculation fully analogous to the unintegrated cross section, particularly convenient since it obviates performing a separate numerical integration over q_T.

Kinematic cuts

When kinematic selections are applied to the data, such as those on the final state due to experimental constraints, the analytic bin integration over q_T discussed above cannot be performed. The reason is that implementing these cuts effectively inserts a q_T-dependent factor $\mathcal{P}$[4] into the integrand:

$$\frac{d\sigma}{dQdydq_T} \propto \int_0^\infty db_T\, q_T J_0(b_T q_T) \mathcal{P}(q_T) \dots\,, \tag{B.9}$$

which prevents the direct use of Eq. (B.2). Since $\mathcal{P}$ varies slowly with q_T across a typical bin, we approximate the bin integral as

$$\int_{q_{T,\min}}^{q_{T,\max}} dq_T\, q_T J_0(b_T q_T) \mathcal{P}(q_T) \simeq \mathcal{P}\left(\frac{q_{T,\max}+q_{T,\min}}{2}\right) \int_{q_{T,\min}}^{q_{T,\max}} dq_T\, q_T J_0(b_T q_T) \\ = \mathcal{P}\left(\frac{q_{T,\max}+q_{T,\min}}{2}\right) \frac{1}{b_T} \left[q_{T,\max} J_1(b_T q_{T,\max}) - q_{T,\min} J_1(b_T q_{T,\min})\right]. \tag{B.10}$$

This structure is, however, inconvenient because it mixes the two bin edges, hindering a recursive computation. To go a step further, and assuming the bin is sufficiently narrow, we expand $\mathcal{P}$ about either edge

$$\mathcal{P}\left(\frac{q_{T,\max}+q_{T,\min}}{2}\right) = \mathcal{P}\left(q_{T,\min}+\Delta q_T\right) = \mathcal{P}\left(q_{T,\min}\right) + \mathcal{P}'\left(q_{T,\min}\right)\Delta q_T + \mathcal{O}\left(\Delta q_T^2\right),$$

$$\mathcal{P}\left(\frac{q_{T,\max}+q_{T,\min}}{2}\right) = \mathcal{P}\left(q_{T,\max}-\Delta q_T\right) = \mathcal{P}\left(q_{T,\max}\right) - \mathcal{P}'\left(q_{T,\max}\right)\Delta q_T + \mathcal{O}\left(\Delta q_T^2\right), \tag{B.11}$$

[4] In fact, $\mathcal{P}$ also depends on the invariant mass Q and rapidity y of the lepton pair, which must likewise be integrated over.

with

$$\Delta q_T = \frac{q_{T,\max} - q_{T,\min}}{2} \,. \tag{B.12}$$

Therefore,

$$b_T \int_{q_{T,\min}}^{q_{T,\max}} dq_T\, q_T J_0(b_T q_T)\mathcal{P}(q_T) \simeq q_{T,\max} J_1(b_T q_{T,\max}) \left[\mathcal{P}\left(q_{T,\max}\right) - \mathcal{P}'\left(q_{T,\max}\right)\Delta q_T\right]$$

$$- q_{T,\min} J_1(b_T q_{T,\min}) \left[\mathcal{P}\left(q_{T,\min}\right) + \mathcal{P}'\left(q_{T,\min}\right)\Delta q_T\right] \,. \tag{B.13}$$

Compared to Eq. (B.10), the advantage is that each term now depends on a single bin edge in q_T, rather than on a combination of adjacent edges. Consequently, in the presence of kinematic cuts, the primitive K of Eq. (B.6), whose explicit form without cuts is given in Eq. (B.7), becomes

$$\begin{aligned} K(Q, y, q_T) = {} & \frac{\sigma_0}{2} H(Q,\mu) \left[\mathcal{P}\left(Q, y, q_T\right) \pm \mathcal{P}'\left(Q, y, q_T\right)\Delta q_T\right] \\ & \times \int_0^\infty db\, J_1(bq_T)\overline{F}_g(x_1, b_T; \mu, \zeta)\overline{F}_g(x_2, b_T; \mu, \zeta) f_{\rm NP}(x_1, b_T, \zeta) f_{\rm NP}(x_2, b_T, \zeta) \,, \end{aligned} \tag{B.14}$$

where we have made explicit the dependence of $\mathcal{P}$ and its q_T-derivative $\mathcal{P}'$ on Q and y. In the square brackets of Eq. (B.14), the minus sign applies when q_T is the upper edge of the bin, and the plus sign when it is the lower edge, in accordance with Eq. (B.13). As discussed below, when integrating over bins in Q and y, one should also integrate $\mathcal{P}$ and $\mathcal{P}'$. Nevertheless, in the interpolation strategy outlined later, these functions can be factored out of the Q and y integrals in a controlled way, avoiding repeated evaluations of the computationally expensive function $\mathcal{P}$ and greatly simplifying the structure of the resulting interpolation tables.

B.2 Integrating over Q and y

As a final step, we need to evaluate the integrals over Q and y defined in Eq. (3.14). These can only be performed numerically. Since the integration over q_T has been reduced to the difference of the two terms on the r.h.s. of Eq. (B.6)[5], we focus on integrating the function K over Q and y at fixed q_T:

$$\widetilde{K}(q_T) = \int_{Q_{\min}}^{Q_{\max}} dQ \int_{y_{\min}}^{y_{\max}} dy\, K(Q, y, q_T) \,. \tag{B.15}$$

In this way, the cross section

$$\widetilde{\sigma} = \int_{Q_{\min}}^{Q_{\max}} dQ \int_{y_{\min}}^{y_{\max}} dy \int_{q_{T,\min}}^{q_{T,\max}} dq_T \left[\frac{d\sigma}{dQ dy dq_T}\right] \,, \tag{B.16}$$

[5]For now we ignore the complications due to final-state cuts discussed in Sec. B.1; we will return to them at the end of this section.

can be calculated as

$$\widetilde{\sigma} = \widetilde{K}(q_{T,\max}) - \widetilde{K}(q_{T,\min})\,. \tag{B.17}$$

To proceed, it is convenient to make explicit the dependence of x_1 and x_2 on Q and y. For simplicity, we identify the scales μ and $\sqrt{\zeta}$ with Q (scale variations can be reinstated later) and thus drop one of the arguments from the TMD distributions $\overline{F}$ and from the hard factor H. This gives

$$\begin{aligned}\widetilde{K}(q_T) = \int_0^\infty db_T\, J_1(b_T q_T) \int_{Q_{\min}}^{Q_{\max}} dQ \int_{e^{y_{\min}}}^{e^{y_{\max}}} \frac{d\xi}{\xi} \frac{\sigma_0(Q)}{2} H(Q) \\ \times \overline{F}_g\left(\frac{Q}{\sqrt{s}}\xi, b_*(b_T); Q\right) \overline{F}_g\left(\frac{Q}{\sqrt{s}}\frac{1}{\xi}, b_*(b_T); Q\right) f_{\rm NP}\left(\frac{Q}{\sqrt{s}}\xi, b_T; Q\right) f_{\rm NP}\left(\frac{Q}{\sqrt{s}}\frac{1}{\xi}, b_T; Q\right),\end{aligned} \tag{B.18}$$

where we have changed variables to $\xi = e^y$. We now define one grid in ξ, $\{\xi_\alpha\}$, with $\alpha = 0, \ldots, N_\xi$, and one grid in Q, $\{Q_\tau\}$, with $\tau = 0, \ldots, N_Q$, each equipped with the corresponding interpolating functions $\mathcal{I}$.
The grid's boundaries satisfy $\xi_0 = e^{y_{\min}}$ and $\xi_{N_\xi} = e^{y_{\max}}$, and $Q_0 = Q_{\min}$ and $Q_{N_Q} = Q_{\max}$. This allows us to interpolate the product of the two $f_{\rm NP}$ factors in Eq. (B.18) for generic (ξ, Q) as

$$\begin{aligned}f_{\rm NP}\left(\frac{Q}{\sqrt{s}}\xi, b_T; Q\right) f_{\rm NP}\left(\frac{Q}{\sqrt{s}}\frac{1}{\xi}, b_T; Q\right) \simeq \\ \sum_{\alpha=0}^{N_\xi}\sum_{\tau=0}^{N_Q} \mathcal{I}_\alpha(\xi)\mathcal{I}_\tau(Q) f_{\rm NP}\left(\frac{Q_\tau}{\sqrt{s}}\xi_\alpha, b_T; Q_\tau\right) f_{\rm NP}\left(\frac{Q_\tau}{\sqrt{s}}\frac{1}{\xi_\alpha}, b_T; Q_\tau\right).\end{aligned} \tag{B.19}$$

Inserting this into Eq. (B.18) yields

$$\begin{aligned}\widetilde{K}(q_T) \simeq \int_0^\infty db\, J_1(b_T q_T) \sum_{\tau=0}^{N_Q}\sum_{\alpha=0}^{N_\xi} \Bigg[\int_{Q_{\min}}^{Q_{\max}} dQ\, \mathcal{I}_\tau(Q) \frac{\sigma_0(Q)}{2} H(Q) \\ \times \int_{e^{y_{\min}}}^{e^{y_{\max}}} d\xi\, \mathcal{I}_\alpha(\xi) \frac{1}{\xi} \overline{F}_g\left(\frac{Q}{\sqrt{s}}\xi, b_*(b_T); Q\right) \overline{F}_g\left(\frac{Q}{\sqrt{s}}\frac{1}{\xi}, b_*(b_T); Q\right) \Bigg] \\ \times f_{\rm NP}\left(\frac{Q_\tau}{\sqrt{s}}\xi_\alpha, b_T; Q_\tau\right) f_{\rm NP}\left(\frac{Q_\tau}{\sqrt{s}}\frac{1}{\xi_\alpha}, b_T; Q_\tau\right).\end{aligned} \tag{B.20}$$

Finally, the b_T integral is evaluated with the Ogata quadrature as before, giving

$$\begin{aligned}\widetilde{K}(q_T) \simeq \sum_{n=1}^{N}\sum_{\tau=0}^{N_Q}\sum_{\alpha=0}^{N_\xi} \Bigg[w_n^{(1)} \int_{Q_{\min}}^{Q_{\max}} dQ\, \mathcal{I}_\tau(Q) \frac{\sigma_0(Q)}{2} H(Q) \\ \times \int_{e^{y_{\min}}}^{e^{y_{\max}}} d\xi\, \mathcal{I}_\alpha(\xi) \frac{1}{\xi} \overline{F}_g\left(\frac{Q}{\sqrt{s}}\xi, b_*\left(\frac{z_n}{q_T}\right); Q\right) \overline{F}_g\left(\frac{Q}{\sqrt{s}}\frac{1}{\xi}, b_*\left(\frac{z_n}{q_T}\right); Q\right) \Bigg] \\ \times f_{\rm NP}\left(\frac{Q_\tau}{\sqrt{s}}\xi_\alpha, \frac{z_n}{q_T}; Q_\tau\right) f_{\rm NP}\left(\frac{Q_\tau}{\sqrt{s}}\frac{1}{\xi_\alpha}, \frac{z_n}{q_T}; Q_\tau\right).\end{aligned} \tag{B.21}$$

In conclusion, by defining

$$W_{n\tau\alpha}(q_T) \equiv w_n^{(1)} \int_{Q_{\min}}^{Q_{\max}} dQ\, \mathcal{I}_\tau(Q)\, \frac{\sigma_0(Q)}{2} H(Q) \times \int_{e^{y_{\min}}}^{e^{y_{\max}}} d\xi\, \mathcal{I}_\alpha(\xi)\, \frac{1}{\xi} \overline{F}_g\left(\frac{Q}{\sqrt{s}}\xi, b_*\left(\frac{z_n}{q_T}\right); Q\right) \overline{F}_g\left(\frac{Q}{\sqrt{s}}\frac{1}{\xi}, b_*\left(\frac{z_n}{q_T}\right); Q\right), \tag{B.22}$$

we obtain

$$\widetilde{K}(q_T) \simeq \sum_{n=1}^{N} \sum_{\tau=0}^{N_Q} \sum_{\alpha=0}^{N_\xi} W_{n\tau\alpha}(q_T) f_{\rm NP}\left(\frac{Q_\tau}{\sqrt{s}}\xi_\alpha, \frac{z_n}{q_T}; Q_\tau\right) f_{\rm NP}\left(\frac{Q_\tau}{\sqrt{s}}\frac{1}{\xi_\alpha}, \frac{z_n}{q_T}; Q_\tau\right). \tag{B.23}$$

The advantage of Eq. (B.23) is that the weights $W_{n\tau\alpha}$, which depend on q_T and on the intervals $[Q_{\min} : Q_{\max}]$ and $[y_{\min} : y_{\max}]$, can be precomputed once for each experimental point used in the fit and then reused to extract $f_{\rm NP}$. This provides a fast prediction tool that greatly facilitates the determination of the non-perturbative component of the TMDs.

We now discuss how the weights in Eq. (B.22) are modified by the cuts described in Sec. B.1. In principle, the square-bracket factor in Eq. (B.14) should appear under the integrals in Eq. (B.22) and be integrated over Q and $\xi = e^y$. This is numerically challenging because evaluating the phase-space reduction factor $\mathcal{P}$ is expensive to compute; moreover, since the factor between square brackets in Eq. (B.14) depends on whether q_T is a lower or upper bin edge, one would effectively need duplicate sets of weights. To simplify, we assume that $\mathcal{P}$ and its derivative $\mathcal{P}'$ vary slowly in Q and y across the typical grid spacings, and we note that the interpolating functions $\mathcal{I}_\tau(Q)$ and $\mathcal{I}_\alpha(\xi)$ are strongly peaked at Q_τ and ξ_α. Under these conditions, we can pull $\mathcal{P}$ and $\mathcal{P}'$ out of the integrals and replace Eq. (B.22) by

$$W_{n\tau\alpha}(q_T) \to \left[\mathcal{P}\left(Q_\tau, \ln(\xi_\alpha), q_T\right) \pm \mathcal{P}'\left(Q_\tau, \ln(\xi_\alpha), q_T\right) \Delta q_T\right] W_{n\tau\alpha}(q_T). \tag{B.24}$$

In practice, the only extra inputs needed to implement the cuts are the values of $\mathcal{P}$ and $\mathcal{P}'$ on the (Q, ξ) grid for all q_T bin edges. Equation (B.24) then permits to use the weights computed over the full phase space.

C Phase space reduction factor

In this appendix we detail the computation of the phase–space reduction factor $\mathcal{P}$ (introduced in Eq. (3.4)) for final states with two and four particles. The factor $\mathcal{P}$ encodes the effect of fiducial selections and detector–level kinematic requirements on the theoretical cross section. We begin with the diphoton channel, $H \to \gamma\gamma$, where our derivation follows Ref. [51]. This serves to fix the notation and reproduce the known result for the two–body case. We then extend the calculation to the four–lepton channel, $H \to 4\ell$, generalising the construction of $\mathcal{P}$ to accommodate the additional decay kinematics and fiducial cuts specific to a four–particle final state.

C.1 Cuts on the two-particle final state

The phase-space reduction factor $\mathcal{P}$ is defined as

$$\mathcal{P}(Q,y,q_T) = \mathcal{P}(q) = \frac{\int_{\text{fid. reg.}} d^4p_1 d^4p_2\, \delta(p_1^2)\delta(p_2^2)\theta(p_{1,0})\theta(p_{2,0})\delta^{(4)}(p_1+p_2-q)\,|\mathcal{M}(p_1,p_2)|^2}{\int d^4p_1 d^4p_2\, \delta(p_1^2)\delta(p_2^2)\theta(p_{1,0})\theta(p_{2,0})\delta^{(4)}(p_1+p_2-q)\,|\mathcal{M}(p_1,p_2)|^2}\,, \tag{C.1}$$

where p_1 and p_2 are the four-momenta of the outgoing photons and $\mathcal{M}(p_1,p_2)$ is the amplitude of the decay $H\to\gamma\gamma$[6], that reads

$$\mathcal{M} = \frac{e^2 g}{(4\pi)^2 m_W} F\,(p_1\cdot p_2\, g^{\mu\nu} - p_2^\mu p_1^\nu)\,\epsilon_\mu(p_1)\epsilon_\nu(p_2)\,, \tag{C.2}$$

so that

$$|\mathcal{M}|^2 \;\propto\; F^2 \frac{(p_1+p_2)^4}{2}\,, \tag{C.3}$$

where F includes contributions from W and fermion loops

$$F = F_W(\beta_W) + \sum_f N_c\, Q_f^2\, F_f(\beta_f)\,. \tag{C.4}$$

Here N_c is a colour factor ($N_c=1$ for leptons, $N_c=3$ for quarks) and

$$\beta_W = \frac{4m_W^2}{m_H^2}\,, \qquad \beta_f = \frac{4m_f^2}{m_H^2}\,, \tag{C.5}$$

with

$$F_W(\beta) = 2 + 3\beta + 3\beta(2-\beta)\,f(\beta), \tag{C.6}$$

$$F_f(\beta) = -2\beta\Big[\,1 + (1-\beta)\,f(\beta)\,\Big]\,, \tag{C.7}$$

where

$$f(\beta) = \begin{cases} \arcsin^2\!\Big(\dfrac{1}{\sqrt{\beta}}\Big), & \beta \geq 1, \\ -\dfrac{1}{4}\left[\ln\!\left(\dfrac{1+\sqrt{1-\beta}}{1-\sqrt{1-\beta}}\right) - i\pi\right]^2, & \beta < 1\,. \end{cases} \tag{C.8}$$

The integral in the denominator of Eq. (C.1) is restricted to some fiducial region. Finally, we find:

$$\mathcal{P}(q) = \frac{\int_{\text{fid. reg.}} d^4p_1 d^4p_2\, \delta(p_1^2)\delta(p_2^2)\theta(p_{1,0})\theta(p_{2,0})\delta^{(4)}(p_1+p_2-q)(p_1+p_2)^4}{\int d^4p_1 d^4p_2\, \delta(p_1^2)\delta(p_2^2)\theta(p_{1,0})\theta(p_{2,0})\delta^{(4)}(p_1+p_2-q)(p_1+p_2)^4}\,. \tag{C.9}$$

The effect of integrating over the fiducial region can be implemented by defining a generalised θ-function, $\Phi(p_1,p_2)$, that is equal to one inside the fiducial region and zero outside.

[6] Unlike Drell–Yan, which involves the contracted leptonic tensor, the Higgs is a spin-0 scalar; therefore only the decay amplitude is required.

This allows one to integrate also the numerator of Eq. (C.9) over the full phase-space of the two outgoing photons.

$$\mathcal{P}(q) = \frac{\int d^4p_1 d^4p_2\, \delta(p_1^2)\delta(p_2^2)\theta(p_{1,0})\theta(p_{2,0})\delta^{(4)}(p_1+p_2-q)\Phi(p_1,p_2)(p_1+p_2)^4}{\int d^4p_1 d^4p_2\, \delta(p_1^2)\delta(p_2^2)\theta(p_{1,0})\theta(p_{2,0})\delta^{(4)}(p_1+p_2-q)(p_1+p_2)^4}\,. \tag{C.10}$$

Now we can integrate over one of the outgoing momenta, say p_2, exploiting the momentum-conservation δ-function both in the numerator and in the denominator. Specifically, the numerator of Eq. (C.10) gives:

$$\begin{aligned}&\int d^4p_1 d^4p_2\, \delta(p_1^2)\delta(p_2^2)\theta(p_{1,0})\theta(p_{2,0})\delta^{(4)}(p_1+p_2-q)\Phi(p_1,p_2)(p_1+p_2)^4 = \\ &Q^4 \int d^4p_1 \delta(p_1^2)\delta((q-p_1)^2)\theta(p_{1,0})\theta(q_0-p_{1,0})\Phi(p_1,q-p_1)\,,\end{aligned} \tag{C.11}$$

and likewise in the denominator setting $\Phi(p_1,p_2)=1$. Finally, renaming $p_1 = p$, the phase-space reduction factor reads:

$$\mathcal{P}(q) = \frac{\int d^4p\, \delta(p^2)\delta((q-p)^2)\theta(p_0)\theta(q_0-p_0)\Phi(p,q-p)}{\int d^4p\, \delta(p^2)\delta((q-p)^2)\theta(p_0)\theta(q_0-p_0)}\,. \tag{C.12}$$

The two δ-functions can now be used to fix two of the components of the four-momentum p. In particular, the on shell constraint $\delta(p_2^2)$ is typically used to set the first component of p (the energy). Since the photons are massless, this gives

$$\int d^4p\, \delta(p^2)\theta(p_0) = \int d^4p\, \delta(E^2-|\mathbf{p}|^2)\theta(E) = \int \frac{dE\, d^3\mathbf{p}}{2|\mathbf{p}|}\delta(E-|\mathbf{p}|) = \int \frac{d^3\mathbf{p}}{2|\mathbf{p}|}\,. \tag{C.13}$$

Accordingly, the four-momentum p appearing in the integrand has to be taken on shell ($E=|\mathbf{p}|$). We then write the three-dimensional measure $d^3\mathbf{p}$ in spherical coordinates as

$$d^3\mathbf{p} = |\mathbf{p}|^2 d|\mathbf{p}| d(\cos\theta) d\phi\,. \tag{C.14}$$

Next, we make a change of variable from $(|\mathbf{p}|, \cos\theta)$ to $(|\mathbf{p}_T|, \eta)$, since the fiducial cuts are defined in terms of these quantities. This proceeds via the standard relations:

$$\begin{cases} |\mathbf{p}| = |\mathbf{p}_T| \cosh\eta\,, \\ \cos\theta = \tanh\eta\,. \end{cases} \tag{C.15}$$

It follows that

$$\int \frac{d^3\mathbf{p}}{2|\mathbf{p}|} = \frac{1}{2}\int |\mathbf{p}| d|\mathbf{p}| d(\cos\theta) d\phi = \frac{1}{2}\int |\mathbf{p}_T| d|\mathbf{p}_T| d\eta d\phi = \frac{1}{2}\int d^2\mathbf{p}_T d\eta\,. \tag{C.16}$$

Now we consider the second δ-function,

$$\frac{1}{2}\int d^2\mathbf{p}_T d\eta\, \delta((q-p)^2)\theta(q_0-p_0) = \frac{1}{2}\int_{-\infty}^{\infty} d\eta \int_0^{2\pi} d\phi \int_0^{\infty} |\mathbf{p}_T| d|\mathbf{p}_T|\, \delta(Q^2-2p\cdot q)\theta(q_0-p_0)\,, \tag{C.17}$$

being $q^2 = Q^2$ and $p^2 = 0$. It is convenient to express the four-vector q in terms of Q, y, and $\mathbf{q}_T$:

$$q = (M \cosh y, \mathbf{q}_T, M \sinh y) \ . \tag{C.18}$$

with $M = \sqrt{Q^2 + |\mathbf{q}_T|^2}$. While

$$p = (|\mathbf{p}_T| \cosh \eta, \mathbf{p}_T, |\mathbf{p}_T| \sinh \eta) \ , \tag{C.19}$$

therefore

$$p \cdot q = |\mathbf{p}_T| M \left(\cosh \eta \cosh y - \sinh \eta \sinh y\right) - \mathbf{p}_T \cdot \mathbf{q}_T = |\mathbf{p}_T| M \cosh\left(\eta - y\right) - \mathbf{p}_T \cdot \mathbf{q}_T \ . \tag{C.20}$$

We may, without loss of generality, align the two-dimensional vector $\mathbf{q}_T$ is aligned with the x axis so that $\mathbf{p}_T \cdot \mathbf{q}_T = |\mathbf{p}_T||\mathbf{q}_T| \cos\phi$([7]). Thus, the argument of the δ-function in Eq. (C.17) becomes

$$f(|\mathbf{p}_T|, \eta, \phi) = Q^2 - 2|\mathbf{p}_T| \left[M \cosh\left(\eta - y\right) - |\mathbf{q}_T| \cos\phi\right] \ . \tag{C.21}$$

while the argument of the ϑ-function is $M \cosh y - |\mathbf{p}_T| \cosh \eta$. It is then convenient to integrate Eq. (C.17) over $|\mathbf{p}_T|$ first:

$$\frac{1}{2} \int_0^\infty |\mathbf{p}_T| d|\mathbf{p}_T| \, \delta(Q^2 - 2p \cdot q) \theta(q_0 - p_0) = \frac{\overline{p}_T^2}{2Q^2} \vartheta(M \cosh y - \overline{p}_T \cosh \eta) = \frac{\overline{p}_T^2}{2Q^2} \ , \tag{C.22}$$

with([8]):

$$\overline{p}_T(\cos\phi) = \frac{Q^2}{2\left[M \cosh\left(\eta - y\right) - |\mathbf{q}_T| \cos\phi\right]} = \frac{Q^2}{2|\mathbf{q}_T|} \frac{1}{\left[\frac{M \cosh(\eta - y)}{|\mathbf{q}_T|} - \cos\phi\right]} \ . \tag{C.23}$$

Now we consider the integral over $d\phi$. For this purpose, the following relations are useful:

$$\int_0^{2\pi} d\phi \, f(\cos\phi) = \int_{-1}^{1} \frac{dx}{\sqrt{1 - x^2}} \left[f(x) + f(-x)\right] \ . \tag{C.24}$$

and

$$\int \frac{dx}{(a \pm x)^2 \sqrt{1 - x^2}} = \frac{2x\sqrt{1 - x^2}}{(a^2 - 1)(x^2 - a^2)} + \frac{2a}{(a^2 - 1)^{3/2}} \tan^{-1}\left(\frac{x\sqrt{a^2 - 1}}{a\sqrt{1 - x^2}}\right) \tag{C.25}$$

For the definite integral, one finds

$$\int_{-1}^{1} \frac{dx}{(a \pm x)^2 \sqrt{1 - x^2}} = \frac{\pi a}{(a^2 - 1)^{3/2}} \ . \tag{C.26}$$

[7] In the general case where $\mathbf{q}_T$ makes an angle β with the x axis, the scalar product is $|\mathbf{p}_T||\mathbf{q}_T| \cos(\phi - \beta)$. However, β can always be absorbed into a redefinition of the integration angle ϕ in Eq. (C.17).

[8] Notice that the ϑ-function has no effect.This has been verified numerically.

We now use Eqs. (C.24)-(C.26) to evaluate

$$\begin{aligned}
&\frac{1}{2Q^2}\int_0^{2\pi} d\phi\,[\overline{p}_T(\cos\phi)]^2 = \frac{Q^2}{8|\mathbf{q}_T|^2}\int_0^{2\pi}\frac{d\phi}{\left[\frac{M\cosh(\eta-y)}{|\mathbf{q}_T|}-\cos\phi\right]^2}\\
&= \frac{Q^2}{8|\mathbf{q}_T|^2}\int_{-1}^{1}\frac{dx}{\sqrt{1-x^2}}\left[\frac{1}{\left(\frac{M\cosh(\eta-y)}{|\mathbf{q}_T|}-x\right)^2}+\frac{1}{\left(\frac{M\cosh(\eta-y)}{|\mathbf{q}_T|}+x\right)^2}\right]\\
&= \frac{Q^2}{8}\Bigg\{\frac{2|\mathbf{q}_T|^2x\sqrt{1-x^2}}{(M^2\cosh^2(\eta-y)-|\mathbf{q}_T|^2)(x^2|\mathbf{q}_T|^2-M^2\cosh^2(\eta-y))}\\
&- \frac{M\cosh(\eta-y)}{(M^2\cosh^2(\eta-y)-|\mathbf{q}_T|^2)^{3/2}}\left[\tan^{-1}\left(\frac{|\mathbf{q}_T|-xM\cosh(\eta-y)}{\sqrt{(M^2\cosh^2(\eta-y)-|\mathbf{q}_T|^2)}\sqrt{1-x^2}}\right)\right.\\
&\left.- \tan^{-1}\left(\frac{|\mathbf{q}_T|+xM\cosh(\eta-y)}{\sqrt{(M^2\cosh^2(\eta-y)-|\mathbf{q}_T|^2)}\sqrt{1-x^2}}\right)\right]\Bigg\}_{-1}^{1}\\
&= \frac{\pi Q^2M\cosh(\eta-y)}{4(M^2\cosh^2(\eta-y)-|\mathbf{q}_T|^2)^{3/2}}
\end{aligned} \tag{C.27}$$

We can proceed further and also perform the integral in η,

$$\begin{aligned}
&\int d^4p\,\delta(p^2)\delta((q-p)^2)\theta(p_0)\theta(q_0-p_0) = \int_{-\infty}^{\infty}d\eta\frac{\pi Q^2M\cosh(\eta-y)}{4(M^2\cosh^2(\eta-y)-|\mathbf{q}_T|^2)^{3/2}} =\\
&\frac{\pi}{4}\frac{Q^2}{M^2}\int_{-\infty}^{\infty}\frac{d(\sinh\eta)}{\left(\sinh^2(\eta-y)+\frac{Q^2}{M^2}\right)^{3/2}} = \frac{\pi}{4}\frac{Q^2}{M^2}\left[\frac{M^2}{Q^2}\frac{\sinh\eta}{\sqrt{\sinh^2\eta+\frac{Q^2}{M^2}}}\right]_{-\infty}^{\infty} = \frac{\pi}{2}\,.
\end{aligned} \tag{C.28}$$

Notably, this result reproduces the denominator of Eq. (C.12). We now need the numerator, which is obtained by inserting the appropriate function Φ. In this case, we will consider symmetric cuts for the two outgoing particles, (in the next section we will also consider asymmetric constraints)

$$\eta_{\min} < \eta_{1(2)} < \eta_{\max} \quad \text{and} \quad |\mathbf{p}_{T,1(2)}| > p_{T,\min}\,. \tag{C.29}$$

Consequently, the function Φ factorises into two identical functions as

$$\Phi(p_1,p_2) = \Theta(p_1)\Theta(p_2)\,, \tag{C.30}$$

with

$$\Theta(p) = \vartheta(\eta-\eta_{\min})\vartheta(\eta_{\max}-\eta)\vartheta(|\mathbf{p}_T|-p_{T,\min})\,. \tag{C.31}$$

Using Eq. (C.12) and the relation above, we obtain

$$q-p = (M\cosh y - |\mathbf{p}_T|\cosh\eta, \mathbf{q}_T-\mathbf{p}_T, M\sinh y - |\mathbf{p}_T|\sinh\eta)\,. \tag{C.32}$$

we thus have

$$\begin{aligned}
&\Phi(p, q-p) = \Theta(p)\Theta(q-p) = \\
&\vartheta(\eta - \eta_{\min})\vartheta(\eta_{\max} - \eta)\times \\
&\vartheta(|\mathbf{p}_T| - p_{T,\min})\times \\
&\vartheta\left(\frac{1}{2}\ln\left(\frac{M\cosh y - |\mathbf{p}_T|\cosh\eta + M\sinh y - |\mathbf{p}_T|\sinh\eta}{M\cosh y - |\mathbf{p}_T|\cosh\eta - M\sinh y + |\mathbf{p}_T|\sinh\eta}\right) - \eta_{\min}\right)\times \\
&\vartheta\left(\eta_{\max} - \frac{1}{2}\ln\left(\frac{M\cosh y - |\mathbf{p}_T|\cosh\eta + M\sinh y - |\mathbf{p}_T|\sinh\eta}{M\cosh y - |\mathbf{p}_T|\cosh\eta - M\sinh y + |\mathbf{p}_T|\sinh\eta}\right)\right)\times \\
&\vartheta(|\mathbf{q}_T - \mathbf{p}_T| - p_{T,\min}) =
\end{aligned} \tag{C.33}$$

$$\begin{aligned}
1):\quad & \vartheta(\eta - \eta_{\min}) \times \vartheta(\eta_{\max} - \eta)\times \\
2):\quad & \vartheta(\overline{p}_T - p_{T,\min})\times \\
3):\quad & \vartheta\left(\frac{1}{2}\ln\left(\frac{Me^{y} - \overline{p}_T e^{\eta}}{Me^{-y} - \overline{p}_T e^{-\eta}}\right) - \eta_{\min}\right) \times \vartheta\left(\eta_{\max} - \frac{1}{2}\ln\left(\frac{Me^{y} - \overline{p}_T e^{\eta}}{Me^{-y} - \overline{p}_T e^{-\eta}}\right)\right)\times \\
4):\quad & \vartheta(\sqrt{|\mathbf{q}_T|^2 + \overline{p}_T^2 - 2|\mathbf{q}_T|\overline{p}_T\cos\phi} - p_{T,\min})\,,
\end{aligned}$$

where in the last step we have replaced $|\mathbf{p}_T|$ with $\overline{p}_T$ defined Eq. (C.23). Our next task is to characterise the integration domain specified by $\Phi(p, q-p)$ in the $(\eta, \cos\phi)$-plane. Since the θ-functions in Eq. (C.12) will appear inside a double nested integral over $x = \cos\phi$ first and η second, it is convenient to rewrite $\Phi(p, q-p)$ from Eq. (C.33) as follows

$$\begin{aligned}
\Phi(p, q-p) = {} & \vartheta(\eta - \eta_{\min}) \times \vartheta(\eta_{\max} - \eta) \\
& \times \vartheta(x - f^{(2)}(\eta, p_{T,\min})) \\
& \times \vartheta(f^{(3)}(\eta, \eta_{\min}) - x) \times \vartheta(f^{(3)}(\eta, \eta_{\max}) - x) \\
& \times \vartheta(f^{(4)}(\eta, p_{T,\min}) - x)\,,
\end{aligned} \tag{C.34}$$

with

$$\begin{aligned}
f^{(2)}(\eta, p_{T,\mathrm{cut}}) &= \frac{2Mp_{T,\min}\cosh(\eta - y) - Q^2}{2p_{T,\mathrm{cut}}|\mathbf{q}_T|}\,, \\
f^{(3)}(\eta, \eta_{\mathrm{cut}}) &= \frac{M\cosh(\eta - y)}{|\mathbf{q}_T|} - \frac{Q^2\left(\sinh(\eta - y)\coth(y - \eta_{\mathrm{cut}}) + \cosh(\eta - y)\right)}{2|\mathbf{q}_T|M}\,, \\
f^{(4)}(\eta, p_{T,\mathrm{cut}}) &= \frac{M\cosh(\eta - y)(Q^2 - 2p_{T,\mathrm{cut}}^2 + 2|\mathbf{q}_T|^2) - Q^2\sqrt{M^2\sinh^2(\eta - y) + p_{T,\mathrm{cut}}^2}}{2|\mathbf{q}_T|\left(M^2 - p_{T,\mathrm{cut}}^2\right)}\,.
\end{aligned} \tag{C.35}$$

Because $-1 \leq \cos\phi \leq 1$, the domain is confined to this interval. Therefore, Eq. (C.34) can be recast in an even more convenient form

$$\begin{aligned}
\Phi(p, q-p) = {} & \vartheta(\eta - \eta_{\min})\vartheta(\eta_{\max} - \eta) \\
& \times \vartheta(x - \max[f^{(2)}(\eta, p_{T,\min}), -1]) \\
& \times \vartheta(\min[f^{(3)}(\eta, \eta_{\min}), f^{(3)}(\eta, \eta_{\max}), f^{(4)}(\eta, p_{T,\min}), 1] - x)
\end{aligned} \tag{C.36}$$

such that a double integral over η and x would read

$$\int_{-\infty}^{\infty} d\eta \int_{-1}^{1} dx\, \Phi(p, q-p) \cdots = \int_{\eta_{\min}}^{\eta_{\max}} d\eta\, \vartheta(x_2(\eta) - x_1(\eta)) \int_{x_1(\eta)}^{x_2(\eta)} dx \ldots . \tag{C.37}$$

where

$$x_1(\eta) = \max[f^{(2)}(\eta, p_{T,\min}), -1] \tag{C.38}$$

and

$$x_2(\eta) = \min[f^{(3)}(\eta, \eta_{\min}), f^{(3)}(\eta, \eta_{\max}), f^{(4)}(\eta, p_{T,\min}), 1]\,. \tag{C.39}$$

Collecting all ingredients, the final expression for the phase-space reduction factor becomes

$$\mathcal{P}(Q, y, q_T) = \int_{\eta_{\min}}^{\eta_{\max}} d\eta\, \vartheta(x_2(\eta) - x_1(\eta))\, [F(x_2(\eta), \eta) - F(x_1(\eta), \eta)] \tag{C.40}$$

with

$$\begin{aligned} F(x, \eta) = \frac{1}{4\pi} \frac{Q^2}{E_q^2 - q_T^2} \Bigg\{ & \frac{2 q_T^2 x \sqrt{1-x^2}}{x^2 q_T^2 - E_q^2} \\ & - \frac{E_q}{\sqrt{E_q^2 - q_T^2}} \left[\tan^{-1}\left(\frac{q_T - x E_q}{\sqrt{E_q^2 - q_T^2}\sqrt{1-x^2}} \right) - \tan^{-1}\left(\frac{q_T + x E_q}{\sqrt{E_q^2 - q_T^2}\sqrt{1-x^2}} \right) \right] \Bigg\} \end{aligned} \tag{C.41}$$

where we define $E_q = M \cosh(\eta - y)$ and $q_T = |\mathbf{q}_T|$. Let us consider the case $y = q_T = 0$, assuming $\eta_{\min} = -\eta_{\max}$. The result is

$$\mathcal{P}(Q, 0, 0) \vartheta(Q - 2p_{T,\min}) \tanh(\max[\eta_{\max}, \overline{\eta}])\,. \tag{C.42}$$

with $\bar{\eta}$ defined as

$$\overline{\eta} = \cosh^{-1}\left(\frac{Q}{2p_{T,\min}} \right)\,. \tag{C.43}$$

This result can be written more explicitly as:

$$\mathcal{P}(Q, 0, 0) = \begin{cases} 0 & Q < 2p_{T,\min}\,, \\ \tanh(\overline{\eta}) = \left(1 + \dfrac{2p_{T,\min}}{Q}\right) \sqrt{1 - \dfrac{4p_{T,\min}}{Q + 2p_{T,\min}}} & 2p_{T,\min} \le Q < 2p_{T,\min} \cosh \eta_{\max}\,, \\ \tanh(\eta_{\max}) & Q \ge 2p_{T,\min} \cosh \eta_{\max}\,. \end{cases} \tag{C.44}$$

C.2 Asymmetric cuts

In some cases, asymmetric cuts are required to match the experimental measurements. More specifically, the two outgoing photons are subjected to different cuts depending on their hierarchy (Tab. 3). Usually, one defines the (sub)leading photon as the particle with the (smallest)largest p_T and according to whether the particle is leading or subleading

a different cut on the p_T is enforced. In this situation, the cut function Φ needs to be generalises to

$$\Phi(p_1,p_2) = \vartheta(p_{T,1}^2 - p_{T,2}^2)\Theta^{(1)}(p_1)\Theta^{(2)}(p_2) + \vartheta(p_{T,2}^2 - p_{T,1}^2)\Theta^{(1)}(p_2)\Theta^{(2)}(p_1)\,, \tag{C.45}$$

where

$$\Theta^{(i)}(p) = \vartheta(\eta - \eta_{\min})\vartheta(\eta_{\max} - \eta)\vartheta(p_T - p_{T,\min}^{(i)})\,, \quad i = 1,2\,, \tag{C.46}$$

and, in general, $p_{T,\min}^{(1)} \neq p_{T,\min}^{(2)}$. As shown above, the photon four-momenta p_1 and p_2 are constrained kinematically so that effectively $p_1 = p$ and $p_2 = q - p$ with $p_{T,1} = \overline{p}_T$ (where $\overline{p}_T$ is defined in Eq. (C.23)) and

$$p_{T,2}^2 = q_T^2 + \overline{p}_T^2 - 2q_T\overline{p}_T\cos\phi\,. \tag{C.47}$$

Therefore, the functions $\vartheta(p_{T,1}^2 - p_{T,2}^2)$ and $\vartheta(p_{T,2}^2 - p_{T,1}^2)$ can be reduced to the following ϑ-functions on the azimuthal angle ϕ:

$$\vartheta(p_{T,1}^2 - p_{T,2}^2) = \vartheta\left(\cos\phi - \frac{q_T\cosh(\eta - y)}{M}\right)\,, \quad \vartheta(p_{T,2}^2 - p_{T,1}^2) = \vartheta\left(\frac{q_T\cosh(\eta - y)}{M} - \cos\phi\right)\,. \tag{C.48}$$

Generalising the procedure detailed above for the implementation of the cuts, we introduce the additional function

$$f^{(1)}(\eta) = \frac{q_T\cosh(\eta - y)}{M}\,, \tag{C.49}$$

such that

$$\Phi(p, q-p) = \vartheta(\eta - \eta_{\min})\vartheta(\eta_{\max} - \eta)\left[\vartheta(x - x_1^{(1)})\vartheta(x_2^{(1)} - x) + \vartheta(x - x_1^{(2)})\vartheta(x_2^{(2)} - x)\right]\,, \tag{C.50}$$

where we have defined

$$\begin{aligned}
x_1^{(1)}(\eta) &= \max[f^{(1)}(\eta), f^{(2)}(\eta, p_{T,\min}^{(1)}), -1]\,,\\
x_2^{(1)}(\eta) &= \min[f^{(3)}(\eta, \eta_{\min}), f^{(3)}(\eta, \eta_{\max}), f^{(4)}(\eta, p_{T,\min}^{(2)}), 1]\,,\\
x_1^{(2)}(\eta) &= \max[f^{(2)}(\eta, p_{T,\min}^{(2)}), -1]\,,\\
x_2^{(2)}(\eta) &= \min[f^{(1)}(\eta), f^{(3)}(\eta, \eta_{\min}), f^{(3)}(\eta, \eta_{\max}), f^{(4)}(\eta, p_{T,\min}^{(1)}), 1]\,.
\end{aligned} \tag{C.51}$$

It follows that

$$\begin{aligned}
\int_{-\infty}^{\infty} d\eta \int_{-1}^{1} dx\, \Phi(p, q-p)\ldots = \int_{\eta_{\min}}^{\eta_{\max}} d\eta \Bigg[&\vartheta(x_2^{(1)}(\eta) - x_1^{(1)}(\eta)) \int_{x_1^{(1)}(\eta)}^{x_2^{(1)}(\eta)} dx \ldots\\
&+ \vartheta(x_2^{(2)}(\eta) - x_1^{(2)}(\eta)) \int_{x_1^{(2)}(\eta)}^{x_2^{(2)}(\eta)} dx \ldots \Bigg]\,.
\end{aligned} \tag{C.52}$$

Finally, exploiting the primitive of the integral in x, the phase-space reduction factor for asymmetric cuts can be written as

$$\begin{aligned}
\mathcal{P}(Q, y, q_T) = \int_{\eta_{\min}}^{\eta_{\max}} d\eta \Big\{ &\vartheta(x_2^{(1)}(\eta) - x_1^{(1)}(\eta)) \left[\overline{F}(x_2^{(1)}(\eta), \eta) - \overline{F}(x_1^{(1)}(\eta), \eta)\right]\\
&+ \vartheta(x_2^{(2)}(\eta) - x_1^{(2)}(\eta)) \left[\overline{F}(x_2^{(2)}(\eta), \eta) - \overline{F}(x_1^{(2)}(\eta), \eta)\right] \Big\}\,,
\end{aligned} \tag{C.53}$$

with F defined in Eq. (C.40).

C.3 Cuts on the four-particle final state

In this appendix, we extend the calculation of the phase–space–reduction factor $\mathcal{P}$ to the four–lepton final state,

$$\mathcal{P}(Q, y, q_T) = \frac{\int_{\text{fid. reg.}} d\Phi_4 \; |\mathcal{M}(p_1, p_2, p_3, p_4)|^2}{\int d\Phi_4 \; |\mathcal{M}(p_1, p_2, p_3, p_4)|^2}\,, \tag{C.54}$$

where p_i are the lepton four-momentum, $\mathcal{M}$ is the decay amplitude for $H \to ZZ \to 4\ell$, and $d\Phi_4$ is the four–body Lorentz invariant phase space,

$$d\Phi_4 \equiv (2\pi)^4 \delta^{(4)}(q - \sum_i^4 p_i) \prod_i^4 \frac{d^4 p_i}{(2\pi)^3}\, \delta(p_i^2)\, \theta(p_{i_0}) \tag{C.55}$$

As in the two photon case, the decay amplitude can be written in terms of the HZZ vertex, the two Z propagators and the leptonic currents. Using

$$g_Z = e/(\sin\theta_W \cos\theta_W)\,, v_f = I_{3,f} - 2Q_f \sin^2\theta_W\,, a_f = I_{3,f} \tag{C.56}$$

with $I_{3,\ell} = -\frac{1}{2}$, $Q_\ell = -1$ for leptons, we can write

$$\mathcal{M} = i\, g_z\, M_Z\, g_{\mu\nu} \left\{ \frac{-i\, g^{\mu\lambda}}{(p_1+p_2)^2 - M_Z^2 + i\Gamma_Z M_Z} \; \frac{-ig_Z}{2} \bar{u}_e^{s_1}(p_1) \left[ie\, \gamma_\lambda\, (v_f - a_f\gamma_5) \right] v_e^{s_2}(p_2) \right\} \tag{C.57}$$

$$\times \left\{ \frac{-i\, g^{\nu\rho}}{(p_3+p_4)^2 - M_Z^2 + i\Gamma_Z M_Z} \; \frac{-ig_Z}{2} \bar{u}_\mu^{s_3}(p_3) \left[ie\, \gamma_\rho\, (v_f - a_f\gamma_5) \right] v_\mu^{s_4}(p_4) \right\}. \tag{C.58}$$

After the spin sum, the squared amplitude takes the schematic form

$$|\mathcal{M}|^2 \propto \frac{[((v_\ell^2 + a_\ell^2)^2 + 4g v_\ell^2 a_\ell^2)(p_1\cdot p_3)(p_2\cdot p_4) + ((v_\ell^2 - a_\ell^2)^2 (p_1\cdot p_4)(p_2\cdot p_3)]}{\left[((p_1+p_2)^2 - m_Z^2)^2 + \Gamma_Z^2 M_Z^2\right] \left[((p_3+p_4)^2 - m_Z^2)^2 + \Gamma_Z^2 M_Z^2\right]} \tag{C.59}$$

so that the explicit dependence on all lepton momenta prevents further analytic simplifications of Eq. (C.54) in the general kinematics (Q, y, q_T).

To enable an efficient numerical evaluation and a transparent implementation of fiducial cuts, we factorise the four–body phase space into a sequence of two–body phase spaces, reflecting the tree structure of the LO decay. To do so, we introduce the intermediate four–momenta

$$q_1 = p_1 + p_2, \qquad q_2 = p_3 + p_4, \qquad q_1 + q_2 = q, \tag{C.60}$$

with virtualities $Q_1^2 \equiv q_1^2$ and $Q_2^2 \equiv q_2^2$. Then

$$d\Phi_4(q; p_1, p_2, p_3, p_4) = \frac{dQ_1^2\, dQ_2^2}{(2\pi)^2}\, d\Phi_2(q; k_1, k_2)\, d\Phi_2(k_1; p_1, p_2)\, d\Phi_2(k_2; p_3, p_4)\,. \tag{C.61}$$

This $1\to2\to2\to2$ factorisation matches the Monte Carlo mapping used in our calculation: it reduces the dimensionality of the integrations at each step, allows us to impose the fiducial requirements (p_T thresholds, $|\eta|$ windows, Z_1/Z_2 mass windows, ordered lepton cuts) at particle level, and leads to a stable and efficient numerical implementation of Eq. (C.54).

This $1 \to 2 \to 2 \to 2$ factorization makes the calculation suitable to a Monte Carlo integration: each step lowers the effective dimensionality and exposes simple two–body kinematics, so the fiducial selections of Table 2 (p_T thresholds, $|\eta|$ windows, m_{Z_1}/m_{Z_2} mass windows, ordered–lepton cuts) can be imposed directly at particle level. In this way, Eq. (C.54) is evaluated numerically in a stable and efficient manner.

Conclusions

This thesis advances the three–dimensional description of hadrons in momentum space within the Transverse Momentum Dependent (TMD) framework along two complementary directions: the study of azimuthal distributions of hadron pairs produced in photon–photon collisions, where we formulated the kinematics and helicity formalism and derived the pattern of azimuthal modulations proportional to the TMD fragmentation functions, and the use of the low-q_T Higgs spectrum at the LHC to probe the gluon sector, where the colour–singlet final state and $q_T \ll m_H$ justify rigorous TMD factorisation and make the shape of the spectrum directly sensitive to the gluon distribution. We investigated azimuthal asymmetries for inclusive production of light–hadron pairs in three leading–order channels,

$$\ell^+\ell^- \to \gamma^*\gamma \to q\bar{q} \to h_1 h_2 + X, \quad \ell^+\ell^- \to \gamma\gamma \to q\bar{q} \to h_1 h_2 + X, \quad \mathcal{N}\mathcal{N} \to \gamma\gamma \to q\bar{q} \to h_1 h_2 + X,$$

requiring the two hadrons to be almost back to back and with large transverse momenta in the photon–photon c.m. frame. The proposed measurements would stimulate TMD studies in photon–photon scattering at a time when future lepton colliders are under discussion. They can improve the determination of quark TMD fragmentation functions with more effective flavour separation than SIDIS or $\ell^+\ell^-$ annihilation, since d, s, b contributions are suppressed by a charge weight factor of $1/16$ relative to u, c. Moreover, while $\ell^+\ell^-$ colliders operate at fixed c.m. energy, photon–photon scattering allows one to vary the perturbative scale via the photon virtualities (or the hadron pair transverse momentum) and thus to study the scale dependence of TMD fragmentation functions within the same process and setup.

For the $\ell^+\ell^- \to \gamma^*\gamma$ case, the azimuthal asymmetries and their moments (Table 2.1) involve ratios of unpolarised and Collins TMD FFs, with prefactors that depend on the kinematics, the initial–state polarisation and the dynamics of the hard process; comparing their relative weights across DIS and SIDIS–like configurations provides a validation of the approach. We presented preliminary estimates for the azimuthal moments of the unpolarised differential cross section and of the double–longitudinal spin asymmetry in two–pion production, for like– and unlike–charged pion pairs at fixed Q^2, as functions of z_2 in z_1 bins, with the remaining variables integrated over the allowed range. The ζ integration in $A_{U,L}$ and $B_{U,L}$ is analytic; by symmetry, the antisymmetric coefficients $A_{U,L}^{\cos\phi_q}$ vanish on the full range and are therefore evaluated over half of it, and the same

prescription is adopted for A_U in the corresponding moments.

The coefficients were evaluated using unpolarised and longitudinal Weizsäcker–Williams photon distributions [82, 83], with $Q^2_{\min}$ and $Q^2_{\max}$ fixed by θ_c as in Eq. (2.34), and illustrative collider parameters in Table 2.2. Fragmentation was described by a factorised Gaussian ansatz for unpolarised TMD FFs (Eq. (2.35)), with $\langle p_\perp^2 \rangle = 0.12$ GeV^2 and DSS collinear FFs [87]. The Collins FF was taken to be proportional to the TMD FF as in Eq. (2.36), with favoured/unfavoured normalisations and a free parameter M_C, following Refs. [85, 86]. Scale evolution was included through a simplified DGLAP treatment of the collinear components; full TMD evolution in the Collins–Soper–Sterman approach, already available for e^+e^-, is left for future phenomenology, in line with current indications that evolution effects are mild for spin and azimuthal asymmetries.

For FCC–ee kinematics (Table 2.2), we showed central-value estimates of $\langle \, \mathrm{d}\sigma^{\mathrm{unp}} \, | \, n, 1 \, \rangle$ at fixed Q^2, and analogous results for $\langle \, A_{LL} \, | \, n, 1 \, \rangle$. In the considered setups, the unpolarised azimuthal moments are small but in some cases reach a few percent in size and may be within experimental reach; A_{LL} moments are at the per–mille level and likely unmeasurable. Their size depends on weighted combinations of Collins and unpolarised FFs and on prefactors related to $A_{U,L}$ and $B_{U,L}$, with a crucial dependence on the Q^2, x_B and ξ ranges. A complete exploration of phase space is necessary to maximise the moments while avoiding excessive suppression of the unpolarised cross section; this study is in progress. The same formalism can be applied to photon–photon scattering in linear lepton colliders with Compton back–scattered photons, and extended to hadron pairs including spin–1/2 particles (e.g. Λ), allowing studies of spontaneous Λ polarisation and quark–flavour effects. We also extended the calculation to hadron–pair production in collisions of two quasi–real photon at lepton colliders, implementing the same methodology as in the $\gamma^*\gamma$ case and deriving compact expressions for the differential cross section, the double–longitudinal asymmetry A_{LL} and their azimuthal moments. An analogous computation was performed for inclusive hadron–pair production in ultraperipheral heavy–ion collisions within the Equivalent Photon Approximation, using both the thrust–axis method and the Gottfried–Jackson frame, obtaining results parallel to the lepton–collider case. The feasibility ultimately depends on achievable luminosities and centre–of–mass energies in the photon–photon mode and should be assessed in future collider studies.

Inclusive Higgs production in proton–proton collisions provides a clean and sensitive probe of the unpolarised gluon TMD $f_1^g(x, \boldsymbol{k}_\perp)$. In the small–$q_T$ region the cross section factorises into a hard function and a convolution of two gluon TMDs with the soft factor and Collins–Soper evolution, making the Higgs q_T distribution directly sensitive to f_1^g (with possible modifications from $h_1^{\perp g}$). Methodologically, the perturbative ingredients for gluon TMDs (matching and evolution) are available at high accuracy and can be deployed consistently in precision phenomenology.

We implemented a TMD analysis of Higgs production using NangaParbat. The calculation is performed in b_T space, with evolution and matching organised through the

b_* prescription and a nonperturbative factor $f_{\rm NP}$; the Hankel transform is evaluated efficiently via the Ogata quadrature, allowing precomputation of weights and fast predictions. The modular structure ensures a like–for–like comparison across datasets while keeping factorisation and evolution consistent. Fiducial selections are incorporated through a phase–space reduction factor $\mathcal{P}$, and the comparison to data uses a $\chi^2 = \chi^2_D + \chi^2_\lambda$ with shifted theory curves for visualisation of correlated systematics.

We confronted these predictions with ATLAS and CMS measurements of the Higgs transverse–momentum spectrum in the $\gamma\gamma$ and 4ℓ channels (and their combinations), restricting to the TMD–validity region $q_T/Q \lesssim 0.3$ and retaining 36 data points. As a preliminary consistency test, we adopted the DWS ansatz for $f_{\rm NP}$ with $(g_1, g_2) = (1, 1)$ and performed a central–replica fit at N^{3}LL accuracy. The overall quality, $\chi^2 \simeq 2.10$, is mixed but encouraging: several spectra are well described (e.g. ATLAS Run II $H \to 4\ell$), while others (e.g. CMS Run II $H \to 4\ell$ and ATLAS 8 TeV $H \to \gamma\gamma$) drive the tension. This pattern suggests genuine sensitivity of current data to TMD effects, but also points to limited flexibility in the present non-perturbative model.

These results motivate a refined analysis with more flexible parametrisations of $f_{\rm NP}$, an improved handling of uncorrelated uncertainties and a more detailed implementation of fiducial cuts. Within such an enhanced setup, the same methodology can enable robust extractions of the unpolarised gluon TMD from Higgs q_T spectra with quantified theoretical and experimental uncertainties, while continued work on photon–photon channels can tighten constraints on TMD fragmentation functions within a unified helicity–based framework.

Bibliography

[1] M. Breidenbach, J. I. Friedman, H. W. Kendall, E. D. Bloom, D. H. Coward, H. DeStaebler, J. Drees, L. W. Mo, and R. E. Taylor. Observed behavior of highly inelastic electron-proton scattering. *Phys. Rev. Lett.*, 23:935–939, Oct 1969. doi: 10.1103/PhysRevLett.23.935. URL https://link.aps.org/doi/10.1103/PhysRevLett.23.935.

[2] J. D. Bjorken. Asymptotic sum rules at infinite momentum. *Physical Review*, 179 (5):1547–1553, 1969. doi: 10.1103/PhysRev.179.1547.

[3] Jr. Callan, C. G. and D. J. Gross. Crucial test of a theory of currents. *Physical Review Letters*, 21(5):311–313, 1968. doi: 10.1103/PhysRevLett.21.311.

[4] Richard P. Feynman. Very high-energy collisions of hadrons. *Physical Review Letters*, 23(24):1415–1417, 1969. doi: 10.1103/PhysRevLett.23.1415.

[5] D. J. Gross and F. Wilczek. Ultraviolet behavior of non-abelian gauge theories. *Physical Review Letters*, 30(26):1343–1346, 1973. doi: 10.1103/PhysRevLett.30.1343.

[6] H. D. Politzer. Reliable perturbative results for strong interactions? *Physical Review Letters*, 30(26):1346–1349, 1973. doi: 10.1103/PhysRevLett.30.1346.

[7] Yu. L. Dokshitzer. Calculation of the structure functions for deep inelastic scattering and e^+e^- annihilation by perturbation theory in QCD. *Soviet Physics JETP*, 46: 641–653, 1977. Zh. Eksp. Teor. Fiz. **73** (1977) 1216–1240.

[8] V. N. Gribov and L. N. Lipatov. Deep inelastic *ep* scattering in perturbation theory. *Soviet Journal of Nuclear Physics*, 15:438–450, 1972. URL https://cds.cern.ch/record/427157.

[9] G. Altarelli and G. Parisi. Asymptotic freedom in parton language. *Nuclear Physics B*, 126:298–318, 1977. doi: 10.1016/0550-3213(77)90384-4.

[10] J. J. Aubert et al. Measurements of the nucleon structure functions f_2^n in deep inelastic muon scattering from deuterium and comparison with those from hydrogen and iron. *Nuclear Physics B*, 293:740–786, 1987. doi: 10.1016/0550-3213(87)90090-3.

[11] A. C. Benvenuti et al. Test of QCD and a measurement of λ from scaling violations in the proton structure function $f_2(x, q^2)$ at high q^2. *Physics Letters B*, 223:490–496, 1989. doi: 10.1016/0370-2693(89)91638-9.

[12] T. Ahmed, S. Aid, A. Akhundov, V. Andreev, B. Andrieu, R. D. Appuhn, et al. A measurement of the proton structure function $f_2(x, q^2)$. *Nuclear Physics B*, 439(3): 471–502, 1995. doi: 10.1016/0550-3213(95)98236-U.

[13] John C. Collins, Davison E. Soper, and George F. Sterman. Factorization of hard processes in QCD. In A. H. Mueller, editor, *Perturbative Quantum Chromodynamics*, volume 5 of *Advanced Series on Directions in High Energy Physics*, pages 1–91. World Scientific, Singapore, 1989. doi: 10.1142/9789814503266_0001.

[14] Xiang-dong Ji, Jian-Ping Ma, and Feng Yuan. QCD factorization for spin-dependent cross sections in DIS and Drell-Yan processes at low transverse momentum. *Phys. Lett. B*, 597:299–308, 2004. doi: 10.1016/j.physletb.2004.07.026.

[15] Xiang-dong Ji, Jian-ping Ma, and Feng Yuan. QCD factorization for semi-inclusive deep-inelastic scattering at low transverse momentum. *Phys. Rev. D*, 71:034005, 2005. doi: 10.1103/PhysRevD.71.034005.

[16] John Collins. *Foundations of Perturbative QCD*, volume 32. Cambridge University Press, 2011. doi: 10.1017/9781009401845.

[17] Miguel G. Echevarria, Ahmad Idilbi, and Ignazio Scimemi. Factorization Theorem For Drell-Yan At Low q_T And Transverse Momentum Distributions On-The-Light-Cone. *JHEP*, 07:002, 2012. doi: 10.1007/JHEP07(2012)002.

[18] P. J. Mulders and R. D. Tangerman. The complete tree-level result up to order $1/q$ for polarized deep-inelastic leptoproduction. *Nucl. Phys. B*, 461:197–237, 1996. doi: 10.1016/0550-3213(95)00632-X.

[19] A. Bacchetta, M. Diehl, K. Goeke, A. Metz, P. J. Mulders, and M. Schlegel. Semi-inclusive deep inelastic scattering at small transverse momentum. *JHEP*, 02:093, 2007. doi: 10.1088/1126-6708/2007/02/093.

[20] M. Anselmino, M. Boglione, U. D'Alesio, S. Melis, F. Murgia, E. R. Nocera, and A. Prokudin. General Helicity Formalism for Polarized Semi-Inclusive Deep Inelastic Scattering. *Phys. Rev. D*, 83:114019, 2011. doi: 10.1103/PhysRevD.83.114019.

[21] S. Arnold, A. Metz, and M. Schlegel. Dilepton production from polarized hadron hadron collisions. *Phys. Rev. D*, 79:034005, 2009. doi: 10.1103/PhysRevD.79.034005.

[22] D. Boer, R. Jakob, and P. J. Mulders. Asymmetries in polarized hadron production in e^+e^- annihilation up to order $1/Q$. *Nucl. Phys. B*, 504:345–380, 1997. doi: 10.1016/S0550-3213(97)00456-2.

[23] U. D'Alesio, F. Murgia, and M. Zaccheddu. General helicity formalism for two-hadron production in e^+e^- annihilation within a TMD approach. *JHEP*, 10:078, 2021. doi: 10.1007/JHEP10(2021)078.

[24] D. Boer, W. J. den Dunnen, C. Pisano, M. Schlegel, and W. Vogelsang. Linearly Polarized Gluons and the Higgs Transverse Momentum Distribution. *Phys. Rev. Lett.*, 108:032002, 2012. doi: 10.1103/PhysRevLett.108.032002.

[25] P. Sun, Bo-Wen Xiao, and F. Yuan. Gluon Distribution Functions and Higgs Boson Production at Moderate Transverse Momentum. *Phys. Rev. D*, 84:094005, 2011. doi: 10.1103/PhysRevD.84.094005.

[26] Jian-wei Qiu, M. Schlegel, and W. Vogelsang. Probing Gluonic Spin-Orbit Correlations in Photon Pair Production. *Phys. Rev. Lett.*, 107:062001, 2011. doi: 10.1103/PhysRevLett.107.062001.

[27] F. Scarpa, D. Boer, M. G. Echevarria, J. P. Lansberg, C. Pisano, and M. Schlegel. Studies of gluon TMDs and their evolution using quarkonium-pair production at the LHC. *Eur. Phys. J. C*, 80:87, 2020. doi: 10.1140/epjc/s10052-020-7619-1.

[28] W. J. den Dunnen, J. P. Lansberg, C. Pisano, and M. Schlegel. Accessing the Transverse Dynamics and Polarization of Gluons inside the Proton at the LHC. *Phys. Rev. Lett.*, 112:212001, 2014. doi: 10.1103/PhysRevLett.112.212001.

[29] D. Boer and C. Pisano. Polarized gluon studies with charmonium and bottomonium at LHCb and AFTER. *Phys. Rev. D*, 86:094007, 2012. doi: 10.1103/PhysRevD.86.094007.

[30] N. Kato, L. Maxia, and C. Pisano. Spin asymmetries for C-even quarkonium production as a probe of gluon distributions. *Phys. Rev. D*, 110:034038, 2024. doi: 10.1103/PhysRevD.110.034038.

[31] T. C. Rogers and P. J. Mulders. No Generalized TMD-Factorization in Hadro-Production of High Transverse Momentum Hadrons. *Phys. Rev. D*, 81:094006, 2010. doi: 10.1103/PhysRevD.81.094006.

[32] R. Boussarie et al. TMD Handbook.

[33] Gerard 't Hooft and Martinus J. G. Veltman. Regularization and renormalization of gauge fields. *Nucl. Phys. B*, 44:189–213, 1972. doi: 10.1016/0550-3213(72)90279-9.

[34] Alexandre Deur. The qcd running coupling, 2025. URL https://arxiv.org/abs/2502.06535. Commissioned article for the Encyclopedia of Particle Physics.

[35] Dennis Sivers. Single-spin production asymmetries from the hard scattering of point-like constituents. *Phys. Rev. D*, 41:83–90, Jan 1990. doi: 10.1103/PhysRevD.41.83. URL https://link.aps.org/doi/10.1103/PhysRevD.41.83.

[36] J. C. Collins. Fragmentation of transversely polarized quarks probed in transverse momentum distributions. *Nucl. Phys. B*, 396:161–182, 1993. doi: 10.1016/0550-3213(93)90262-N.

[37] Stanley J. Brodsky, Dae Sung Hwang, and Ivan Schmidt. Final-state interactions and single-spin asymmetries in semi-inclusive deep inelastic scattering. *Physics Letters B*, 530(1):99–107, 2002. ISSN 0370-2693. doi: https://doi.org/10.1016/S0370-2693(02)01320-5. URL https://www.sciencedirect.com/science/article/pii/S0370269302013205.

[38] John C. Collins. Leading-twist single-transverse-spin asymmetries: Drell–yan and deep-inelastic scattering. *Physics Letters B*, 536(1):43–48, 2002. ISSN 0370-2693. doi: https://doi.org/10.1016/S0370-2693(02)01819-1. URL https://www.sciencedirect.com/science/article/pii/S0370269302018191.

[39] Stanley J. Brodsky, Dae Sung Hwang, and Ivan Schmidt. Initial-state interactions and single-spin asymmetries in drell–yan processes. *Nuclear Physics B*, 642(1):344–356, 2002. ISSN 0550-3213. doi: https://doi.org/10.1016/S0550-3213(02)00617-X. URL https://www.sciencedirect.com/science/article/pii/S055032130200617X.

[40] A.M. Kotzinian and P.J. Mulders. Probing transverse quark polarization via azimuthal asymmetries in leptoproduction. *Physics Letters B*, 406(4):373–380, 1997. ISSN 0370-2693. doi: https://doi.org/10.1016/S0370-2693(97)00708-9. URL https://www.sciencedirect.com/science/article/pii/S0370269397007089.

[41] R. D. Tangerman and P. J. Mulders. Intrinsic transverse momentum and the polarized drell-yan process. *Phys. Rev. D*, 51:3357–3372, Apr 1995. doi: 10.1103/PhysRevD.51.3357. URL https://link.aps.org/doi/10.1103/PhysRevD.51.3357.

[42] A. M. Kotzinian and P. J. Mulders. Longitudinal quark polarization in transversely polarized nucleons. *Phys. Rev. D*, 54:1229–1232, Jul 1996. doi: 10.1103/PhysRevD.54.1229. URL https://link.aps.org/doi/10.1103/PhysRevD.54.1229.

[43] D. Boer and P. J. Mulders. Time-reversal odd distribution functions in leptoproduction. *Phys. Rev. D*, 57:5780–5786, May 1998. doi: 10.1103/PhysRevD.57.5780. URL https://link.aps.org/doi/10.1103/PhysRevD.57.5780.

[44] P.J Mulders and R.D Tangerman. The complete tree-level result up to order 1/q for polarized deep-inelastic leptoproduction. *Nuclear Physics B*, 461(1):197–237, 1996. ISSN 0550-3213. doi: https://doi.org/10.1016/0550-3213(95)00632-X. URL https://www.sciencedirect.com/science/article/pii/055032139500632X.

[45] M. Anselmino, M. Boglione, U. D'Alesio, E. Leader, S. Melis, and F. Murgia. The general partonic structure for hadronic spin asymmetries. *Phys. Rev. D*, 73:014020, 2006. doi: 10.1103/PhysRevD.73.014020.

[46] J. C. Collins and D. E. Soper. Back-To-Back Jets in QCD. *Nucl. Phys. B*, 193, 1981. doi: 10.1016/0550-3213(81)90339-4.

[47] Wojciech Bizoń, Xuan Chen, Aude Gehrmann-De Ridder, Thomas Gehrmann, Nigel Glover, Alexander Huss, Pier Francesco Monni, Emanuele Re, Luca Rottoli, and Paolo Torrielli. Fiducial distributions in higgs and drell-yan production at n3ll+nnlo. *Journal of High Energy Physics*, 2018(12), December 2018. ISSN 1029-8479. doi: 10.1007/jhep12(2018)132. URL http://dx.doi.org/10.1007/JHEP12(2018)132.

[48] John Collins and Ted C. Rogers. Connecting different tmd factorization formalisms in qcd. *Phys. Rev. D*, 96:054011, Sep 2017. doi: 10.1103/PhysRevD.96.054011. URL https://link.aps.org/doi/10.1103/PhysRevD.96.054011.

[49] Stefano Catani, Leandro Cieri, Daniel de Florian, Giancarlo Ferrera, and Massimiliano Grazzini. Vector-boson production at hadron colliders: hard-collinear coefficients at the nnlo. *The European Physical Journal C*, 72(11), November 2012. ISSN 1434-6052. doi: 10.1140/epjc/s10052-012-2195-7. URL http://dx.doi.org/10.1140/epjc/s10052-012-2195-7.

[50] Miguel G. Echevarria, Ignazio Scimemi, and Alexey Vladimirov. Unpolarized transverse momentum dependent parton distribution and fragmentation functions at next-to-next-to-leading order. *Journal of High Energy Physics*, 2016(9), September 2016. ISSN 1029-8479. doi: 10.1007/jhep09(2016)004. URL http://dx.doi.org/10.1007/JHEP09(2016)004.

[51] Alessandro Bacchetta, Valerio Bertone, Chiara Bissolotti, Giuseppe Bozzi, Filippo Delcarro, Fulvio Piacenza, and Marco Radici. Transverse-momentum-dependent parton distributions up to n3ll from drell-yan data. *Journal of High Energy Physics*, 2020(7), July 2020. ISSN 1029-8479. doi: 10.1007/jhep07(2020)117. URL http://dx.doi.org/10.1007/JHEP07(2020)117.

[52] Stefano Catani. Higher-order qcd corrections in hadron collisions: Soft-gluon resummation and exponentiation. *Nuclear Physics B - Proceedings Supplements*, 54

(1–2):107–113, March 1997. ISSN 0920-5632. doi: 10.1016/s0920-5632(97)00024-8. URL http://dx.doi.org/10.1016/S0920-5632(97)00024-8.

[53] Thomas Becher, Matthias Neubert, and Daniel Wilhelm. Electroweak gauge-boson production at small q t: Infrared safety from the collinear anomaly. *Journal of High Energy Physics*, 2012(2), February 2012. ISSN 1029-8479. doi: 10.1007/jhep02(2012)124. URL http://dx.doi.org/10.1007/JHEP02(2012)124.

[54] Thomas Becher, Matthias Neubert, and Daniel Wilhelm. Higgs-boson production at small transverse momentum. *Journal of High Energy Physics*, 2013(5), May 2013. ISSN 1029-8479. doi: 10.1007/jhep05(2013)110. URL http://dx.doi.org/10.1007/JHEP05(2013)110.

[55] Andrea Banfi, Heather McAslan, Pier Francesco Monni, and Giulia Zanderighi. Two-jet rate in e^+e^- at next-to-next-to-leading-logarithmic order. *Phys. Rev. Lett.*, 117:172001, Oct 2016. doi: 10.1103/PhysRevLett.117.172001. URL https://link.aps.org/doi/10.1103/PhysRevLett.117.172001.

[56] Giuseppe Bozzi, Stefano Catani, Daniel de Florian, and Massimiliano Grazzini. Transverse-momentum resummation and the spectrum of the higgs boson at the lhc. *Nuclear Physics B*, 737(1–2):73–120, March 2006. ISSN 0550-3213. doi: 10.1016/j.nuclphysb.2005.12.022. URL http://dx.doi.org/10.1016/j.nuclphysb.2005.12.022.

[57] Stefano Catani, Leandro Cieri, Daniel de Florian, Giancarlo Ferrera, and Massimiliano Grazzini. Universality of transverse-momentum resummation and hard factors at the nnlo. *Nuclear Physics B*, 881:414–443, April 2014. ISSN 0550-3213. doi: 10.1016/j.nuclphysb.2014.02.011. URL http://dx.doi.org/10.1016/j.nuclphysb.2014.02.011.

[58] Marcin Bury, Francesco Hautmann, Sergio Leal-Gomez, Ignazio Scimemi, Alexey Vladimirov, and Pia Zurita. Pdf bias and flavor dependence in tmd distributions. *Journal of High Energy Physics*, 2022(10), October 2022. ISSN 1029-8479. doi: 10.1007/jhep10(2022)118. URL http://dx.doi.org/10.1007/JHEP10(2022)118.

[59] Valentin Moos, Ignazio Scimemi, Alexey Vladimirov, and Pia Zurita. Extraction of unpolarized transverse momentum distributions from fit of drell-yan data at n^4ll, 2024. URL https://arxiv.org/abs/2305.07473.

[60] Ignazio Scimemi and Alexey Vladimirov. Non-perturbative structure of semi-inclusive deep-inelastic and drell-yan scattering at small transverse momentum. *Journal of High Energy Physics*, 2020(6), June 2020. ISSN 1029-8479. doi: 10.1007/jhep06(2020)137. URL http://dx.doi.org/10.1007/JHEP06(2020)137.

[61] J. C. Collins, D. E. Soper, and G. Sterman. Transverse Momentum Distribution in Drell-Yan Pair and W and Z Boson Production. *Nucl. Phys. B*, 250:199, 1985. doi: 10.1016/0550-3213(85)90479-1.

[62] J. Collins, L. Gamberg, A. Prokudin, T. C. Rogers, N. Sato, and B. Wang. Relating transverse-momentum-dependent and collinear factorization theorems in a generalized formalism. *Phys. Rev. D*, 94:034014, Aug 2016. doi: 10.1103/PhysRevD.94.034014. URL https://link.aps.org/doi/10.1103/PhysRevD.94.034014.

[63] Alessandro Bacchetta, Filippo Delcarro, Cristian Pisano, Marco Radici, and Andrea Signori. Extraction of partonic transverse momentum distributions from semi-inclusive deep-inelastic scattering, drell-yan and z-boson production. *Journal of High Energy Physics*, 2017(6), June 2017. ISSN 1029-8479. doi: 10.1007/jhep06(2017)081. URL http://dx.doi.org/10.1007/JHEP06(2017)081.

[64] V. M. Budnev, I. F. Ginzburg, G. V. Meledin, and V. G. Serbo. The Two photon particle production mechanism. Physical problems. Applications. Equivalent photon approximation. *Phys. Rept.*, 15:181–281, 1975. doi: 10.1016/0370-1573(75)90009-5.

[65] I. F. Ginzburg, G. L. Kotkin, V. G. Serbo, and V. I. Telnov. Colliding γe and $\gamma\gamma$ Beams Based on the Single Pass Accelerators (of Vlepp Type). *Nucl. Instrum. Meth.*, 205:47–68, 1983. doi: 10.1016/0167-5087(83)90173-4.

[66] I. F. Ginzburg, G. L. Kotkin, S. L. Panfil, V. G. Serbo, and V. I. Telnov. Colliding γe and $\gamma\gamma$ Beams Based on the Single Pass e^+e^- Accelerators. 2. Polarization Effects. Monochromatization Improvement. *Nucl. Instrum. Meth. A*, 219:5–24, 1984. doi: 10.1016/0167-5087(84)90128-5.

[67] H. Kolanoski. *Two-photon physics at e^+e^- storage rings*, volume 105. Berlin, Springer-Verlag, 1984. doi: 10.1007/BFb0045900.

[68] L. Schoeffel, C. Baldenegro, H. Hamdaoui, S. Hassani, C. Royon, and M. Saimpert. Photon–photon physics at the LHC and laser beam experiments, present and future. *Prog. Part. Nucl. Phys.*, 120:103889, 2021. doi: 10.1016/j.ppnp.2021.103889.

[69] C. F. von Weizsacker. Radiation emitted in collisions of very fast electrons. *Z. Phys.*, 88:612–625, 1934. doi: 10.1007/BF01333110.

[70] E. J. Williams. Nature of the high-energy particles of penetrating radiation and status of ionization and radiation formulae. *Phys. Rev.*, 45:729–730, 1934. doi: 10.1103/PhysRev.45.729.

[71] J. C. Collins and A. Metz. Universality of soft and collinear factors in hard-scattering factorization. *Phys. Rev. Lett.*, 93:252001, 2004. doi: 10.1103/PhysRevLett.93.252001.

[72] F. Yuan. Azimuthal Asymmetric Distribution of Hadrons Inside a Jet at Hadron Collider. *Phys. Rev. Lett.*, 100:032003, 2008. doi: 10.1103/PhysRevLett.100.032003.

[73] L. P. Gamberg, A. Mukherjee, and P. J. Mulders. A model independent analysis of gluonic pole matrix elements and universality of TMD fragmentation functions. *Phys. Rev. D*, 83:071503, 2011. doi: 10.1103/PhysRevD.83.071503.

[74] J. C. Collins and D. E. Soper. Back-To-Back Jets: Fourier Transform from b to k_T. *Nucl. Phys. B*, 197:446–476, 1982. doi: 10.1016/0550-3213(82)90453-9.

[75] M. G. Echevarria, A. Idilbi, A. Schäfer, and I. Scimemi. Model-Independent Evolution of Transverse Momentum Dependent Distribution Functions (TMDs) at NNLL. *Eur. Phys. J. C*, 73:2636, 2013. doi: 10.1140/epjc/s10052-013-2636-y.

[76] M. G. Echevarria, A. Idilbi, and I. Scimemi. Soft and Collinear Factorization and Transverse Momentum Dependent Parton Distribution Functions. *Phys. Lett. B*, 726:795–801, 2013. doi: 10.1016/j.physletb.2013.09.003.

[77] U. D'Alesio, L. Gamberg, F. Murgia, and M. Zaccheddu. Transverse Λ polarization in e^+e^- processes within a TMD factorization approach and the polarizing fragmentation function. *JHEP*, 12:074, 2022. doi: 10.1007/JHEP12(2022)074.

[78] U. D'Alesio, L. Gamberg, F. Murgia, and M. Zaccheddu. Transverse Λ polarization in e^+e^- annihilations and in SIDIS processes at the EIC within TMD factorization. *Phys. Rev. D*, 108:094004, 2023. doi: 10.1103/PhysRevD.108.094004.

[79] C. Pisano, D. Boer, S. J. Brodsky, M. G. A. Buffing, and P. J. Mulders. Linear polarization of gluons and photons in unpolarized collider experiments. *JHEP*, 10: 024, 2013. doi: 10.1007/JHEP10(2013)024.

[80] K. Schilling and G. Wolf. How to analyze vector meson production in inelastic lepton scattering. *Nucl. Phys. B*, 61:381–413, 1973. doi: 10.1016/0550-3213(73)90371-4.

[81] M. Anselmino, M. Bertini, F. Murgia, and B. Pire. Off diagonal helicity density matrix elements for heavy vector mesons inclusively produced in NN, γN and ℓN interactions. *Phys. Lett. B*, 438:347–352, 1998. doi: 10.1016/S0370-2693(98)00978-2.

[82] Stefano Frixione, Michelangelo L. Mangano, Paolo Nason, and Giovanni Ridolfi. Improving the Weizsacker-Williams approximation in electron - proton collisions. *Phys. Lett. B*, 319:339–345, 1993. doi: 10.1016/0370-2693(93)90823-Z.

[83] Daniel de Florian and Stefano Frixione. Jet cross-sections in polarized photon hadron collisions. *Phys. Lett. B*, 457:236–244, 1999. doi: 10.1016/S0370-2693(99)00544-4.

[84] S. Navas et al. Review of particle physics. *Phys. Rev. D*, 110(3):030001, 2024. doi: 10.1103/PhysRevD.110.030001.

[85] Mariaelena Boglione, Umberto D'Alesio, Carlo Flore, Josè Osvaldo Gonzalez-Hernandez, Francesco Murgia, and Alexei Prokudin. Simultaneous reweighting of Transverse Momentum Dependent distributions. *Phys. Lett. B*, 854:138712, 2024. doi: 10.1016/j.physletb.2024.138712.

[86] M. Anselmino, M. Boglione, J. O. Gonzalez Hernandez, S. Melis, and A. Prokudin. Unpolarised Transverse Momentum Dependent Distribution and Fragmentation Functions from SIDIS Multiplicities. *JHEP*, 04:005, 2014. doi: 10.1007/JHEP04(2014)005.

[87] Daniel de Florian, Rodolfo Sassot, and Marco Stratmann. Global analysis of fragmentation functions for pions and kaons and their uncertainties. *Phys. Rev. D*, 75:114010, 2007. doi: 10.1103/PhysRevD.75.114010.

[88] E. Fermi. On the Theory of the impact between atoms and electrically charged particles. *Z. Phys.*, 29:315–327, 1924. doi: 10.1007/BF03184853.

[89] John David Jackson. *Classical Electrodynamics*. Wiley, 1998. ISBN 978-0-471-30932-1.

[90] Daniel Boer. Angular dependences in inclusive two-hadron production at BELLE. *Nucl. Phys. B*, 806:23–67, 2009. doi: 10.1016/j.nuclphysb.2008.06.011.

[91] R. Keith Ellis, W. James Stirling, and B. R. Webber. *QCD and collider physics*, volume 8. Cambridge University Press, 2 2011. ISBN 978-0-511-82328-2, 978-0-521-54589-1. doi: 10.1017/CBO9780511628788.

[92] H. Ogata. A numerical integration formula based on the bessel functions. URL http://www.kurims.kyoto-u.ac.jp/$\sim$okamoto/paper/Publ_RIMS_DE/41-4-40.pdf.

[93] CMS Collaboration. Measurement and interpretation of differential cross sections for higgs boson production at $\sqrt{s} = 13$ tev. *Phys. Lett. B*, 792:369–396, 2019. doi: 10.1016/j.physletb.2019.03.059.

[94] ATLAS Collaboration. Combined measurement of differential and total cross sections in the $h \to \gamma\gamma$ and $h \to zz^* \to 4\ell$ decay channels at $\sqrt{s} = 13$ tev with the atlas detector. *Phys. Lett. B*, 786:114–133, 2018. doi: 10.1016/j.physletb.2018.09.019.

[95] CMS Collaboration. Measurement of the higgs boson inclusive and differential fiducial production cross sections in the diphoton decay channel with pp collisions at $\sqrt{s} = 13$ tev. 2022. Submitted to JHEP.

[96] CMS Collaboration. Measurements of the higgs boson inclusive and differential fiducial cross sections in the $h \to zz \to 4\ell$ decay channel at $\sqrt{s} = 13$ tev. 2023. Submitted to JHEP.

[97] CMS Collaboration. Measurement of differential cross sections for higgs boson production in the diphoton decay channel in pp collisions at $\sqrt{s} = 8$ tev. *Eur. Phys. J. C*, 76(1):13, 2016. doi: 10.1140/epjc/s10052-015-3853-3.

[98] ATLAS Collaboration. Measurements of the higgs boson inclusive and differential fiducial cross-sections in the diphoton decay channel with pp collisions at $\sqrt{s} = 13$ tev with the atlas detector. *JHEP*, 08:027, 2022. doi: 10.1007/JHEP08(2022)027.

[99] ATLAS Collaboration. Measurements of the higgs boson inclusive and differential fiducial cross sections in the 4
ell decay channel at $\sqrt{s} = 13$ tev. *Eur. Phys. J. C*, 80:942, 2020. doi: 10.1140/epjc/s10052-020-8223-0.

[100] ATLAS Collaboration. Measurements of higgs boson properties in the diphoton decay channel with 36 fb^{-1} of pp collision data at $\sqrt{s} = 13$ tev with the atlas detector. *Phys. Rev. D*, 98:052005, 2018. doi: 10.1103/PhysRevD.98.052005.

[101] ATLAS Collaboration. Fiducial and differential cross sections of higgs boson production measured in the four-lepton decay channel in pp collisions at $\sqrt{s} = 8$ tev with the atlas detector. *Phys. Lett. B*, 738:234–253, 2014. doi: 10.1016/j.physletb.2014.09.054.

[102] ATLAS Collaboration. Measurements of fiducial and differential cross sections for higgs boson production in the diphoton decay channel at $\sqrt{s} = 8$ tev with atlas. *JHEP*, 09:112, 2014. doi: 10.1007/JHEP09(2014)112.

[103] Valerio Bertone, Ignazio Scimemi, and Alexey Vladimirov. Extraction of unpolarized quark transverse momentum dependent parton distributions from drell-yan/z-boson production. *Journal of High Energy Physics*, 2019(6), June 2019. ISSN 1029-8479. doi: 10.1007/jhep06(2019)028. URL http://dx.doi.org/10.1007/JHEP06(2019)028.

[104] Richard D. Ball, Stefano Carrazza, Luigi Del Debbio, Stefano Forte, Jun Gao, Nathan Hartland, Joey Huston, Pavel Nadolsky, Juan Rojo, Daniel Stump, Robert S. Thorne, and C.-P. Yuan. Parton distribution benchmarking with lhc data. *Journal of High Energy Physics*, 2013(4), April 2013. ISSN 1029-8479. doi: 10.1007/jhep04(2013)125. URL http://dx.doi.org/10.1007/JHEP04(2013)125.

[105] Richard D. Ball, Valerio Bertone, Stefano Carrazza, Luigi Del Debbio, Stefano Forte, Patrick Groth-Merrild, Alberto Guffanti, Nathan P. Hartland, Zahari Kassabov, José I. Latorre, Emanuele R. Nocera, Juan Rojo, Luca Rottoli, Emma Slade,

and Maria Ubiali. Parton distributions from high-precision collider data: Nnpdf collaboration. *The European Physical Journal C*, 77(10), October 2017. ISSN 1434-6052. doi: 10.1140/epjc/s10052-017-5199-5. URL http://dx.doi.org/10.1140/epjc/s10052-017-5199-5.

[106] C.T.H. Davies, B.R. Webber, and W.J. Stirling. Drell-yan cross sections at small transverse momentum. *Nuclear Physics B*, 256:413–433, 1985. ISSN 0550-3213. doi: https://doi.org/10.1016/0550-3213(85)90402-X. URL https://www.sciencedirect.com/science/article/pii/055032138590402X.

[107] Ming-xing Luo, Tong-Zhi Yang, Hua Xing Zhu, and Yu Jiao Zhu. Unpolarized quark and gluon tmd pdfs and ffs at n3lo. *Journal of High Energy Physics*, 2021(6), June 2021. ISSN 1029-8479. doi: 10.1007/jhep06(2021)115. URL http://dx.doi.org/10.1007/JHEP06(2021)115.